SUPRAMOLECULAR ARCHITECTURES: PROPERTIES AND APPLICATIONS

Francesco Di Stasio

Department of Physics and Astronomy
London Centre for Nanotechnology

University College London

A dissertation submitted for the degree of Doctor of Philosophy

I, Francesco Di Stasio confirm that the work presented in this thesis is my own. Where information has been derived from other sources, I confirm that this has been indicated in the thesis.

London, 2012

Supervisor: Prof. Franco Cacialli,
Department of Physics and Astronomy and London Centre for Nanotechnology, University College London

Second Supervisor: Dr. Oliver Fenwick
Department of Physics and Astronomy and London Centre for Nanotechnology, University College London

Abstract

Supramolecular architectures represent an increasingly interesting playground both in the chemistry and physics field. In fact, they give us the possibility to tailor the physical and chemical properties of conjugated systems, opening the doors to new applications.

In this dissertation I will present my findings regarding different types of supramolecular structures.

The first part is dedicated to the study of the optical properties of conjugated polyrotaxanes: conjugated polymers such as poly(4,4’-diphenylene vinylene) threaded through cyclodextrin macrocycles rings, that sterically impose increased intermolecular distances, leading to preserved single-molecule excitonic photophysics even in high concentration regimes, due to reduced π–π stacking of the chromophores. In particular, I will show how it is possible to tune their photoluminescence properties for different applications like polarized emission and optically pumped lasers.

The incorporation of polyrotaxanes and their unthreaded analogue in a stretch-oriented polyvinyl alcohol matrix gives rise to a strongly polarized photoluminescence parallel to the stretching direction which I studied using steady-state and time-resolved optical techniques. Furthermore, by exploiting the water-solubility of polyrotaxanes is possible to embed them in three-dimensional photonic crystal and tune their radiative rate to achieve low-threshold optically pumped lasers.

In the second part, I will present the application of supramolecular structures in light-emitting diodes. In fact, self-assembled monolayers represent an interesting system to tune the work function of commonly used electrodes in the plastic electronics field, therefore changing the injection barriers for holes at the interface between the organic semiconductor and the metallic electrode. Furthermore, I will show how supramolecular architectures are used to obtain efficient near-infrared photoluminescence and electroluminescence introducing a three-dimensional π conjugation. Moreover, by adding a pyridine derivative it is possible to suppress the efficient self-quenching in this class of porphyrin based molecular assembly increasing further their applicability in light-emitting diodes.

Acknowledgements

This dissertation is based on the work carried out at the Organic Semiconductors and Nanostructures group at the Dept. of Physics and Astronomy and London Centre for Nanotechnology, University College London between January 2009 and January 2012.

My PhD was funded by the European Commission Marie Curie Research Training Network THREADMILL (grant number: MRTN-CT-2006-036040) from January 2009 to September 2010, and from the European Commission FP-7 ONE-P large-scale project N. 212311 from October 2010 to January 2012.

First and foremost I would like to thank Prof. Franco Cacialli for the opportunity he gave me, the support, the scientific insights and the huge amount of things that I have learnt from him. Secondly, my deepest gratitude goes to all post-docs that I have met during these three years at UCL: Dr. Oliver J. Fenwick, Dr. Giovanni Mattia Lazzerini and Dr. Sergio Brovelli. You have helped me in every aspect of my "every-day-life", from scientific stuff (how to prepare light-emitting diodes, how to perform time-resolved photoluminescence measurements, how to write a scientific paper, ecc...) to completely scientific unrelated ones. I really hope we will be able to meet again.

Another big thank to all the other PhD students that shared with me the burden of doing a PhD (even if it is not a really big one): Gustaf Winroth, Yong Sig-shin, Penglei Li, Marten Tolk, Charlotte Flechon, Giulia Tregnago, Francesco Bausi, Giuseppe Paterno`, Ania Pietrzak and Nico Seidler. Thanks to you I had a really great time here at UCL.

A special thank to Prof. Shabbir "Apollo" Mian, the summer spent in room F17 dealing with the IR spectrometer is unforgettable.

Finally, a big thanks to all collaborators from all around the world (Nuria, Platon, Luca, Toru, Prof. A. Tracz, Prof. P. Samori`, Prof. H.A. Anderson and Prof. D. Comoretto), and all the MsC students that spent time with me in the lab: Tanzim, Ahmed, Jonathan and Deepyanti.

As always, I need to thank my family for the huge support they gave me during all my life. If it wasn't for them I would not be here today writing my PhD thesis.

Last but not least, I want to dedicate this dissertation to my partner Martina that three years ago decided to start this adventure in London with me. Everything is much easier when you are not alone.

Contents

List of Figures

5.3 Chemical structures of the two self-assembled monolayers studied and poly(9,9’-dioctylfluorene-alt-benzothiadiazole) (F8BT) used as active layer in light-emitting diodes. Bottom: structure of the light-emitting diodes studied.

5.4 (a) Scheme of the electroabsorption set-up used in this study. (b) Scheme of an LED and how it is driven.

5.5 EA signal as function of the applied voltage for AZO-SAM 1 (filled circles) and AZO-SAM 2 (open circles). The Vnull values are reported as inset

5.6 Current density-voltage (a) and (semi-logarithmic) luminance-voltage (b) plots for all OLEDs. Color code is the same in both panels.

5.7 Steady-state PL (a) and EL (b) spectra of all devices investigated (from top to bottom, ITO, Au, AZO-SAM 1 and AZO-SAM 2, curves have been offset for clarity). All measurements were conducted at room temperature, and the PL was excited by a pulsed diode laser (Eex = 3.3 eV, pulse width ~ 40 ps).

5.8 Temporal evolution of the PL collected at 2.24 eV for all OLEDs (from top to bottom, ITO, Au, AZO-SAM 1 and AZO-SAM 2, curves have been offset for clarity). A single exponential decay of the type: $I(t) = I_0+I\exp(-t/\tau)$ is used to fit the decay of all the samples (values of τ are reported in figure). All measurements were conducted at room temperature.

6.1 Scheme of energy levels alignment for ITO/PPV/CN-PPV/cathode OLEDs. (Reproduced from ref. 2)

6.2 Chemical structure of Poly(9,9’-dioctylfluorene-alt-N-(4-butylphenyl) -diphenylamine) (TFB, top) and poly(9,9’-dioctylfluorene-alt-benzothiadiazole) (F8BT, bottom)

6.3 Current density-voltage (logJ-V) and luminance-voltage (logL-V) curves for ITO/TFB(t_i)/F8BT(120 nm)/Ca-Al OLEDs for t_i=0, 29, 90, 395 and 1800 nm (pixel area = 0.35 mm^2). Luminance progressively increases upon insertion of the TFB layer up t_i=395 nm. A drastic reduction of J and L is measured for t_i=1800 nm.

6.4 Energy bands diagram of OLEDs components before contact is created. ITO and Ca work function values and TFB and F8BT polaronic levels (conduction band and valence band). The energy barrier at the TFB/F8BT for electrons injected trough the Ca/Al cathode increases the charge carrier balance in the device.

6.5 (a) PL and (b) EL spectra for OLEDs with different initial TFB layer thickness. PL spectra were collected at room temperature in air, using the TCSPC system described in chapter 4. As excitation source a pulsed laser diode was used (E = 3.3 eV, ~40 ps)

6.6 Normalised PL time-resolved measurements collected at 2.28 eV, comparing the time decay of the samples with different initial TFB thicknesses. A single exponential decay is used to fit the decay of the reference sample, whereas a triple exponential is used for all others. The presence of exciplexes is confirmed by the longer decay time for the samples with TFB.

6.7 Energy level scheme for excitons in F8BT, charge-separated states and exciplexes at the TFB/F8BT interface. (*Reproduced and adapted from ref. 27*)

7.1 (a) Chemical structures of the porphyrin hexamers used and the complex of the linear hexamer, P6, with 4-benzyl pyridine, BP. (Ar = 3,5-bis(octyloxy)phenyl in P6 and 3,5-bis(tert-butyl)phenyl in c P6T.) (b)

Optical absorption (solid lines) and photoluminescence (dashed lines) spectra of pure F8BT and blended films. Insets show the overlap of the absorption and emission of the hexamer component of the spectrum. (c) Excitation-emission spectrum for an F8BT : c-P6T blend for a collection wavelength of 1090 nm, plotted alongside the absorption intensity. (*Reproduced from ref. 3*)

7.2 (a) Energy levels of electrodes, F8BT and the porphyrin hexamers, P6 and c-P6T. OLEDs were fabricated with the structure ITO\PEDO:PSS(85 nm)\active layer(70 nm)\Ca(45 nm)\Al (150 nm). The device area was 3.5 mm2. (b) Electroluminescence spectrum of an F8BT:c-P6T OLED measured at 15.5 V. (c) Current density and radiance plotted against driving voltage for a typical F8BT:c-P6T device. The inset shows the external quantum efficiency (EQE) as a function of current density, where the EQE has been calculated for the full spectrum including 6 % of the emission that originates from the F8BT. (*Reproduced from ref. 3*)

7.3 Current density and light emission plotted against driving voltage for typical F8BT blended devices with P6 and P6-BP. b Electroluminescence spectra for the F8BT:P6 and F8BT:P6BP devices recorded at 16 V and 14 V respectively. The difference in spectral shape of the NIR component is ascribed to the insulating behavior of the BP around the P6 hexamer. c External quantum efficiency (EQE) plotted as a function of current density for the same devices as a. The EQE is calculated for the full range of wavelengths (including residual F8BT emission), though for P6BP, > 99% of the emission is from the hexamer. Devices were fabricated with the structure ITO\PEDOT:PSS (85 nm)\active layer (70 nm)\Ca (45 nm)\Al (150 nm), where the active layer was a blend of P6 or P6BP in F8BT (10% P6) spin-coated from a 2% solution in xylene. The device area was 3.5 mm2. (*Reproduced from ref. 3*)

List of Tables

3.1 Polarisation and dichroic ratios for films embedding PDV.Li or PDV.Li$\subset\beta$-CD.

3.2 Life time values (τ_1 and τ_2) used in the fit-curves and the Φ_{PL} value for solutions and films.

4.1 Lifetime values (τ_1, τ_2, τ_3) used in the fit-curves the temporal evolution of the PL (the relative contribute of each time constant is included in parentheses). We estimated an error of 5% on the measured value

4.2 Radiative (K_R) and non-radiative (K_{NR}) rates for PDV.Li$\subset\beta$-CD incorporated inside the PhC and in the reference sample. All rates were calculated using the model proposed in the text. We include an error of 10% on the calculated value.

7.1 Table of key optical parameters for the blends, and performance parameters of devices. [a] Defined as the voltage at which the current density reaches 5 x 10-5 mA/cm2 [b] Defined as the voltage at which light output reaches 5 x 10-5 mW/cm2 (~5 times the noise level) [c] EQE has been adjusted to account for an estimated 25% that is missed through lack of sensitivity of our detector in the region beyond 1100 nm. [d] Maximum radiance at current densities ≤ 160 mA/cm2. [e] Defined as the % of emission at wavelengths longer than 750 nm. [f] Peak emission in PL was at 920 nm for c-P6T, 873 nm for P6 and 882 nm for

P6BP. [g] Peak EL emission was at 960 nm for c-P6T, 883 nm for P6 and 883 nm for P6BP. (*Reproduced from ref. 3*)

List of Publications

1 *Photoinduced work function changes by isomerization of a densely packed azobenzene-based SAM on Au a joint experimental and theoretical study*

N. Crivillers, A. Liscio, F. Di Stasio, C. Van Dyck, S. Osella, D. Cornil, S. Mian, G. M. Lazzerini, O. Fenwick, E. Orgiu, F. Reinders, S. Braun, M. Fahlman, M. Mayor, J. Cornil, V. Palermo, F. Cacialli, P. Samorì, *Physical Chemistry Chemical Physics* **2011** *13*, 14302

2 *Highly Polarized Emission from Oriented Films Incorporating Water-Soluble Conjugated Polymers in a Polyvinyl Alcohol Matrix*

F. Di Stasio, P. Korniychuk, S. Brovelli, P. Uznanski, S. O. McDonnell, G. Winroth, H. L. Anderson, A. Tracz, F. Cacialli, *Advanced Materials* **2011** *23*, 1855-1859

3 *Linear and Cyclic Porphyrin Hexamers as Near-Infrared Emitters in Organic Light-Emitting Diodes*

O. Fenwick, J. K. Sprafke, J. Binas, D. V. Kondratuk, F. Di Stasio, H. L. Anderson, F. Cacialli, *Nano Letters* **2011** *11*, 2451-2456

4 *White Luminescence from Single-layer Devices of Nonresonant Polymer Blends*

S. Brovelli, H. Guan, G. Winroth, O. Fenwick, F. Di Stasio, R. Daik, W. J. Feast, F. Meinardi, F. Cacialli, *Applied Physics Letters* **2010** *96*, 213301

5 *Low-temperature treatment of semiconducting interlayers for high-efficiency light-emitting diodes based on a green-emitting polyfluorene derivative*

G. M. Lazzerini, F. Di Stasio, C. Flechon, D. Caruana, F. Cacialli, *Applied Physics Letters* **2011**, *99*, 243305 (2011)

6 *Radiative-rate modifications in a polystyrene photonic crystal self assembled with water-soluble conjugated polyrotaxanes*

F. Di Stasio, L. Berti, S. O. McDonnel, H. L. Anderson, D. Comoretto, F. Cacialli, **In preparation**

7 *Increasing the efficiency of green-emitting polyfluorene derivative light-emitting diodes with self-assembled monolayers functionalized anodes*

G. M. Lazzerini, F. Di Stasio, S. Mian, N. Crivillers, E. Orgiu, P. Samorì, F. Cacialli, **In preparation**

8 *Large Au work function shift caused by a novel polyfluorophenyl-terminated azobenzene self –assembled monolayers*

N. Crivillers, A. Liscio, G.M. Lazzerini, C. Van Dyck S. Osella, D. Cornil, S. Mian, F. Di Stasio, O. Fenwick E. Orgiu, F. Reinders, S. Braun, M. Fahlman, M. Mayor, J. Cornil, V. Palermo, F. Cacialli, P. Samorì, **In preparation**

9 *Scanning near-field optical lithography of PPV from its xanthate precursor*

F. Di Stasio, O. Fenwick, Y. Zhang, D. Taneja, J. Yu, P. Burns, F. Cacialli, **In preparation**

10 *Efficient red emission from copolymers based on F8BT and incorporating small concentrations of low-gap units*

O. Fenwick, T. Baig, S. Fusco, F. Di Stasio, T. Steckler, M. Anderson, F. Cacialli, **In preparation**

11 *Selenium-containing polymers as efficient near-infrared emitters in organic light-emitting diodes*

O. Fenwick, D. Breusov, C. Flechon, F. Di Stasio, S. Yilmaz, D. Caruana, D. Warner, S. Allard, U. Scherf, F. Cacialli, **In preparation**

12 *A blend of a small molecule and a polyfluorene for near-infrared organic light-emitting diodes*

O. Fenwick, J. Ellingsen, G. M. Lazzerini, F. Di Stasio, S. Yilmaz, S. Allard, U. Scherf, F. Cacialli, **In preparation**

INTRODUCTION

Conjugated polymers are interesting materials as they possess both, the electronic properties of semiconductors and the processing advantages and mechanical properties of plastic materials. Since the discovery of their electrical conductivity in 1977,[1] and their electroluminescence in 1990,[2-4] they have attracted increasing attention due to interesting optoelectronics properties and processing advantages for the realization of low cost light emitting diodes,[2] light emitting electrochemical cells,[5-7] photovoltaic devices[8, 9] and field-effect transistors.[10, 11]

Conducting polymers soluble in either water or in organic solvents have been synthesized, enabling processing of films, fibres and blends. Thanks to solution-based processing (i.e. drop-casting, spin-casting, layer-by-layer deposition, ink-jet printing ...) organic devices can be produced at very low costs, on very large area and on flexible substrates. From a more fundamental point of view, conjugated polymers offer many scientific challenges. These materials lie on the edge of organic chemistry and condensed matter physics, thus revealing new properties that can be understood only within the joint framework of these disciplines.

An important aspect in the field of conjugated polymers is the control of electronics interactions taking place between conjugated chains, namely interchain interactions.

Interchain interactions profoundly change the chemical, biological and physical properties of a huge variety of systems.[12] They influence phenomena as protein folding,[13] cellular organization[14] as well as the photophysics of organic semiconductors.[15-17] This phenomenon has been brought under increasing attention for polymer based devices and its control is needed for the optimal development and exploitation of conjugated systems.

Such a control can be achieved by using supramolecular architectures like, for example, conjugated polyrotaxanes,[18-20] which are conjugated oligomers threaded through α or β-cyclodextrin rings.[21, 22] They are a model system for studying the influence of interchain interactions on the electronic dynamics of organic semiconductors.[23, 24] Cyclodextrin insulation suppresses intermolecular interactions that control their photophysics, in particular regarding the tendency to form excimers (excited states delocalised on more than one molecule)[25, 26] which can red-shift and quench the luminescence[27] and are detrimental for colour purity.[28]

Another interesting aspect of supramolecular architectures is the possibility to use these structures to modify the surface properties of various materials. An example of this functionalization is self-assembled monolayers chemisorbed on specific metallic surfaces.[29, 30] In fact, self-assembled monolayers are of technological interest as they can be incorporated in devices like sensors[31] and organic thin-film transistors[32] to modify the metal/organic semiconductor interface properties, hence devices performance. Among various functions of self-assembled monolayers, in this dissertation I will show how they can be used to introduce an interfacial dipole at the metal/semiconductor interfaces to tune the work function of metallic contacts, thus optimizing the charge injection in light-emitting diodes, achieving a better balance between electrons and holes in the organic active layer, hence moving the recombination zone of charge carries.[33-35]

This dissertation is divided in 7 different chapters:

In chapter 1 and 2 I will briefly introduce the general properties of conjugated polymers and supramolecular architectures, their applications in light-emitting diodes and photovoltaic cells.

In chapter 3, the optical properties of stretch-aligned film embedding polyrotaxanes are discussed. In particular, I will discuss how the supramolecular architecture can influence the mechanical properties, i.e. the possibility of align the conjugated chains, of polyrotaxanes with respect to the unthreaded oligomers.

In chapter 4, the properties of polyrotaxanes self-assembled with a three dimensional photonic crystals are shown. The high photoluminescence quantum yield granted by the cyclodextrin insulation and the water solubility of polyrotaxanes can be exploited to obtain low lasing-threshold optically pumped lasers based on synthetic polystyrene opals.

In chapter 5 I will present how it is possible to improve the efficiency of polymeric light-emitting diodes using azo-benzene based self-assembled monolayers to lower the injection barrier at electrode/active layer interfaces.

In chapter 6, a low-temperature treatment of electron blocking layers shows how it is possible to obtain multilayer polymeric structures for light-emitting diodes without using a high-temperatures annealing step in the processing.

Finally, in chapter 7 I will show the properties of two types of porphyrin based systems: one linear and one cyclic. In particular, I will show how it is possible to increase their photoluminescence quantum yield by creating a supramolecular architecture of the linear hexamer and 4-benzyl pyridine, thus increasing the overall efficiency of near-infrared light-emitting diodes based on this class of materials.

References

[1] C. K. Chiang, C. R. Fincher, Y. W. Park, A. J. Heeger, H. Shirakawa, E. J. Louis, S. C. Gau, A. G. Macdiarmid, *Physical Review Letters* **1977**, *39*, 1098.

[2] J. H. Burroughes, D. D. C. Bradley, A. R. Brown, R. N. Marks, K. Mackay, R. H. Friend, P. L. Burns, A. B. Holmes, *Nature* **1990**, *347*, 539.

[3] R. H. Partridge, *Polymer* **1983**, *24*, 748.

[4] R. H. Partridge, *Polymer* **1983**, *24*, 755.

[5] J. Morgado, R. H. Friend, F. Cacialli, B. S. Chuah, S. C. Moratti, A. B. Holmes, *Journal of Applied Physics* **1999**, *86*, 6392.

[6] J. Morgado, F. Cacialli, R. H. Friend, B. S. Chuah, H. Rost, A. B. Holmes, *Macromolecules* **2001**, *34*, 3094.

[7] P. Matyba, K. Maturova, M. Kemerink, N. D. Robinson, L. Edman, *Nature Materials* **2009**, *8*, 672.

[8] B. Oregan, M. Gratzel, *Nature* **1991**, *353*, 737.

[9] H. Hoppe, D. A. M. Egbe, D. Muhlbacher, N. S. Sariciftci, *Journal of Materials Chemistry* **2004**, *14*, 3462.

[10] L. Burgi, T. J. Richards, R. H. Friend, H. Sirringhaus, *Journal of Applied Physics* **2003**, *94*, 6129.

[11] H. Sirringhaus, N. Tessler, R. H. Friend, *Scienze* **1998**, *280*, 1741.

[12] J. M. Lehn, *Reports on Progress in Physics* **2004**, *67*, 249.

[13] A. Ansari, S. V. Kuznetsov, *Journal of Physical Chemistry B* **2005**, *109*, 12982.

[14] P. O'Shea, *Biochemical Society Transactions* **2003**, *31*, 990.

[15] J. Gierschner, M. Ehni, H. J. Egelhaaf, B. Milian Medina, D. Beljonne, H. Benmansour, G. C. Bazan, *Journal of Chemical Physics* **2005**, *123*, 9.

[16] L. Poulsen, M. Jazdzyk, J. E. Communal, J. C. Sancho-Garcia, A. Mura, G. Bongiovanni, D. Beljonne, J. Cornil, M. Hanack, H. J. Egelhaaf, J. Gierschner, *Journal of the American Chemical Society* **2007**, *129*, 8585.

[17] J. C. Sancho-Garcia, L. Poulsen, J. Gierschner, R. Martinez-Alvarez, E. Hennebicq, M. Hanack, H. J. Egelhaaf, D. Oelkrug, D. Beljonne, J. L. Bredas, J. Cornil, *Advanced Materials* **2004**, *16*, 1193.

[18] F. Cacialli, J. S. Wilson, J. J. Michels, C. Daniel, C. Silva, R. H. Friend, N. Severin, P. Samori, J. P. Rabe, M. J. O'Connell, P. N. Taylor, H. L. Anderson, *Nature Materials* **2002**, *1*, 160.

[19] J. S. Wilson, M. J. Frampton, J. J. Michels, L. Sardone, G. Marletta, R. H. Friend, P. Samori, H. L. Anderson, F. Cacialli, *Advanced Materials* **2005**, *17*, 2659.

[20] M. J. Frampton, H. L. Anderson, *Angewandte Chemie-International Edition* **2007**, *46*, 1028.

[21] J. J. Michels, M. J. O'Connell, P. N. Taylor, J. S. Wilson, F. Cacialli, H. L. Anderson, *Chemistry-a European Journal* **2003**, *9*, 6167.

[22] P. N. Taylor, M. J. O'Connell, L. A. McNeill, M. J. Hall, R. T. Aplin, H. L. Anderson, *Angewandte Chemie-International Edition* **2000**, *39*, 3456.

[23] S. R. Forrest, *Nature* **2004**, *428*, 911.

[24] R. H. Friend, R. W. Gymer, A. B. Holmes, J. H. Burroughes, R. N. Marks, C. Taliani, D. D. C. Bradley, D. A. Dos Santos, J. L. Bredas, M. Logdlund, W. R. Salaneck, *Nature* **1999**, *397*, 121.

[25] S. A. Jenekhe, J. A. Osaheni, *Science* **1994**, *265*, 765.

[26] J. Kim, T. M. Swager, *Nature* **2001**, *411*, 1030.

[27] J. Cornil, A. J. Heeger, J. L. Bredas, *Chemical Physics Letters* **1997**, *272*, 463.

[28] I. D. W. Samuel, G. Rumbles, C. J. Collison, *Physical Review B* **1995**, *52*, 11573.

[29] J. C. Love, L. A. Estroff, J. K. Kriebel, R. G. Nuzzo, G. M. Whitesides, *Chemical Reviews* **2005**, *105*, 1103.

[30] N. Crivillers, A. Liscio, F. Di Stasio, C. Van Dyck, S. Osella, D. Cornil, S. Mian, G. M. Lazzerini, O. Fenwick, E. Orgiu, F. Reinders, S. Braun, M. Fahlman, M. Mayor, J. Cornil, V. Palermo, F. Cacialli, P. Samori, *Physical Chemistry Chemical Physics*, **2011** *13*, 14302.

[31] D. Samanta, A. Sarkar, *Chemical Society Reviews*, **2011** *40*, 2567.

[32] S. A. DiBenedetto, A. Facchetti, M. A. Ratner, T. J. Marks, *Advanced Materials* **2009**, *21*, 1407.

[33] X. Cheng, Y.-Y. Noh, J. Wang, M. Tello, J. Frisch, R.-P. Blum, A. Vollmer, J. P. Rabe, N. Koch, H. Sirringhaus, *Advanced Functional Materials* **2009**, *19*, 2407.

[34] K. Asadi, F. Gholamrezaie, E. C. P. Smits, P. W. M. Blom, B. de Boer, *Journal of Materials Chemistry* **2007**, *17*, 1947.

[35] P. Stoliar, R. Kshirsagar, M. Massi, P. Annibale, C. Albonetti, D. M. de Leeuw, F. Biscarini, *Journal of the American Chemical Society* **2007**, *129*, 6477.

1. Conjugated polymers

1.1. Electronic properties

As I briefly described in the introduction, after the discovery of the electrical conductivity of doped polyacetylene in 1977 by MacDiarmid, Shirakawa and Heeger,[1, 2] conjugated systems have attracted an increasing attention from both the scientific community and industry.

The electrical properties of conjugated polymers are directly connected to the electronic configuration of the carbon atom: $1s^2\ 2s^2\ 2p^2$.[3] From this electronic configuration only 2 electrons in the p orbital ($2p^2$) can be used to form bonds with another atom. Nevertheless, carbon atoms have four valence electrons. This can be explained by taking in consideration the hybridisation between atomic orbitals. In fact, this process leads to more stable chemical bonds which better match the spatial geometry of carbon based molecules.[3, 4] Three different types of hybridisation are possible: sp^3, sp^2 and sp^1 (Fig. 1.1).

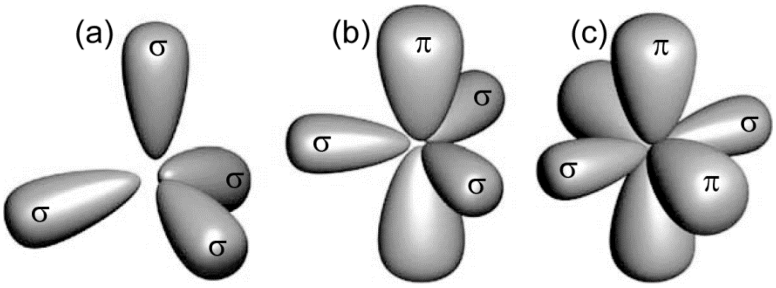

Figure 1.1 (a) In the sp^3 hybridisation 4 σ bonds are formed, therefore it possesses a tetrahedral structure with an angle of 109.5° between the bonding orbitals. (b) The sp^2 hybridisation shows a trigonal-planar geometry with an angle of 120° between the 3 σ bonds. (c) The sp hybridisation has only 2 σ bonds, hence a planar geometry with an angle of 180° between the bonding orbitals.

In saturated polymers, the four valence electrons of the carbon atoms are sp^3 hybridised and every carbon is bonded to four neighbouring atoms, therefore molecular orbitals are fully saturated. The classical example is poly(ethylene), in which each carbon atom is σ-bonded to two neighbouring carbons and two hydrogen atoms. Saturated polymers are insulators because to promote an electron from a bonding σ-orbital to an anti-bonding σ*-orbital requires an energy $E = 8$ eV or more. Furthermore, excitation of electrons into the σ*-anti bonding-orbital usually destroy the polymer chain since σ-orbitals are essentials for holding the carbon atoms together.

Conjugated polymers differ from saturated polymers in the sp^2 hybridisation; each carbon is bonded to only three other atoms. The simplest conjugated polymer is the polyacetylene, i.e. a linear chain of CH units bonded by single (σ) and double (σ and π) covalent bonds (Fig. 1.2).

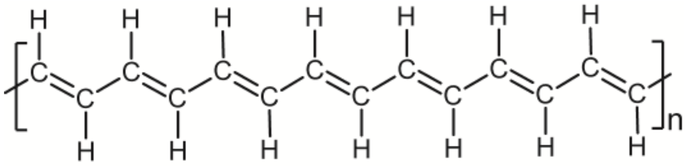

Figure 1.2 Chemical structure of *trans*-polyacetylene

This alternation creates delocalised states along the chain due to the hybridisation of the sp^2 molecular orbital. Only three electrons of each carbon atom reside in the three σ-bonding molecular orbital, forming covalent bonds with other atoms. The remaining unpaired valence electron resides in the delocalised $2p_z$ orbital with its charge density lobes perpendicular to the plane defined by the σ-bonds (Fig. 1.1b). For a simple C_2H_4 molecule, the p_z orbitals of neighbouring carbons overlap to form new and extended orbitals with an energy splitting, namely π-bonds and π*-anti-bonds (Fig. 1.3). The energy splitting between these new orbitals depends on the energy and overlap of the original orbitals, in general, stronger is the overlap, larger is the splitting.[3, 5] The bonding π–orbital is occupied (in the ground state, highest occupied molecular orbital, HOMO), instead the anti-bonding π*-orbital is unoccupied (lowest unoccupied molecular orbital, LUMO).

By adding more CH_2 units to the C_2H_4 molecule more bonding and anti-bonding orbitals are added causing a degeneration of the energy levels. If the number of carbon atoms is infinite we create two different energy bands. For real polymers, the number of carbon atoms is clearly not infinite, therefore is more correct to refer to the LUMO and HOMO as quasi-continuous energy bands.[3, 5] More interestingly, to promote an electron from the π-orbital (HOMO) to the π^*-orbital only 2-3 eV are necessary and this process does not compromise the integrity of the polymer chain.[6]

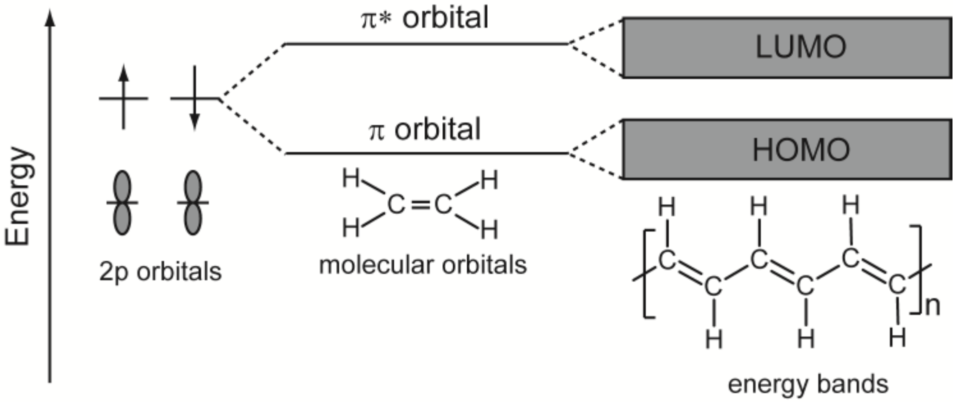

Figure 1.3 Scheme of the energy splitting of 2p orbitals into 2 different molecular orbitals: a bonding π-orbital and an anti-bonding π^*-orbital. Adding other CH_2 units (increasing the conjugation length) leads to an increase in the degeneration of energy levels, thus forming two different energy quasi-bands, namely the highest occupied molecular orbital (HOMO) and the lowest unoccupied molecular orbital (LUMO).

In general, the electronic structure of conjugated polymers has been theoretically studied using many different models; the most frequently used is the Tight-binding model (Linear combination of atomic orbitals, LCAO).[6, 7]

Both σ and π are directional intramolecular covalent bonds. In the solid state different polymeric chains interact through Van der Waals forces resulting in disordered solids in which molecules have no long range order. Furthermore, the intermolecular wavefunction overlaps are very small. Therefore, as stated previously, the electronic behaviour of conjugated polymers can be described approximately by considering their molecular energy levels.[8]

1.1.1. Semiconducting behaviour

In the very first theoretical studies, conjugated polymers were expected to show a metallic behaviour instead of a semiconducting one. In fact, if we consider once more the polyacetylene chain, we can expect that a complete delocalisation of the electron wavefunction on the entire polymer would lead to a minimisation of the molecular energy (like for Benzene). This would generate a constant distance between carbon atoms (Fig. 1.4a). Therefore, we can consider this chain as a crystal of N atoms with a periodicity a. Since the volume of 1 electronic state in the k-space is $V = 2\pi/Na$, and we can accommodate 2N electrons in the volume of the Brillouin zone ($V_{BZ} = 2\pi/a$), by calculating the ratio $V_{BZ}/V = 2(2\pi/a)/(2\pi/Na) = 2N$, we can expect an half-filled band (only N electrons are available), i.e. a metallic behaviour.

However, distortion originating from alternating nuclei displacement (Peierls distortion or dimerisation) produces short (double) and long (single) bonds lowering the symmetry of the system (Fig. 4b). Thanks to this distortion, the molecular energy of polyacetylene is decreased further with respect to the complete delocalization. By increasing the periodicity to 2a we obtain: $V_{BZ}/V = 2(\pi/a)/(2\pi/Na) = N$, hence, a fully occupied band. the Peierls distortion has a similar effect to a scattering potential inducing a separation of the bands at the edge of the Brillouin zone, leading to a semiconducting behavior.[7]

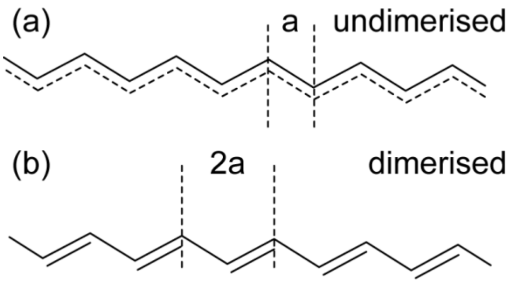

Figure 1.4 (a) an undimerised polyacetylene chain (complete delocalisation of the electron wavefunction). (b) Peierls dimerisation of polyacetylene

The dimerisation of polyacetylene can take place with two different conjugations, i.e. it is possible to interchange single and double bonds. Both dimers possess the same energy; hence the ground state is degenerate.[7, 9, 10] This phenomenon does not take place for conjugated polymers having benzene rings since one of the two possible "configurations" has lower energy than the other one.

1.1.2. Polarons

Photoexcitations in conjugated polymers do not create free-charges. Instead, the structural relaxation of the conjugated system after photoexcitation cause the self-localization of them.[5, 6] These non-linear excitations are: solitons, polarons and bipolarons (Fig. 1.5)

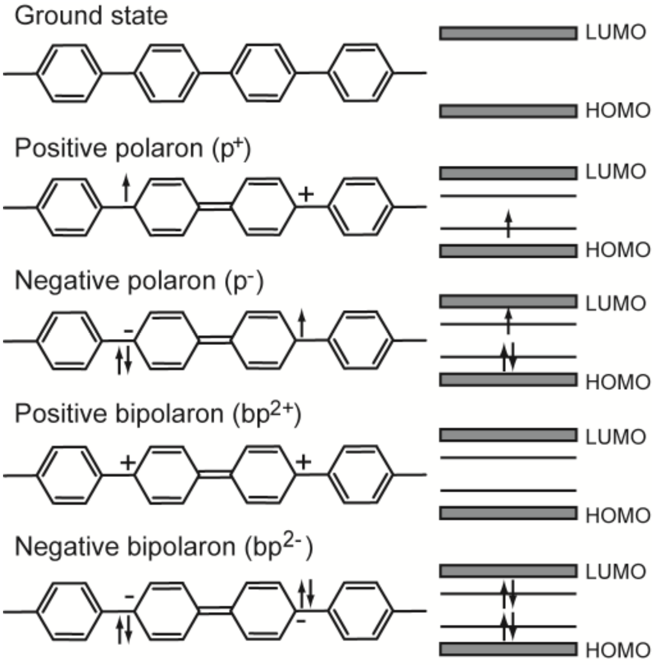

Figure 1.5 Positive and negative polarons and bipolarons in poly(*para*-phenylene). Spins and charges are indicated on the conjugated chain and the corresponding energy diagram is represented on the right.

Solitons are present only in degenerate systems like polyacetylene, while polarons and bipolarons are common in non-degenerate systems (for example poly(*para*-phenylene), Fig. 1.5). They are Fermion quasi-particles consisting of a charge and a polarization field. This field changes the local nuclear geometry creating as a potential well, thus causing the self-localization of the charge carrier. This phenomenon is one of the main limiting factor of charge carriers mobility in organic semiconductors, and causes the appearance of sub-gap energy levels.

Polarons possess a charge $Q = \pm e$ and spin $s = ½$ while bipolarons have $Q = \pm 2e$ and spin $s = 0$.

1.1.3. Excitons

When an excited state is created on a conjugated chain, we must consider two different phenomena:

- The formation of excited species leads to structural modifications of the conjugated chain (polarons and bipolarons).
- Conjugated polymers possess a low dielectric constant (ε_R ~1.8 - 6), therefore electrons-holes, electrons-electrons and holes-holes Coulombic interactions must contribute to the final properties of the excited state.

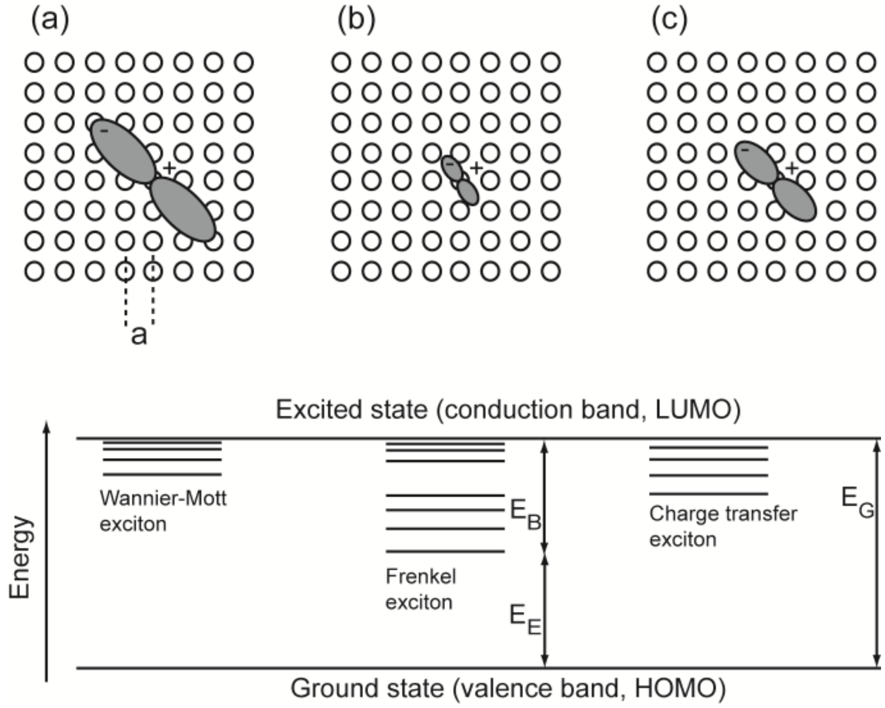

Figure 1.6 (Top) Schematic representation of a Wannier-Mott exciton (a), Frenkel exciton (b) and a charge-transfer exciton (c). (Bottom) Scheme of the energy levels of the three different types of excitons

The binding energy of an exciton (Fig. 1.6, E_B) is defined as the difference between the energy gap (E_G) and the exciton energy (E_E). Excitons can be classified in three different types:

- Wannier-Mott excitons (Fig. 1.6a): named after Gregory Wannier and Nevill Francis Mott, they possess a radius (i.e. distance between electrons and holes) bigger than the lattice parameter. Their binding energy is <0.1 eV, therefore their energy is lying near to the excited state energy (conductivity band). They are usually found in inorganic semiconductors where the large dielectric constant provides an efficient electric field screening.

- Frenkel excitons (Fig. 1.6b): named after Yakov Frenkel, their radius is comparable to the lattice parameter. Their binding energy is around 0.2-1 eV, i. e. Their energy lies inside the energy gap. They are usually found in insulating materials or in organic semiconductors[11] where the dielectric constant is small; hence electric field screening is small.
- Charge-transfer excitons (Fig. 1.6c): they represent an intermediate condition between the Wannier-Mott and the Frenkel excitons. They can be found in organic semiconductors as well.[12]

In general, excitons are neutral, but if the electron and holes are separated they are able to move freely and independently obtaining two free charge carriers. Furthermore, the total quantum spin number S (S = 2s+1) differentiate between singlet (S = 1) and triplet (S = 3) excitons. In conjugated polymers triplet and singlet states coexist/compete determining the fluorescence and phosphorescence properties of the material.

1.2. Optical properties

1.2.1. Photoluminescence properties

Thanks to the versatility of organic chemistry, during the last 20 years many different conjugated polymers photoluminescent in the visible (390 nm > λ_{VIS} < 750 nm) or in the near- infrared range (800 nm > λ_{PL} > 1000 nm) have being synthesised.

Photoluminescence is the emission of light occurring from the decay of an electronically excited state (due to absorption of light) to the ground state. It can be divided in two different processes: fluorescence (emission from singlet excited states) and phosphorescence (emission from triplet excited states).[13] For fluorescence, the electron in the excited state has its spin paired (opposite) to the second electron in the ground state, therefore the recombination is spin-allowed causing a short fluorescence life time (from tens of pico-seconds to tens of nano-second).

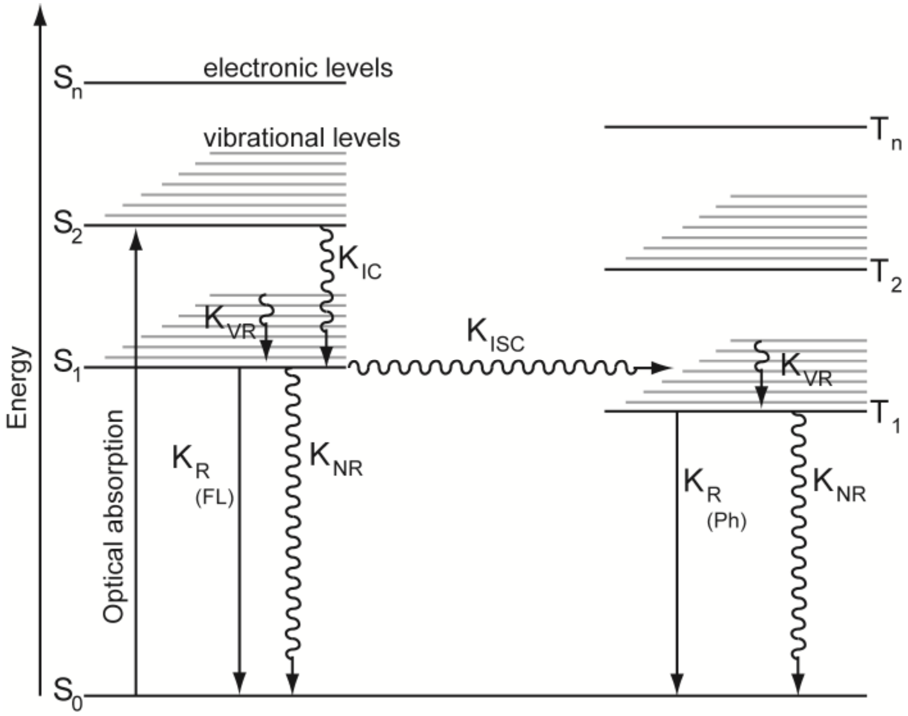

Figure 1.7 Jablonski diagram illustrating the different electronic and vibrational levels in an organic molecule and, the different optical transitions (with their rates K): fluorescence ($K_{R(FL)}$), phosphorescence ($K_{R(Ph)}$), non radiative decay (K_{NR}), internal conversion (K_{IC}), vibrational relaxation (K_{VR}) and intersystem crossing (K_{ISC}).

Instead, for phosphorescence both electrons possess the same spin orientation making the transition to the ground state forbidden, so that phosphorescence life time is tipically in the range of milliseconds.

During this long life time, the exciton is able to diffuse to trap states or bimolecular reactions with other singlet excitons, triplet excitons or charge carriers, preventing the observation of phosphorescence at room temperature, therefore making fluorescence more common in conjugated polymers.[3, 13]

The different energy levels of a molecule and their transitions can be described by the Jablonski diagram (Fig. 1.7).[3, 13] Fluorescence and phosphorescence are both radiative transitions which must compete with non-radiative ones. In fact, many non-radiative transitions decrease the overall efficiency of the light emission process.

Vibrational relaxation (Fig. 1.7, K_{VR}) causes a dissipation of energy from the molecule to its surrounding environment and possess a high rate ($K_{VR} \sim 10^{12}$ s^{-1})and therefore a high yield.[3] As a consequence of this, the emission of photons takes place from the lowest excited state of a given multiplicity (Kasha’s rule, named after Michael Kasha).[14]

Internal conversion (Fig. 1.7, K_{IC}) is a non-radiative process similar to vibrational relaxation. It occurs when a vibrational level of an electronic excited state couples to a iso-energetic vibrational level of a lower electronic state of the same multiplicity.[3]

Intersystem crossing (Fig. 1.7, K_{ISC}) is a spin conversion process to the triplet excited state. This is usually the only way to populate the triplet excited state and to increase the yield of ISC a large spin-orbit coupling must be introduced in the molecule by inserting heavy atoms like bromine and iodine.[13]

Electronic transitions are instantaneous when compared to the time scale of nuclear motions (Born-Oppenheimer approximation).[3] Therefore, electronic transitions between vibrational levels corresponding to minimal change in the nuclear coordinates are favoured. This principle is known as the Frank-Condom principle and is applied to both the absorption and emission of photons. As a consequence, the emission spectrum is red-shifted with respect to the absorption one (Stoke shift).[3, 13]

1.2.2. Photoluminescence quenching and aggregates

The environment surrounding a chromophore is of primary importance, since it can create other decay channels inducing a decrease of the photoluminescence intensity (i.e. the photoluminescence quantum yield). This phenomenon is generally called photoluminescence quenching, and it can be caused by a variety of different processes.

Two general types of quenching are collisional (dynamic), and static quenching. They can be caused, for example, by impurities left by the synthesis of the conjugated system. In both cases, the chromophore must come into contact with the quencher.

Collisional quenching takes place when a chromophore in the excited state comes into contact with a quencher. This process needs the quencher to diffuse toward the chromophore while the latter is still in its excited state. As an example, we can use molecular oxygen. In fact, O_2 is one of the most well known and studied quencher, and the most likely mechanism is that the oxygen causes intersystem crossing in the chromophore diminishing the fluorescence quantum yield inducing phosphorescence, which is usually absent at room temperature, decreasing the overall photoluminescence.[13] For this very reason most of the photoluminescence quantum yield measurements are performed in N_2 atmosphere.

Static quenching involves instead the formation of non-radiative complexes in the ground state between the chromophore and the quencher. In this case, the quenching is not dynamic and it doesn’t depend on the life time of the excited state as for collisional quenching. Therefore, we can imagine the quencher as a chemical compound added directly to the chromophore solution and so, the quenching intensity depends directly from the amount of quencher in the environment surrounding the chromophore.

Both static and dynamic quenching requires the diffusion of the quencher toward the chromophore, i.e. they are common in solutions or liquid phases. In solid state, both these types of quenching are still present but the diffusion range is much lower than in a solution. Nevertheless, the effect of molecular aggregation (i.e. concentration quenching) is usually much stronger than in solution.

Molecular aggregation is caused by intermolecular Van Der Waals-like forces between the molecules and they exhibit distinct changes in the absorption and emission spectrum with respect to the monomer. This process can lead to the formation of different aggregates depending on the relative orientation of the monomers and their transition moment. It is possible to distinguish between two cases: co-facial aggregation of monomers leading to the formation of H-aggregates, and head-to-tail aggregation leading to the formation of J-aggregates.

H-aggregates are much more common than J- ones, since the latter is present almost exclusively in cyanines based molecules and dyes.[15] H-aggregates are extremely detrimental for the photoluminescence quantum yield since they lead to unfavourable level splitting. Furthermore, their oscillator strength resides mainly at the top of the exciton band, causing a blue-shift of the optical absorption and intraband relaxation of the excited state results in low or absent photoluminescence.[15] On the contrary, J-aggregates present a red-shift of the optical absorption and high photoluminescence quantum yield.

H-aggregates are commonly found in conjugated polymer thin-films, causing an overall decrease of the photoluminescence quantum yield and the introduction of a new de-excitation pathway usually characterised by a longer life time than that o the singlet exciton. As I will discuss in the following chapters a possible way to avoid the formation of this aggregates is to prevent the close-packing of the chromophore, like, for example, in conjugated polyrotaxanes.

1.2.3. Resonance energy transfer

Resonance energy transfer (RET, Fig 1.8) is an interaction that occurs over longer distances than static or collisional quenching. RET can be classified as a quenching process since it decreases the photoluminescence intensity of a donor and transfer the energy to an acceptor.[13]

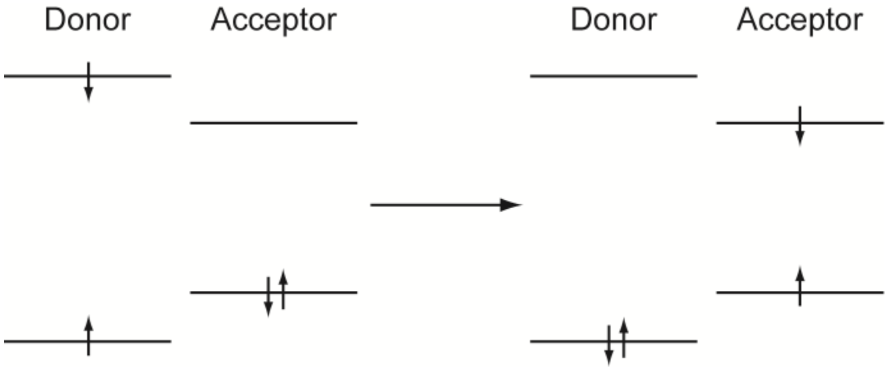

Figure 1.8 Schematic representation of the energy transfer process between a donor and an acceptor molecule.

There are three different types of RET:

- Trivial transfer: the donor molecule emits a photon that is absorbed by the acceptor:

$$D^* \rightarrow D + h\nu_1 ;\, h\nu_1 + A \rightarrow A^*;\, A^* \rightarrow A + h\nu_2$$

  This energy transfer process can be extremely long range and its rate mainly depend on spectral overlap between the photoluminescence of the donor the optical absorption of the acceptor, their photoluminescence quantum yield and extinction coefficient respectively and their concentration.

- Forster transfer: only for spin-allowed transitions (singlets), this energy transfer process can be modelled as the interaction between two point dipoles. Once again, its efficiency mainly depends on the spectral overlap between the donor and acceptor, and the distance (R) between them (~1/R^6). Typically, in conjugated polymers the range of the Forster transfer (Foster radius) is of the order of 10 nm or less.
- Dexter transfer: it is an electron exchange interaction. The electron in the excited state from the donor is exchanged for a ground-state electron from the acceptor. Dexter transfer is in independent from the spin of the electrons involved in the interaction; therefore it occurs both for triplets and singlets. Due to its electron exchange nature, Dexter transfer is strongly dependant on the distance between the donor and acceptor and compare to the Forster transfer (tunnelling process VS antenna effect).

1.3. Optoelectronics conjugated polymers devices

In this paragraph I will briefly described the main applications of conjugated polymers in the optoelectronic field.

1.3.1. Light-emitting diodes

Polymer light-emitting diodes (PLEDs) have been widely studied and investigated during the last 30 years both in academia and industry. The typical PLED consist of a thin-film of polymer sandwiched between a cathode and a transparent anode.[16-23]

The cost of fabrication of such PLEDs (as well as photovoltaic cells and transistors) can be much lower than inorganic ones, and processing over large areas for lighting applications has captured the interest of many companies. For PLEDs to be viable for displays and lighting sources, device lifetimes of many 10,000s of hours must be achieved. This target has been reached for red and green emitting PLEDs, whilst blue-emitting polymers are still the focus of much research.

The fabrication process of a PLEDs starts with the deposition on a substrate of a thin-film of Indium-Tin-Oxide (ITO).[21-23] Afterward, the ITO is usually treated with O_2 plasma to increase its work function and clean it from impurities.[24, 25] On top of the ITO film a layer based of poly(3,4-ethylene dioxythiophene):poly(styrene sulfonic acid) (PEDOT:PSS) is spin-coated.[20, 26-29] PEDOT:PSS is used as a hole-injection layer, due to the doping level and relatively high work function, and still being relatively transparent in visible light. The ITO and PEDOT:PSS form the anode of the PLED.

On top of the anode, the active material is spin-coated. Many different types of materials have been investigated, but recently research has focused on polyfluorene based polymers,[30-33] due to their high photoluminescence quantum yield, electron mobility and ease of injection, and finally for their chemical stability. The active (light emitting) part of a PLED usually is not made by a single layer/material but more complex structures such multilayers[17, 34, 35] or blends[36, 37] have been developed. Of particular interest are multilayer PLEDs, in fact by depositing different layers it is possible to tune the number of holes or electrons in the active layer,[8, 38] therefore moving where the recombination between holes and electrons take place (recombination zone, See Chapter 6).

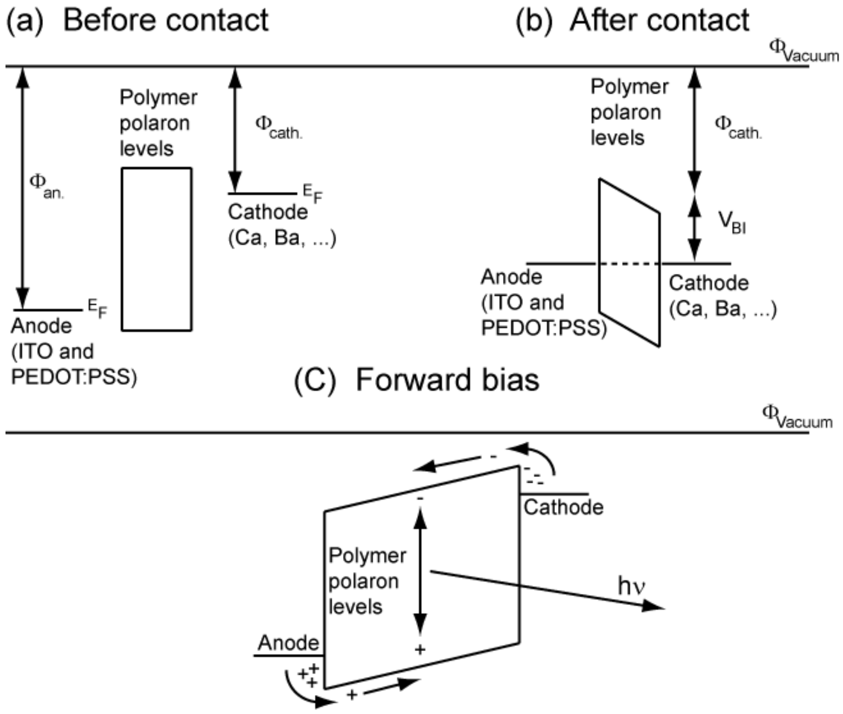

Figure 1.9 (a) Anode and Cathode work functions ($\Phi_{an.}$ and $\Phi_{cath.}$ respectively) and Fermi's energies (E_f) before contact with the polymer layer. (b) After contact, the chemical potential is equilibrated through the heterojunction via electron transfer from the cathode to the anode, creating a potential in the polymer layer (built-in potential, V_{BI}). (c) in forward bias electrons and holes are injected into the polymer film through an energy barrier. When a hole and electron are in close proximity they form an exciton that can radiatively decay.

The top electrode (cathode) is usually a thermally evaporated metallic thin-film. As a requirement, the metal use must possess a low work function.[25, 39, 40] Metal as Ba or Ca are commonly used, but due to their high chemical reactivity (in particular with O_2) a conductive/protective layer is necessary. Therefore, a thick Al film is evaporated on top of them.

The operation of a PLED device is shown in Figure 1.9. Electrons and holes must be injected into the polymeric layer from the cathode and anode respectively. To achieve this, a bias is applied in the direction that allows bipolar injection, i.e. a forward bias in contrast to a reverse one that applies a negative (positive) potential to the anode (cathode). The injected charges (polarons) must then migrate through the device under the applied bias until they get close to a polaron possessing an opposite charge, .i.e. forming an exciton . At this point, the exciton may then decay either radiatively or non-radiatively.

In general, the light emission process can be divided in 4 different parts: injection of charges, diffusion of charges towards the opposite electrode, exciton formation, Radiative decay of the exciton.

The efficiency of PLEDs is determined by several factors (Eq. 1.1):

$$External\ quantum\ efficiency = \gamma \phi_{PL} r_{st} n_{ext} \qquad (1.1)$$

γ represent the exciton formation efficiency per charge injected, Φ_{PL} is the photoluminescence quantum yield, r_{st} is the ratio between singlet and triplet excitons formed in the device (i.e. the amount of excitons that can radiatively decay), and n_{ext} is the optical outcoupling of the emitted light (i.e. the amount of light able to exit the device). In general for a standard device:[8]

- $50\% < \gamma < 100\%$,
- $25\% < r_{s\text{-}t} < 90\%$,
- $20\% < n_{ext} < 40\%$

Therefore, the external quantum efficiency of PLEDs ranges from ~ 2% to ~ 30% of the Φ_{PL} of the light-emitting polymer.

1.3.2. Photovoltaic cells

The first working photovoltaic cell (PV) based on conjugated polymers was presented by Tang et al in 1986.[41] In this first experiment, a bi-layer structure was used achieving an efficiency of 1%.

Photovoltaic cells (PVs) are prepared in the same way as PLEDs. The main difference resides in the active layer which is usually a blend of a donor and acceptor polymer (type II heterojunction). PVs, as PLEDs, have attracted much attention for the low cost of fabrication and high optical absorption coefficients of conjugated polymers compared to inorganic materials used in commercially available PVs.

In general, PVs operate in the reverse mode of an LED. Firstly an incident photon is absorbed exciting an electron from the ground state to the excited state, forming an exciton. The exciton must be split under the influence of a reverse bias and the positively and negatively charged polarons transported to the anode and cathode respectively. By comparison to inorganic materials, exciton binding energies are much higher in conjugated polymers (see Chapter 1.1.3) and a large internal field is often required to effectively split the charges. To solve this issue many different structures have been developed, like bilayer,[42] multilayers[43-45] and bulk heterojunctions,[46] so that the exciton can be separated by the built in field caused by the energy level offset between the donor and the acceptor.

Bulk heterojunction PVs have shown the best power conversion efficiencies.[46-48] in the polymer layer, excitons can only diffuse a certain distance before decaying (exciton diffusion range), this implies that the mean distance that the exciton must travel to a heterojunction in order to dissociate must be shorter than the exciton diffusion range. Using a bulk heterojunction, small domains are created while maintaining a good optical absorption, increasing the surface of the heterojunction interface as well.

Of the 3 different types of heterojunction, type II heterojunction has given the best results so far, since the hole of an exciton generated in the donor does not travel to the electron acceptor, therefore favoring the splitting of the exciton under the applied reverse bias.

References

[1] C. K. Chiang, C. R. Fincher, Y. W. Park, A. J. Heeger, H. Shirakawa, E. J. Louis, S. C. Gau, A. G. Macdiarmid, *Physical Review Letters* **1977**, *39*, 1098.

[2] H. Shirakawa, E. J. Louis, A. G. Macdiarmid, C. K. Chiang, A. J. Heeger, *Journal of the Chemical Society-Chemical Communications* **1977**, 578.

[3] S. Schols, *Device architecture and materials for organic light-emitting devices*, Springer Science+Business Media, New York **2011**.

[4] G. Winroth, *Physical characterisation of interfaces in organic devices*, PhD thesis, London **2010**.

[5] M. Pope, C. E. Swemberg, *Electronic Processes in Organic Crystals and Polymers*, Oxford Science Publications, Oxford **1999**.

[6] W. Barford, *Electronic and optical properties of conjugated polymers*, Clarendon press, Oxford **2005**.

[7] A. J. Heeger, S. Kivelson, J. R. Schrieffer, W. P. Su, *Reviews of Modern Physics* **1988**, *60*, 781.

[8] F. So, *Materials, processing, devices and applications*, CRC press, **2010**.

[9] W. P. Su, J. R. Schrieffer, A. J. Heeger, *Physical Review B* **1980**, *22*, 2099.

[10] W. P. Su, J. R. Schrieffer, A. J. Heeger, *Physical Review Letters* **1979**, *42*, 1698.

[11] P. A. Cox, *The electronic structure and chemistry of solids*, Oxford University Press, New York **1987**.

[12] E. I. Haskal, *Physical Review B* **1995**, *51*, 4449.

[13] J. R. Lakowicz, *Principles of Fluorescence Spectroscopy*, Springer Science+Business Media, New York **2006**.

[14] M. Kasha, *Discussions of the Faraday Society* **1950**, *9*, 14.

[15] S. Siddiqui, F. C. Spano, *Chemical Physics Letters* **1999**, *308*, 99.

[16] J. H. Burroughes, D. D. C. Bradley, A. R. Brown, R. N. Marks, K. Mackay, R. H. Friend, P. L. Burns, A. B. Holmes, *Nature* **1990**, *347*, 539.

[17] N. C. Greenham, S. C. Moratti, D. D. C. Bradley, R. H. Friend, A. B. Holmes, *Nature* **1993**, *365*, 628.

[18] R. H. Friend, R. W. Gymer, A. B. Holmes, J. H. Burroughes, R. N. Marks, C. Taliani, D. D. C. Bradley, D. A. Dos Santos, J. L. Bredas, M. Logdlund, W. R. Salaneck, *Nature* **1999**, *397*, 121.

[19] J. Morgado, F. Cacialli, R. H. Friend, B. S. Chuah, H. Rost, A. B. Holmes, *Macromolecules* **2001**, *34*, 3094.

[20] G. Winroth, G. Latini, D. Credgington, L.-Y. Wong, L.-L. Chua, P. K. H. Ho, F. Cacialli, *Applied Physics Letters* **2008**, *92*.

[21] J. S. Kim, F. Cacialli, R. Friend, *Thin Solid Films* **2003**, *445*, 358.

[22] J. S. Kim, F. Cacialli, M. Granström, R. H. Friend, N. Johansson, W. R. Salaneck, R. Daik, W. J. Feast, *Synthetic Metals* **1999**, *101*, 111.

[23] J. S. Kim, M. Granstrom, R. H. Friend, N. Johansson, W. R. Salaneck, R. Daik, W. J. Feast, F. Cacialli, *Journal of Applied Physics* **1998**, *84*, 6859.

[24] T. M. Brown, F. Cacialli, *Journal of Polymer Science Part B-Polymer Physics* **2003**, *41*, 2649.

[25] T. M. Brown, G. M. Lazzerini, L. J. Parrott, V. Bodrozic, L. Burgi, F. Cacialli, *Organic Electronics* **2011**, *12*, 623.

[26] M. Dobbelin, R. Marcilla, C. Tollan, J. A. Pomposo, J. R. Sarasua, D. Mecerreyes, *Journal of Materials Chemistry* **2008**, *18*, 5354.

[27] M. Dobbelin, C. Pozo-Gonzalo, R. Marcilla, R. Blanco, J. L. Segura, J. A. Pomposo, D. Mecerreyes, *Journal of Polymer Science Part a-Polymer Chemistry* **2009**, *47*, 3010.

[28] B. L. Groenendaal, F. Jonas, D. Freitag, H. Pielartzik, J. R. Reynolds, *Advanced Materials* **2000**, *12*, 481.

[29] S. Kirchmeyer, K. Reuter, *Journal of Materials Chemistry* **2005**, *15*, 2338.

[30] V. Bodrozic, T. M. Brown, S. Mian, D. Caruana, M. Roberts, N. Phillips, J. J. Halls, I. Grizzi, J. H. Burroughes, F. Cacialli, *Advanced Materials* **2008**, *20*, 2410.

[31] S. A. Choulis, V. E. Choong, A. Patwardhan, M. K. Mathai, F. So, *Advanced Functional Materials* **2006**, *16*, 1075.

[32] M. Grell, W. Knoll, D. Lupo, A. Meisel, T. Miteva, D. Neher, H. G. Nothofer, U. Scherf, A. Yasuda, *Advanced Materials* **1999**, *11*, 671.

[33] Z. J. Zheng, K. H. Yim, M. S. M. Saifullah, M. E. Welland, R. H. Friend, J. S. Kim, W. T. S. Huck, *Nano Letters* **2007**, *7*, 987.

[34] A. C. Morteani, A. S. Dhoot, J. S. Kim, C. Silva, N. C. Greenham, C. Murphy, E. Moons, S. Cina, J. H. Burroughes, R. H. Friend, *Advanced Materials* **2003**, *15*, 1708.

[35] A. C. Morteani, R. H. Friend, C. Silva, *Chemical Physics Letters* **2004**, *391,* 81.

[36] S. Brovelli, H. Guan, G. Winroth, O. Fenwick, F. Di Stasio, R. Daik, W. J. Feast, F. Meinardi, F. Cacialli, *Applied Physics Letters* **2010**, *96,* 213301

[37] S. Brovelli, F. Meinardi, G. Winroth, O. Fenwick, G. Sforazzini, M. J. Frampton, L. Zalewski, J. A. Levitt, F. Marinello, P. Schiavuta, K. Suhling, H. L. Anderson, F. Cacialli, *Advanced Functional Materials* **2010**, *20*, 272.

[38] A. C. Morteani, R. H. Friend, C. Silva, *Organic Light Emitting Devices: Synthesis, Properties and Applications*, WILEY-VCH, Winheim, **2006**

[39] T. M. Brown, R. H. Friend, I. S. Millard, D. J. Lacey, T. Butler, J. H. Burroughes, F. Cacialli, *Journal of Applied Physics* **2003**, *93*, 6159.

[40] T. M. Brown, J. S. Kim, R. H. Friend, F. Cacialli, R. Daik, W. J. Feast, *Applied Physics Letters* **1999**, *75*, 1679.

[41] C. W. Tang, *Applied Physics Letters* **1986**, *48*, 183.

[42] N. S. Sariciftci, D. Braun, C. Zhang, V. I. Srdanov, A. J. Heeger, G. Stucky, F. Wudl, *Applied Physics Letters* **1993**, *62*, 585.

[43] A. Hadipour, B. de Boer, J. Wildeman, F. B. Kooistra, J. C. Hummelen, M. G. R. Turbiez, M. M. Wienk, R. A. J. Janssen, P. W. M. Blom, *Advanced Functional Materials* **2006**, *16,* 1897.

[44] V. D. Mihailetchi, H. X. Xie, B. de Boer, L. J. A. Koster, P. W. M. Blom, *Advanced Functional Materials* **2006**, *16*, 699.

[45] Z. Q. Liang, K. L. Dzienis, J. Xu, Q. Wang, *Advanced Functional Materials* **2006**, *16*, 542.

[46] G. Yu, J. Gao, J. C. Hummelen, F. Wudl, A. J. Heeger, *Science* **1995**, *270*, 1789.

[47] G. Yu, A. J. Heeger, *Journal of Applied Physics* **1995**, *78*, 4510.

[48] J. J. M. Halls, C. A. Walsh, N. C. Greenham, E. A. Marseglia, R. H. Friend, S. C. Moratti, A. B. Holmes, *Nature* **1995**, *376*, 498.

2. Supramolecular architectures

In this chapter I will present a short summary of the properties of two different types of supramolecular architectures: conjugated polyrotaxanes and self-assembled monolayers.

2.1. Conjugated polyrotaxanes

Conjugated polyrotaxanes[1-5] are organic semiconductors consisting of a conjugated moiety threaded through cyclodextrin macrocycles (Fig 2.1) which act like a non-conjugated "spacer" between the conjugated chains providing control over the interchain interactions.[6, 11] Thanks to this property, they represent a model compounds to study fundamental physical properties of conjugated semiconductors, since their electronic and optical properties, are controlled both by molecular structure of the conjugated backbone, and by supramolecular interactions. During the last 10 years they have been successfully used in white-light-emitting diodes and electrochemical cells[6-8] and optically pumped laser.[9, 10]

In the last two decades, the attention has been focused on tailoring/control of "intramolecular functionality" (π -conjugation). Control at the intermolecular level is more difficult to achieve, but equally important in determining the properties of conjugated materials. In fact, intermolecular interactions can lead to formation of interchain species (aggregates and/or excimers), detrimental for the photophysics of such polymer-based devices.[12-14]

Conjugated polyrotaxanes are a model system for studying the influence of interchain interactions on the electronic dynamics of organic semiconductors. In fact, cyclodextrin insulation suppresses intermolecular interactions, showing photoluminescence decay dynamics which are mono-exponential and independent of concentration, despite the incomplete shielding of the conjugated cores by the cyclodextrins.[15]

Furthermore, by increasing the degree of threading (quantified by the "threading ratio," TR),[11] the progressive encapsulation preserves the intrinsic spectroscopic properties of the isolated chains without suppressing charge transport in solid films, thus yielding enhanced and blue-shifted electroluminescence with respect to unthreaded conjugated polymers. Incorporation of luminescent polymers into cyclodextrin macrocycles also reduces energy transport rates and exciton diffusion to quench sites.[2]

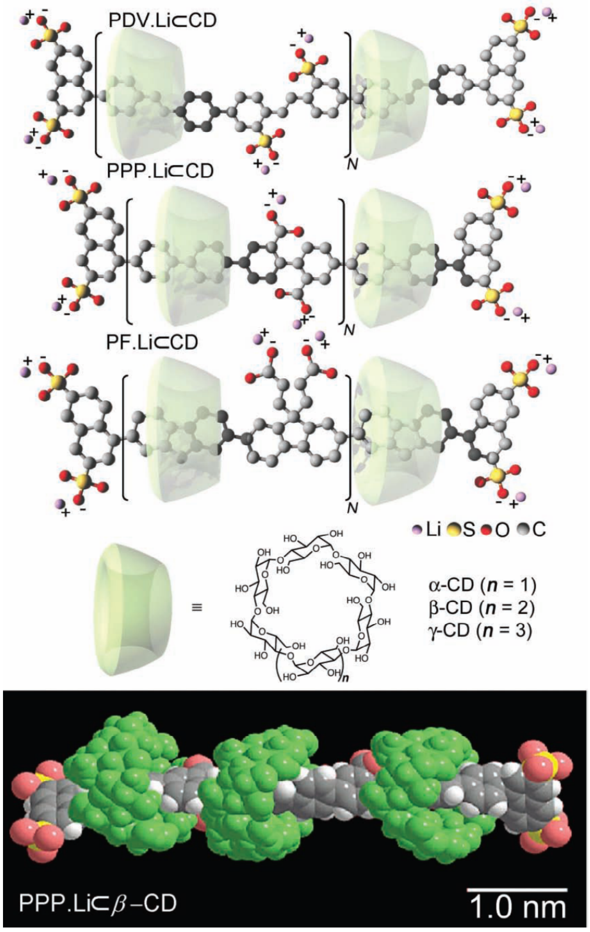

Figure 2.1 (Top) Chemical structures of the cyclodextrin-threaded conjugated polyrotaxanes with poly(4,4'-diphenylene vinylene) (PDV.Li), poly(*para*-phenylene) (PPP.Li) and poly(fluorene) (PF.Li) cores with naphthalene stoppers, average degree of polymerization: *n* = 10. (b) Energy minimized structure of a 2-repeat-unit PPP.Li⊂ β -CD oligorotaxane.
(Reproduced from ref. 1)

Comparison of threaded and unthreaded conjugated chains provides important information on the effect of threading on the formation and decay of interchain and intrachain species.[2] For unthreaded and threaded chains trough β-Cyclodextrin cycles (β-CD) of poly(4,40-diphenylenevinylene) (PDV.Li), steady-state photolumienescence (PL) measurements show the independence of the PL spectra of the polyrotaxanes from solution concentration. On the contrary, the PL spectrum of unthreaded polymer solutions evolves from the polyrotaxane PL spectrum (in the most diluted case) to progressive red-shifted and broadened ones with increasing concentration (Fig 2.1).

Time-resolved PL measurements show a long-lived non-exponential decay strongly dependent on concentration and a red-shifted emission spectrum (fingerprint of interchain species, Fig. 2.3, similar results for derivatives of poly(fluorene) (PF.Li), poly(paraphenylene) (PPP.Li)). In contrast, conjugated polyrotaxanes show dynamics independent of solution concentration over more than two decades.[11, 16]

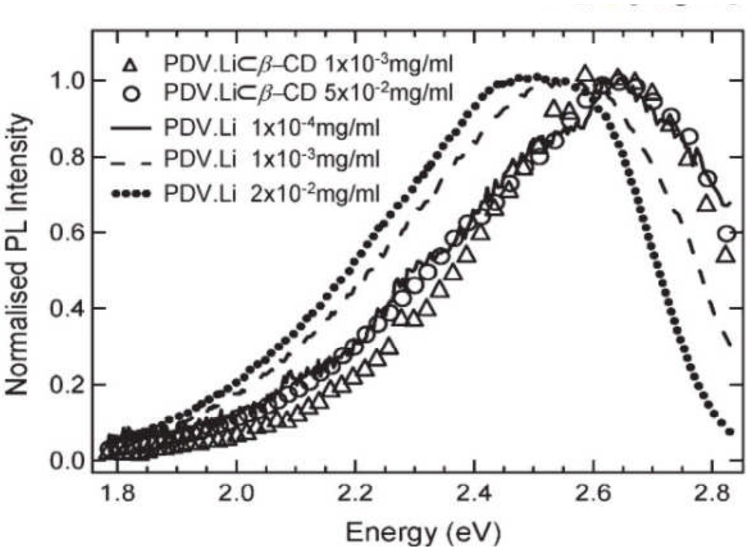

Figure 2.2 Steady-state PL spectra of poly(4,40- diphenylene vinylene) (PDV.Li) polyrotaxane solution at $5x10^{-2}$ mg/mL (opencircles) $1x10^{-4}$ mg/mL (open triangles) and of all the solutions of the unthreaded polymer (labeled with their respective concentrations). The spectrum of the polyrotaxane solution is virtually coincident with that of the most diluted solution of the unthreaded polymer. (Reproduced and adapted from ref. 2)

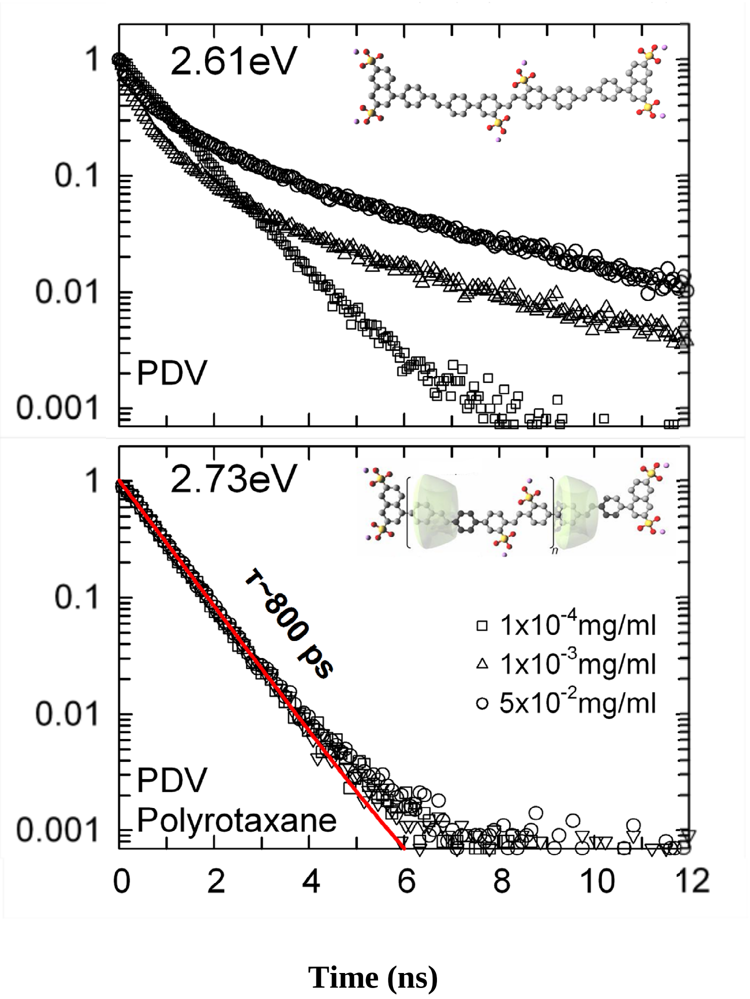

Figure 2.3 Time-dependent decays of solutions of PDV.Li (top panel) at 2.61 eV, and of the threaded polymer at 2.73 eV (bottom panel). The relative fits are also shown for the PDV.Li_β-CD decays, which have been fitted by a simple exponential function.

2.2. Azo-benzene based self-assembled monolayers

Self-assembled monolayers (SAMs) are currently a key component of many electronic devices such as organic thin-film transistors, light-emitting diodes, photovoltaic cells, and memory cells.[17] A particular application of SAMs is the chemical functionalisation of metallic surfaces which allows tuning of the metal work function and simultaneously modifying the surface wettability. Combination of both these effects offer a major flexibility advantage in the design of devices.[18] This modification at the metal/active material interface has great impact on the injection/extraction of electrons and/or holes, as well as on the molecular order (degree of cristallinity) of the semiconductors deposited on top of the SAMS, which can completely alter the transport pathways through the material and thus, the overall performance of devices.

It has been demonstrated that small changes in the chemical structure of the molecules forming the SAMs can dramatically change the resulting properties of the device. This chemical tunability, can be induced from single-component SAMs as well as mixed SAMs in which the ratio of each component alters significantly the resulting properties of the metal.[18, 19].

In Chapter 5, I will show how a photoactive fluorinated thiol derivative containing an azobenzene unit chemisorbed on an Au substrate leads to a large work function shift. This shift is comparable to other fluorinated SAMs on Au such as the pentafluorobenzene thiol (PFBT).[20] Nevertheless, due to the azobenzene group the work function can be later tuned by irradiating the SAM at a specific wavelength, thus widening the functionality of the SAM. Azobenzene derivatives are one of the families of photochromic molecules extensively used due to their accessible and reversible isomerization process that occurs between the *trans* and *cis* states under UV light for the *trans* to *cis* conversion and under visible light or by temperature for the *cis* to *trans*.[21, 22]

References

[1] F. Cacialli, J. S. Wilson, J. J. Michels, C. Daniel, C. Silva, R. H. Friend, N. Severin, P. Samori, J. P. Rabe, M. J. O'Connell, P. N. Taylor, H. L. Anderson, *Nature Materials* **2002**, *1*, 160.

[2] A. Petrozza, S. Brovelli, J. J. Michels, H. L. Anderson, R. H. Friend, C. Silva, F. Cacialli, *Advanced Materials* **2008**, *20*, 3218.

[3] M. J. Frampton, H. L. Anderson, *Angewandte Chemie-International Edition* **2007**, *46*, 1028.

[4] J. J. Michels, M. J. O'Connell, P. N. Taylor, J. S. Wilson, F. Cacialli, H. L. Anderson, *Chemistry-a European Journal* **2003**, *9*, 6167.

[5] P. N. Taylor, M. J. O'Connell, L. A. McNeill, M. J. Hall, R. T. Aplin, H. L. Anderson, *Angewandte Chemie-International Edition* **2000**, *39*, 3456.

[6] S. Brovelli, F. Meinardi, G. Winroth, O. Fenwick, G. Sforazzini, M. J. Frampton, L. Zalewski, J. A. Levitt, F. Marinello, P. Schiavuta, K. Suhling, H. L. Anderson, F. Cacialli, *Advanced Functional Materials* **2010**, *20*, 272.

[7] G. Latini, L. J. Parrott, S. Brovelli, M. J. Frampton, H. L. Anderson, F. Cacialli, *Advanced Functional Materials* **2008**, *18*, 2419.

[8] F. E. Oddy, S. Brovelli, M. T. Stone, E. J. F. Klotz, F. Cacialli, H. L. Anderson, *Journal of Materials Chemistry* **2009**, *19*, 2846.

[9] S. Brovelli, T. Virgili, M. M. Mroz, G. Sforazzini, A. Paleari, H. L. Anderson, G. Lanzani, F. Cacialli, *Advanced Materials* **2010**, *33*, 3690 .

[10] M. M. Mroz, S. Perissinotto, T. Virgili, G. Gigli, M. Salerno, M. J. Frampton, G. Sforazzini, H. L. Anderson, G. Lanzani, *Applied Physics Letters* **2009**, *95*, 3.

[11] S. Brovelli, G. Latini, M. J. Frampton, S. O. McDonnell, F. E. Oddy, O. Fenwick, H. L. Anderson, F. Cacialli, *Nano Letters* **2008**, *8*, 4546.

[12] I. D. W. Samuel, G. Rumbles, C. J. Collison, *Physical Review B* **1995**, *52*, 11573.

[13] T. Q. Nguyen, R. C. Kwong, M. E. Thompson, B. J. Schwartz, *Applied Phyics Letters* **2000**, *76*, 2454.

[14] B. J. Schwartz, *Annual Review of Physical Chemistry* **2003**, *54*, 141.

[15] J. S. Wilson, M. J. Frampton, J. J. Michels, L. Sardone, G. Marletta, R. H. Friend, P. Samori, H. L. Anderson, F. Cacialli, *Advanced Materials* **2005**, *17*, 2659.

[16] S. Brovelli, F. Cacialli, *Small* **2011**, *6*, 2796.

[17] M. Halik, A. Hirsch, *Advanced Materials* **2011**, *23*, 2689.

[18] C.-Y. Chen, K.-Y. Wu, Y.-C. Chao, H.-W. Zan, H.-F. Meng, Y.-T. Tao, *Organic Electronics* **2011**, *12*, 148.

[19] K.-Y. Wu, S.-Y. Yu, Y.-T. Tao, *Langmuir* **2009**, *25*, 6232.

[20] J. Smith, R. Hamilton, Y. Qi, A. Kahn, D. D. C. Bradley, M. Heeney, I. McCulloch, T. D. Anthopoulos, *Advanced Functional Materials* **2010**, *20*, 2330.

[21] Griffith.J, *Chemical Society Reviews* **1972**, *1*, 481.

[22] N. Tamai, H. Miyasaka, *Chemical Reviews* **2000**, *100*, 1875.

3. Oriented films incorporating water-soluble conjugated polyrotaxane

3.1. Introduction

Despite the various solution-processing available for conjugated polymers, optoelectronics devices are typically produced using thin-films by spin-coating or drop-casting of a solution. These techniques hinder the intrinsic anisotropy of electronic states due to delocalization of π electrons along the conjugated polymer backbone. During the last 30 years many techniques have been developed to orientate conjugated polymers in order to study their photophysical and electrical properties. In particular, mechanical techniques have been widely used due to their low cost and simple but effective approach. A first examples is the tensile drawing of polymer,[1] which has been used for poly(*p*-phenylene vinylene) (PPV) to study its infrared-spectrum,[2, 3] polarised electroluminescence[4] and its anisotropic photoluminescence properties.[5, 6]

A different approach to mechanically align films is that of rubbing a conjugated polymer film, for example with a cloth mounted on a rotating drum. This technique has been widely applied to prepare alignment layers for liquid crystals (LCs).[7-9] Good alignment requires high "rubbing strengths"[9] and under this conditions films are aligned throughout their thickness, not just in a thin surface layer.[10]

Other non-mechanical techniques have been developed based for example on "Langmuir-Blodgett" films for preparation of LEDs,[11] photo-alignment of functionalised polyimide films,[12] nanoimprinting of poly(9,9-dioctylfluorene-*co*-benzothiadiazole) (F8BT) in liquid crystalline phase,[13, 14] alignment of poly(9,9-dioctylfluorenyl-2,7-diyl) (PFO) nanowires[15] and "zone-casting" of different polymers.[16, 17]

In view of the increased rigidity of the chains upon rotaxination, the question arises as to whether it might be possible to align the molecules so as to achieve polarised emission. In this chapter, I will show results on the alignment of conjugated polyrotaxanes by stretching a water-soluble matrix of polyvinyl alcohol. Polarization-resolved steady-state and time-resolved photoluminescence experiments reveal that over 95% of the emitted light is polarized along the orientation direction. A hybrid organic-inorganic light-emitting diode was built to investigate the possibility of using these films as polarizing filters for solid-state lighting and display technology.[18]

The film preparation and tensile drawing was carried out at the "Center of Molecular and Macromolecular studies, Polish Academy of Studies" in collaboration with Mr. Platon Korniychuck and

Prof. Adam Tracz. The conjugated polymers were synthesised at the "Chemistry Research Laboratory, Department of Chemistry, University of Oxford" by Dr. Shane O. McDonnel and Prof. Harry L. Anderson. This study was carried out within the Marie Curie research training network THREADMILL (MRTN-CT-2006-036040). Both experimental methods and optical properties here reported are extracted from my Mphil to PhD transfer report submitted September 2010 and the publication: F. Di Stasio, et al., Adv. Mater., 23, 1855-1858 (2011).

3.2. Experimental methods

3.2.1. Film Preparation and Tensile Drawing

Films were prepared by drop-casting onto a glass substrate a 20% by weight water solution of polyvinyl alcohol (PVA, M_w = 72000 g/mol, Fig. 3.1) and poly(4,4'-diphenylene vinylene) (PDV.Li, M_w = 6050 g/mol, PVA:PDV.Li = 99.5:0.5 by weight, Fig. 3.3.1), a polyelectrolytic derivative of poly-*para*-phenylene (PPP) where sulfonated sidegroups balanced by Li^+ ions assure the solubility in polar solvents.

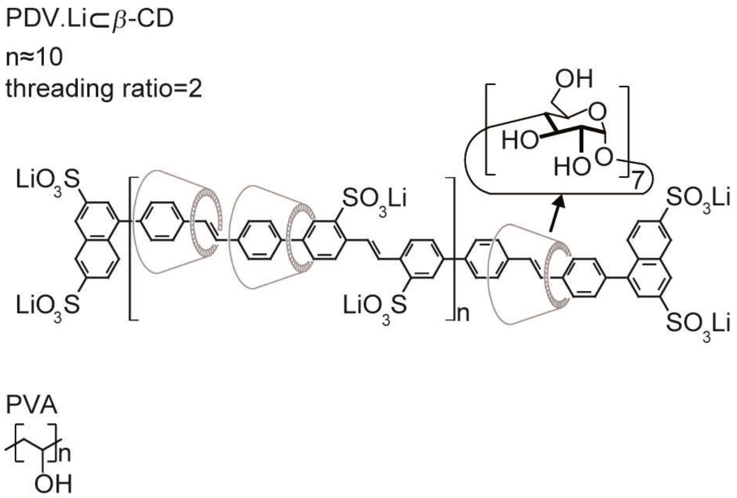

Figure 3.1 Molecular structures of PDV.Li⊂β-CD (PDV.Li posses the same structure but without cyclodextrins) and PVA.

To investigate the effect of rotaxination on the molecular orientation and polarisation anisotropy we used both unthreaded PDV.Li and the same polymer threaded into β-cyclodextrin macrocycles (PDV.Li⊂β-CD, threading ratio=2).[19, 20]

After water evaporation a ~30 μm thick film was obtained and then "peeled-off" the substrate obtaining a free-standing film. The film was then stretched at room temperature in an environment with 100% relative humidity.[21] The stretching process was carried out using a home-made set-up based on a micrometer-screw. Water being a solvent of PVA, increasing the concentration of it decreases the glass transition temperature (T_g) of PVA from 85 °C to below room temperature.[22] This phenomenon can be used to induce a drop in the Young Modulus of the material, allowing the alignment of the polymer while in its "rubbery state" where the material exhibits large elongations under relatively low load. Films were stretched 5 times the original length ($\Delta L/L_0=5$) and at the end of the process they were dried in an elongated condition in Nitrogen gas and then removed from the stretching-rig.

3.2.2. Time correlated single photon counting (TCSPC)

The TCSPC system is a photon counting technique based on the assumption that for low-level, high-repetition-rate signals, the light intensity is so low that the probability of detecting one photon in one excitation pulse is less than 1. In fact, the detection rate is typically 1 photon per 100 excitation pulses. The system measures the time delay of each photon against the excitation pulse, and build up an histogram of the photon-times, after many photons (more than 10000) the distribution of the detection times, i.e. the waveform of the optical pulse, builds up in the system memory.[23]

A typical example of a TCSPC electronic schematic[24] is reported in Fig. 3.2. The experiment starts with the excitation pulse (LASER) that excites the sample (S) and sends a signal to the electronics. This signal is passed through a constant fraction discriminator (CFD), which accurately measures the arrival time of the pulse. Afterward, the same signal is passed to a time-to-amplitude converter (TAC), which generates a voltage ramp that increases linearly with time. In parallel, a second channel detects the pulse from the single photon emitted from the sample. The arrival time of the pulse is accurately measured using the CFD, which sends a signal to stop the voltage ramp. The TAC now contains a voltage proportional to the time delay between the excitation and the emission signals. In the end, the voltage is amplified by a programmable gain amplifier (PGA) and converted to a numerical value by the analog-to-digital converter (ADC).

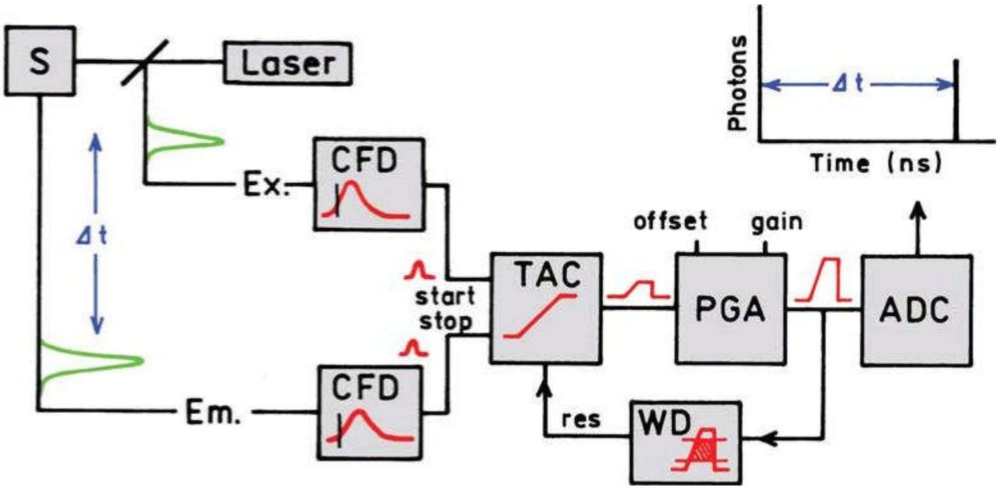

Figure 3.2 Electronics scheme for TCSPC (*Principle of Fluorescence Spectroscopy, J. R. Lakowicz, Springer)*

To minimize false readings the signal is restricted to a given range of voltages. If the signal is not within this range the event is suppressed by a window discriminator (WD). The voltage is converted to a digital value that is stored as a single event with the measured time delay.

Although this principle looks complicated at first glance, TCSPC records light signals with high time-resolution (~ 150 ps).

The time-resolution of a TCSPC system is characterised by its instrument response function (IRF). The IRF not only contains the width of the excitation pulse, but the temporal dispersion in the optical path and the uncertainty in the timing of the light signal (timing jitter) as well, decreasing the time-resolution of the system.

In our case, we used an Edinburg Instruments F900-red TCSPC (time resolution ~150 ps), as excitation light a laser-diode (E_{ex}= 3.3 eV) with a pulse width of ~ 40 ps and a cooled photomultiplier tube coupled with a monochromator as detector.

3.2.3. Photoluminescence quantum yield measurements

The photoluminescence quantum yield (Φ_{PL}) of chromophores is defined as the ratio of the number of photons emitted to the number of photons absorbed.

Solution photoluminescence quantum yields (Φ_{PL}) have been measured relative to a quinine sulphate dehydrate in 0.5M H_2SO_4 solution (~10^{-5}M, $\Phi_{PL} = 0.546 \pm 5\%$, NIST standard reference material SRM# 936a, www.nist.gov/srm).

A general technique used to measure Φ_{PL} for solid-state films is using an integrating sphere.[25] Unfortunately it was impossible to use this simple technique with our films due to the large thickness and scattering from the rough surface of films. Therefore, we calculated the Φ_{PL} by extrapolating the photoluminescence (PL) lifetime (τ) from the PL-kinetics. In fact, Φ_{PL} depends on the emissive rate (K_R) and the rate of non-radiative decay (K_{NR}), as the fraction of chromophores that decay though emission, and hence Φ_{PL}, is given by:

$$\Phi_{PL} = \frac{K_R}{K_R + K_{NR}}, \tag{3.1}$$

In complete absence of non-radiative channels the Φ_{PL} is equal to 1 and in this case the lifetime of the chromophores is called the intrinsic or natural lifetime, and is given by:

$$\tau_n = \frac{1}{K_R}, \tag{3.2}$$

The natural lifetime τ_n is related to the measured PL-lifetime (τ) and Φ_{PL}:

$$\tau_n = \frac{\tau}{\Phi_{PL}}, \tag{3.3}$$

If τ_n is a constant in all different samples, i.e. no changes in the excited-state geometry and emission wavelength[24] but only in the PL-quenching which affects K_{NR}, we calculated the Φ_{PL} of our films using the τ and Φ_{PL} values measured for the each solution:

$$\Phi_{PL\,film} = \frac{\tau_{film}}{\tau_n} \;;\; \Phi_{PL\,sol.} = \frac{\tau_{sol.}}{\tau_n}, \tag{3.4}$$

Obtaining:

$$\frac{\Phi_{sol.}}{\tau_{sol.}} = \frac{\Phi_{film}}{\tau_{film}}, \tag{3.5}$$

Assuming that the natural lifetime does not change is feasible in this case, since all the effects on the PL-lifetime here observed are connected to a reduction in the polymer aggregation and PL-quenching which are only modifying the rate of non-radiative decay (K_{NR}).

3.2.4. Photoluminescence anisotropy

Anisotropy measurements are commonly used in biochemical applications to study the size and shape of proteins or the rigidity of various molecules.

In this case, we have used time-resolved and steady-state anisotropy measurements to study and quantify the alignment of the conjugated chains in stretch-oriented films.

Anisotropy measurements are based on the photoselectivity of the excitation of chromophores by polarised light. Chromophores preferentially absorb photons whose electrical field vectors are aligned parallel to their transition moment. The transition moment has a defined orientation with respect to the molecular axis and its orientation depends on the chromophores structure.

All measurements were carried out using the TCSPC system previously described, a Glan-Taylor polarising prism was used to choose between the photoluminescence polarisations. All spectra presented here have been corrected for the overall system response for all different polarisations. The photoluminescence measurements were collected with the polarizer oriented parallel ($\parallel$) or perpendicular ($\perp$) to the stretching direction (for oriented films) or an arbitrary direction (for un-stretched films).

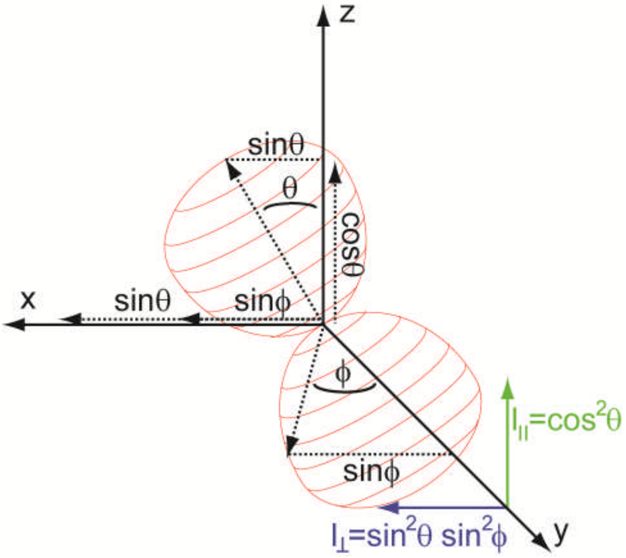

Figure 3.3 Emission intensities for a radiating dipole in a polar coordinate system. The red shape represents the dipole.

The photoluminescence anisotropy is defined as:

$$\gamma = \frac{I_{\parallel} - I_{\perp}}{I_{\parallel} + 2I_{\perp}}, \tag{3.6}$$

The anisotropy (γ) is a dimensionless quantity that is independent on the concentration of chromophores and it is normalized on the total intensity of the emitted light $I_{tot} = I_{\|} + 2I_{\perp}$.

The theory for photoluminescence anisotropy can be simplified and explained considering a single molecule (i.e. a single radiating dipole), assuming that the absorption and emission moments are parallel (collinear) and rotational diffusion of the polarisation (depolarisation) is absent. This single molecule will be oriented at an angle θ relative to the z-axis (Fig. 3.3) and ϕ relative to the y-axis, in an isotropic system (for example, a diluted solution) the ground-state of our molecule will be randomly oriented. If the excitation is polarised parallel to the z-axis then there will be a preferential orientation of the excited-state population along this axis, due to the photoselectivity of the dipole. Fig. 3.3 shows $I_{\|}$ and $I_{\perp}$ being proportional to the projection of the transition moment (i.e. the electric field generated by the dipole) onto the axes, if the dipole is oriented along the z-axis, hence is oriented along the excitation axis, the electric field can be described by:

$$E(\theta, \phi) = k \frac{sin\,\theta}{r} \hat{\theta}, \tag{3.7}$$

Where k is a constant, r is the distance from the chromophore and $\hat{\theta}$ is a unit vector along the θ coordinate. From (3.7) we can calculate the intensity of the emitted light:

$$I_0(\theta, \phi) = k^2 \frac{sin^2\,\theta}{r^2} \hat{r}, \tag{3.8}$$

In this case, $\hat{r}$ is the unit vector in the direction of the propagation. From these considerations, we can calculate the parallel ($I_{\|}$) and perpendicular ($I_{\perp}$) intensities for a dipole with an arbitrary orientation:

$$I_{\|}(\theta, \phi) = I_0 cos^2\,\theta, \tag{3.9}$$

$$I_{\perp}(\theta, \phi) = I_0 sin^2\,\theta\, sin^2\,\phi, \tag{3.10}$$

For excitation polarised parallel to the z-axis, all molecules at an angle ϕ from the y-axis are excited with equal probability; i. e. the population of excited chromophores is symmetrically distributed around the z-axis and oriented with $0 \leq \phi \leq 2\pi$. Hence, we can substitute the ϕ dependence from equation 3.10 with the average value of $\sin^2 \phi$:

$$\langle sin^2\,\phi \rangle = \frac{\int_0^{2\pi} sin^2\,\phi\, d\phi}{\int_0^{2\pi} d\phi} = \frac{1}{2}, \tag{3.11}$$

Obtaining:

$$I_{\|}(\theta) = I_0 cos^2\,\theta, \tag{3.12}$$

$$I_{\perp}(\theta) = \frac{1}{2} I_0 sin^2 \theta, \tag{3.13}$$

In general, a collection of chromophores is studied and not a single one, if we assume that this group of chromophores is oriented relative to the z-axis with a probability f(θ), the measured photoluminescence intensities are:

$$I_{\parallel} = I_0 \int_0^{\frac{\pi}{2}} f(\theta) \cos^2 \theta \, d\theta = a I_0 \langle \cos^2 \theta \rangle, \tag{3.14}$$

$$I_{\perp} = \frac{1}{2} I_0 \int_0^{\frac{\pi}{2}} f(\theta) \sin^2 \theta d\theta = \frac{a}{2} I_0 \langle \sin^2 \theta \rangle, \tag{3.15}$$

Where f(θ) dθ is the probability that a chromophore is oriented between θ and θ + dθ, and a is an instrumental constant. Using eq. 3.6 we find that:

$$\gamma = \frac{3\langle \cos^2 \theta \rangle - 1}{2}, \tag{3.16}$$

The anisotropy is determined by the average value of $\cos^2 \theta$, where θ is the angle of the emission dipole relatives to the z-axis. This expression is only correct for samples that display z-axis symmetry. A different expression is needed to describe the anisotropy of a chromophore with specific θ and ϕ. For a single chromophore oriented along the z-axis (θ = 0) with collinear transitions, eq. 4.16 shows γ = 1. However, it is not possible to have such a perfectly oriented excited-state population since the electric dipole of the chromophore does not need to be precisely aligned with the z-axis to absorb light polarised along this axis. Hence the anisotropy is always less than 1.

For a group of molecule with no preferential orientation, collinear emission and absorption dipoles the probability of absorption is proportional to $\cos^2 \theta$, where θ is the angle between the absorption dipole and the z-axis and is the same angle as for the emission dipole (Fig. 3.3). For the random ground-state distribution which must exist in an isotropic system, the number of molecules at an angle θ and θ + dθ is proportional to $\sin \theta \, d\theta$. This quantity is proportional to the surface area on a sphere within angles θ and θ + dθ. Hence, the distribution of molecules excited by vertically (parallel to the z-axis) polarised light, g(θ), is given by:

$$g(\theta) \, d\theta = \cos^2 \theta \sin \theta \, d\theta, \tag{3.17}$$

The probability distribution given by eq. (3.17) determines the maximum photo-selection that can be obtained using one-photon excitation of an isotropic system. The value of $\langle \cos^2 \theta \rangle$ is given by:

$$\langle cos^2 \theta \rangle = \frac{\int_0^{\frac{\pi}{2}} cos^2 \theta \, g(\theta) d\theta}{\int_0^{\frac{\pi}{2}} g(\theta) d\theta}, \tag{3.18}$$

Substitution of eq. 3.17 into eq. 3.18 yields $\langle \cos^2 \theta \rangle = 3/5$ and a maximum of anisotropy of 0.4 for an isotropic system. This value is observed when absorption and emission dipoles are collinear and when depolarisation is absent. Under these conditions the excited-state population is preferentially oriented along the z-axis and $I_{\parallel} = 3I_{\perp}$. This value is considerably smaller than that possible for a single chromophore oriented along the z-axis.

To study the polarised photoluminescence properties of stretch-oriented films in all conditions we have changed the excitation laser polarisation using a λ/4 wave-plate and a polarising filter, therefore introducing another parameter due to the different excitation polarisation.

To quantify the polarisation resulting from the alignment of the polymeric chains we calculated the PL polarisation ratio (R) for all different excitation/detection configurations (Fig. 3.4). In what follows, we will indicate these with the general notation $R_{xx/xy}=PL_{xx}/PL_{xy}$, $R_{xx/yy}=PL_{xx}/PL_{yy}$ where the first index represents the polarisation of the excitation and the second one represents the polarisation of the PL (parallel ∥ or perpendicular ⊥ to the stretching direction for stretch-oriented films and an arbitrary direction for un-stretched films).

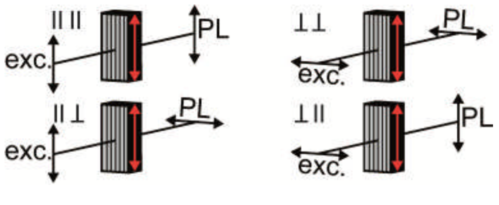

Figure 3.4 Scheme representing the four different configurations used to study the polarised photoluminescence of the PVA films. The red arrow represents the stretching direction for the oriented films and the arbitrary direction for un-stretched films.

These definitions allow us to use a uniform notation for both oriented and un-stretched films, although the rotational symmetry of the un-stretched films considerably reduced the number of independent ratios.

There are 12 ratios of this type overall, but 6 of them are the inverse of the other 6 (e.g. $R_{\parallel\parallel/\perp\perp} = 1/R_{\perp\perp/\parallel\parallel}$ and so on). $R_{\parallel\parallel/\perp\perp}$ provides information on the number of chromophores oriented along the stretching direction and maintaining the initial polarisation, in respect to those oriented at 90° to the stretching direction. $R_{\parallel\parallel/\perp\perp}$ thus characterises the success of the alignment process via tensile drawing. The expected value for a perfect alignment of the chromophores and no exciton migration to perpendicular chromophores is tending to infinite, meaning that all chromophores are aligned along one direction and all of them are emitting photons from excited states maintaining the initial polarisation.

$R_{\parallel\parallel/\parallel\perp}$ provides instead information on the proportion of chromophores oriented along the stretching direction that, once excited, maintain the initial polarisation with respect to those that over their lifetime are able to reach (and decay from) chromophores oriented 90° to the stretching direction. The value of $R_{\parallel\parallel/\parallel\perp}$ expected for a perfect alignment of the chromophores, and no exciton migration to perpendicular chromophores is also tending to infinite. However, the alignment is never found to be perfect, and even when the excitation is parallel to the stretching direction, “orthogonal chromophores” (i.e. oriented perpendicular to the stretching direction) can be excited via both intra- and inter-chain energy transfer. This ratio thus gives information especially on exciton migration processes.

In all these different ratios, the expected value for a film with isotropic alignment and exciton migration is 1, since no differences in orientation can be observed and the emission of photons take place from excited states randomly oriented which are not maintaining the initial polarisation.

We can easily derive the anisotropy γ from these ratios using the equation:

$$\gamma = \frac{R_{xx/xy}-1}{R_{xx/xy}+2}, \tag{3.19}$$

As we will discuss later, γ is usually not a constant,[5, 14] instead it depends on the spectral position ($\gamma(E)$).

3.2.5. Other techniques

Optical absorption measurements were carried out at room temperature, in air using an Agilent 8453 UV-Visible spectrometer and the polarisation of incidence light was selected using a polarising filter.

For the hybrid device, a GaN LEDs array ($E_{peak} = 3.3eV$, maximum light output = 1150mW) was used to excite the film with non-polarised light and spectra were collected with a spectrometer (Andor Shamrock 163i) coupled with a CCD camera (Andor Newton CCD, cooled at -50°C) and a polarising filter was use to select between the polarisation directions.

3.3. Optical properties

3.3.1. Optical absorption spectra

In Fig. 3.5 the optical absorption spectra of stretch-oriented (a, c) films embedding PDV.Li or PDV.Li⊂*β*-CD are presented. The optical absorption spectra of un-stretched films are shown in Fig. 3.5 b and d for direct comparison.

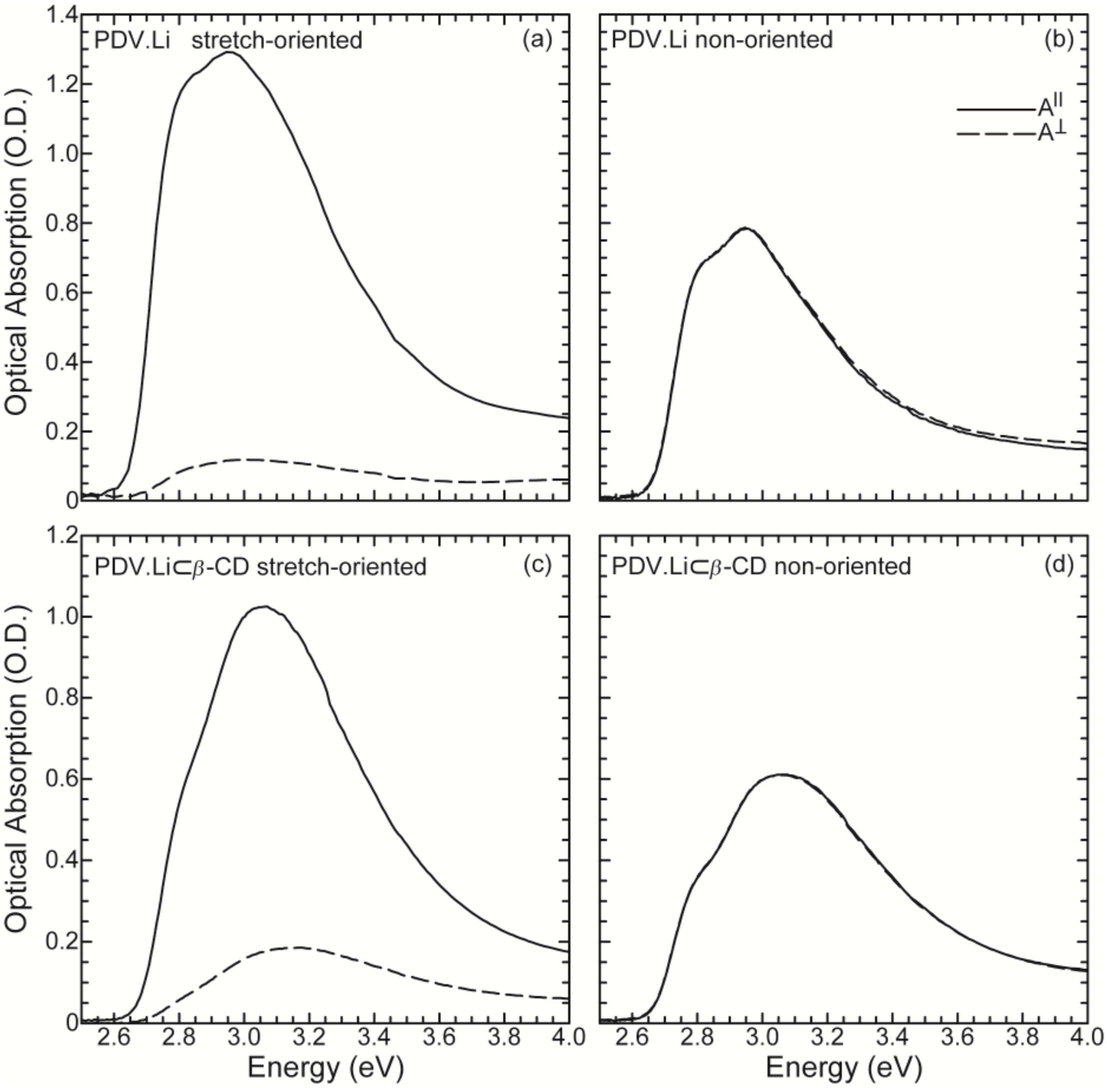

Figure 3.5 Optical absorption spectra for stretch-oriented films (a, c) and un-stretched films (b, d) embedding PDV.Li (a, b) or PDV.Li⊂β-CD (c, d).

According to previous reports, the absorption spectrum of the polyrotaxane is blue-shifted with respect to the unthreaded chain ($\mathrm{Abs}_{\mathrm{MAX\text{-}PDV.Li}\subset\beta\text{-}\mathrm{CD}}$ ~ 3.10 eV, $\mathrm{Abs}_{\mathrm{MAX\text{-}PDV.Li}}$ ~ 2.98 eV).[26] From the absorption spectra with incident light polarised parallel ($A^{\parallel}$) or perpendicular ($A^{\perp}$) to the stretching axis, dichroic ratios are: $D = A^{\parallel}/A^{\perp} \sim 5$ for PDV.Li⊂*β*-CD and D ~ 11 for PDV.Li respectively. The absorption spectrum of PDV.Li⊂β-CD measured with incident light polarised perpendicular to the stretching direction (Fig. 3.5c), is blue-shifted by 80 meV with respect to the one measured with incident light polarised parallel. Such a high dichroic ratio for films doped with PDV.Li suggests that a higher degree of orientation is obtained for the latter than for PDV.Li⊂β-CD.

The dichroic ratio for both un-stretched films is equal to 1, as expected due to the random orientation of the conjugated moieties inside the PVA matrix.[13, 24]

3.3.2. Photoluminescence spectra

In Fig. 3.6 all photoluminescence (PL) spectra for the 4 different configurations (see scheme in Fig. 3.4) are presented. The PL spectra present peaks at 2.54 eV and 2.68 eV for PDV.Li⊂*β*-CD and at 2.51 eV and 2.66 eV for PDV.Li.

The PL does not show any detectable variation in spectral shapes upon stretching and, the relative ratio between the different vibronic peaks is maintained to better than 1%. However, a significant enhancement of the 0-0 transition for the rotaxanes compared to the unthreaded analogues is observed. Furthermore, a small red-shift for the PDV.Li PL with respect to PDV.Li⊂β-CD is still present despite the PVA matrix. This can be ascribed to residual interchain interactions in PDV.Li that are further removed in the polyrotaxane due to β-cyclodextrin encapsulation.

As previously discussed, it is possible to calculate the different polarisation ratios (R) for all different configurations. $R_{\parallel\parallel/\perp\perp}$ is ~ 51 for PDV.Li⊂*β*-CD and 111 for PDV.Li (Fig. 3.6 a,c), which is comparable with the best values reported in literature for tensile-drawing of poly(*p*-phenylene vinylene),[5] photoalignment of polyimide [12] and nanoconfinement of poly(9,9-dioctylfluorene-co-benzothiadiazole) in liquid crystalline phase.[14] This clearly demonstrates the remarkable level of chain alignment obtainable using a stretchable polymeric matrix such as PVA.

Interestingly, these results also show that the presence of the CDs partially hinders the alignment process, probably by reducing the aspect ratio (i.e. ratio of molecular length to width) by increasing the thickness of the polymer strands and by changing the non-covalent interactions between the conjugated polymer and the PVA matrix.

For the ratio $R_{\parallel\parallel/\parallel\perp}$, $R_{\parallel\parallel/\parallel\perp} \sim 22$ for PDV.Li$\subset\beta$-CD and $R_{\parallel\parallel/\parallel\perp} \sim 33$ for PDV.Li. Less significant migration is expected for the rotaxanes compared to the unthreaded analogues, but it is obviously to be connected to the better alignment obtained for the unthreaded molecules compared to the rotaxanes, clearly signalled by the difference in $R_{\parallel\parallel/\perp\perp}$ and in dichroic ratios. Indeed, $R_{\parallel\parallel/\parallel\perp}$ for unrotaxinated and rotaxinated polymers show that the ratio reduces to 1.5, i.e. smaller than the ratios of $R_{\parallel\parallel/\perp\perp}$ ~2.2, and in line with the expectation of suppressed exciton migration in the threaded molecular wires.

For all these different ratios, the expected value for a film with isotropic alignment or rapid exciton migration is one, since no differences in orientation can be observed and the emission of photons typically takes place from excited states not maintaining the initial polarization. Therefore, $R_{\parallel\parallel/\parallel\perp} = R_{\parallel\parallel/\perp\parallel} = R_{\perp\perp/\parallel\perp} = R_{\perp\perp/\perp\parallel}$, which can be simplified in $R_{\perp}$ to indicate the ratio of the luminescence from chromophores oriented parallel to the exciting laser and the PL from chromophores oriented perpendicular to the laser polarisation. Similarly, $R_{\parallel\parallel/\perp\perp} = R_{\perp\perp/\parallel\parallel} \equiv R_{\parallel} \sim 1$. The results (reported in Table 3.1) show that $R_{\perp} \sim 1.75$ for PDV.Li$\subset\beta$-CD and $R_{\perp} \sim 1.60$ for PDV.Li, higher values than expected (1, owing to the discussed lack of any intentional orientation which can be connected to the slow depolarization of the PL). The slightly higher value for the polyrotaxane film is not surprising, due to the additional encapsulation provided by the cyclodextrins with respect to the unthreaded chains.[27] Both $R_{\parallel}$, and the dichroic ratio D (Fig.5b, d), have a value of 1 however, as expected for random chromophores orientation.[13, 24] [27]

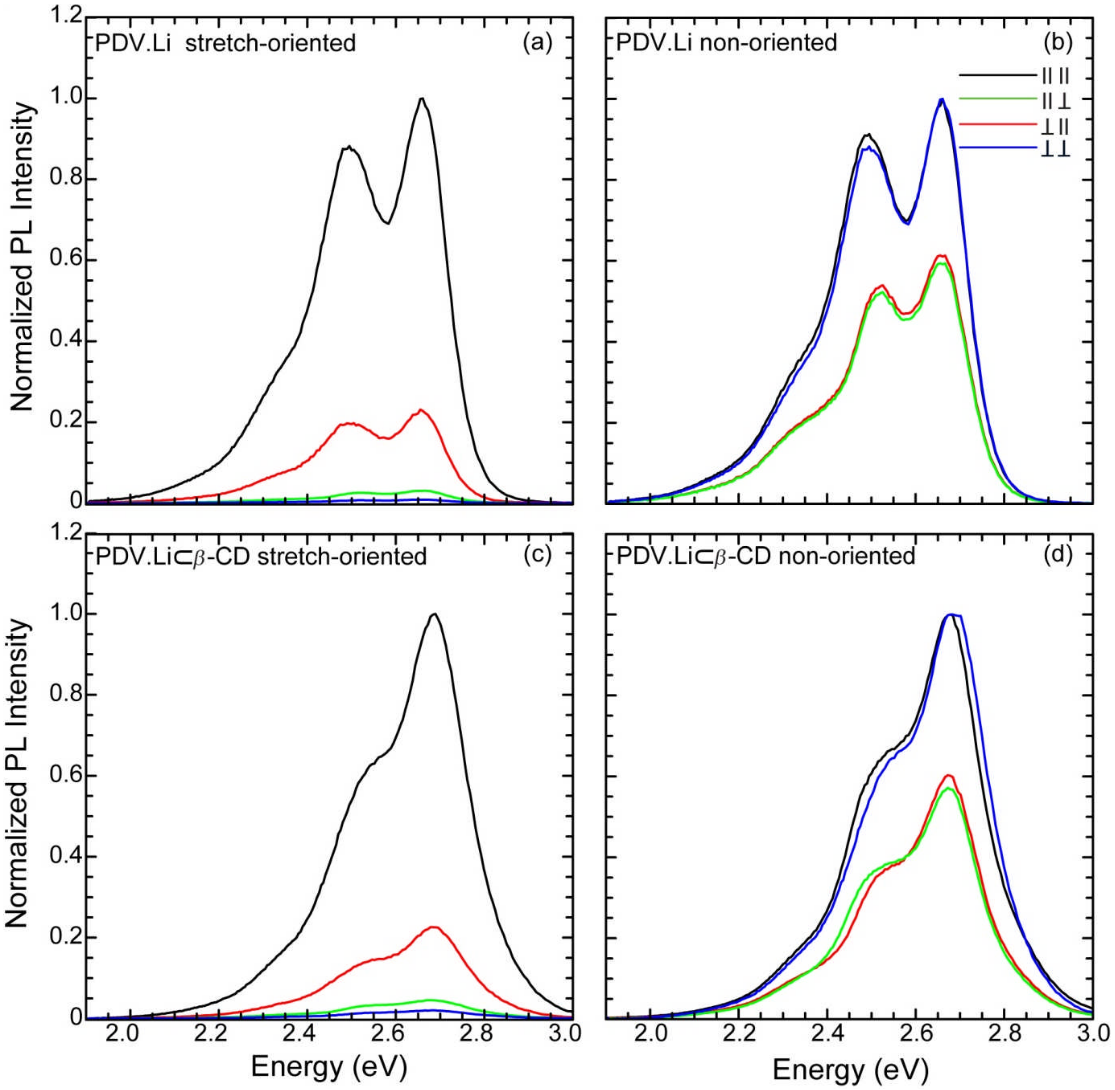

Figure 3.6 PL spectra for stretch-oriented films (a, c) and un-stretched films (b, d) embedding PDV.Li (a, b) or PDV.Li⊂β-CD (c, d). All spectra have been corrected for the overall system response and they were collected using a 3.3 eV laser diode as excitation source.

Interestingly, the results show that the presence of the CDs partially hinders the alignment process. This can be explained by considering that the PVA strands act as the “mediator” of the tensile alignment, and therefore by relating results to the more or less intimate interaction of rotaxanes or analogues with the PVA. For example, the larger cross-section of the rotaxanes should lead to a lower ratio of polymer to PVA strands per unit volume, therefore weakening the effectiveness of PVA as an alignment agent in comparison to the unthreaded material. In addition, the presence of the CDs should partially screen the interaction of PVA with the polar groups, which is conceivably stronger than with the rest of the molecule (rotaxanes or analogues), owing to the polar character of PVA. Furthermore, CDs might also offer preferential interaction points/groups, compared to the polar chains, so that the during the tensile drawing, the straightening of the

PVA strands results in a shuttling of the CDs along the molecular shaft instead of a straightening of the rotaxanes cores.

	$R_{\parallel\parallel/\perp\perp}$	$R_{\parallel\parallel/\perp\parallel}$	$R_{\parallel\parallel/\parallel\perp}$	$R_{\perp\parallel/\parallel\perp}$	$R_{\perp\perp/\parallel\perp}$	$R_{\perp\perp/\perp\parallel}$	D
PDV.Li⊂*β*-CD							
Stretch-oriented	51	4.40	22	5	0.40	0.08	5
Non-stretch-oriented	1	1.70	1.75	1	1.75	1.75	1
PDV.Li							
Stretch-oriented	111	4.40	33	7.40	0.30	0.03	11
Non-stretch-oriented	1	1.60	1.60	1	1.60	1.70	1

Table 3.1 Polarisation and dichroic ratios for films embedding PDV.Li or PDV.Li⊂*β*-CD.

3.3.3. Spectral anisotropy and depolarization

To investigate further the effect of stretching the PL anisotropy $\gamma(E) = (R-1)/(R+2)$ was studied, (Fig. 3.7a, where R(E) is the polarization ratio calculated at energy E), which represents the ratio of the polarised component to the total emitted light, and the time-resolved PL anisotropy (Fig. 3.7b) measurements, $\gamma(t)$ at the PL peak value (~ 2.6 eV) for the configuration $\parallel\parallel/\parallel\perp$ are reported.

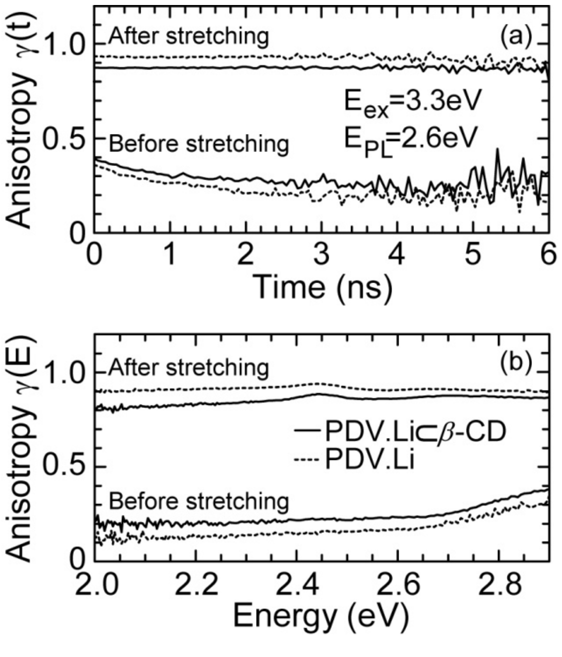

Figure 3.7 (a) PL depolarisation dynamics measured for stretch-oriented and un-stretched films at 2.66 eV for PDV.Li and 2.68 eV for PDV.Li⊂*β*-CD. (b) Spectral dependence of the PL anisotropy obtained by the steady-state spectra in Fig. 3.6 for both stretch-oriented and un-stretched films. The coding is the same in both (a) and (b).

Un-stretched films show $\gamma(t = 0) \sim 0.36$ and $\gamma(t = 0) \sim 0.39$ for PDV.Li and PDV.Li$\subset\beta$-CD respectively. The estimated error on the measurement is 5%, hence both values are near to the maximum theoretical value of $\gamma(t = 0) = 0.4$ for randomly oriented chromophores. This value corresponds to a rotation of the transition moment $\beta = 0°$ hence, the absorption and emission moments of the conjugated chains are collinear.[24] Such level of emission anisotropy is expected for randomly oriented non-interacting chromosphores,[24] as for the polymers dispersed in the PVA matrix investigated here.

Values of $\gamma(t = 0) \sim 0.4$ have been observed before for PDV.Li blends with polyethylene oxide (PEO).[27, 28] $\gamma(t)$ decreases after about 3 ns and stabilizes at a value of ~ 0.17 and ~ 0.22 for PDV.Li and PDV.Li$\subset\beta$-CD respectively, in good agreement with the $\gamma(E)$ values at the PL peak for both films (~ 0.18 and ~ 0.23 for PDV.Li and PDV.Li$\subset\beta$-CD).

The $\gamma(E)$ curves (Fig. 3.7b) show a small increase of the anisotropy between 2 and 2.7 eV and a sharp change at 2.7 eV probably induced by the high self-absorption in this spectral range. A higher value of anisotropy is reported for PDV.Li$\subset\beta$-CD along the whole spectral range, suggesting that rotaxination contributes to the suppression of residual interchain interactions.

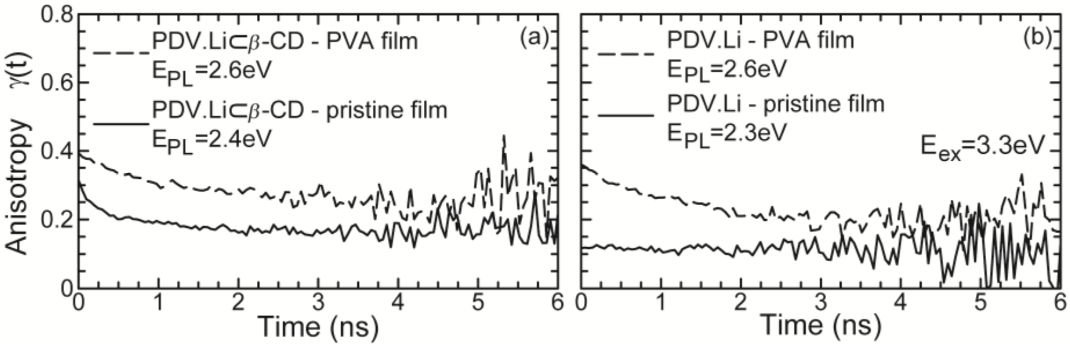

Figure 3.8 PL depolarisation dynamics for un-stretched PVA films (dashed line) and neat films (solid line) of (a) PDV.Li$\subset\beta$-CD and (b) PDV.Li.

For stretched films, it was found instead $\gamma(t) \sim 0.87$ (Fig.7b) and $\gamma(t) \sim 0.93$ for PDV.Li$\subset\beta$-CD and PDV.Li respectively. For both systems, $\gamma(t)$ is constant with time over more than 6 ns, which is approximately one order of magnitude longer than the intrachain exciton lifetime ($\tau \sim 870$ ps). This indicates negligible depolarisation over this time regime. Thus, the data again imply that a remarkable degree of orientation is obtained in both cases, but orientation is slightly better with PDV.Li than with PDV.Li$\subset\beta$-CD, possibly for the reason discussed earlier.

The spectrally-resolved anisotropy, $\gamma(E)$ slowly increases from a value of 0.80 (0.90) at 2 eV to the highest value of 0.88 (0.94) at 2.5 eV for PDV.Li$\subset\beta$-CD (PDV.Li) due to small changes in the PL peaks spectral position between the two configurations.

By comparing the depolarisation dynamics of un-stretched PVA films with those of neat PDV.Li and PDV.Li$\subset\beta$-CD (Fig. 3.8), a major increase in the depolarisation time after the introduction of PVA can be observed. In particular this effect is more pronounced for unthreaded PDV.Li ($\gamma(t = 0) \sim 0.12$ for the pristine PDV.Li film, Fig. 3.8b) where interchain interactions are only suppressed by adding PVA, on the contrary this effect is less intense for PDV.Li$\subset\beta$-CD ($\gamma(t = 0) \sim 0.30$ for the pristine PDV.Li$\subset\beta$-CD film, Fig. 3.8a) where interchain interactions are already reduced by the β-cyclodextrin encapsulation.

3.3.4. Photoluminescence quantum yield and dynamics

The data presented so far indicates that the conjugated polymers are oriented along the stretching direction and PVA strongly suppresses interchain interactions resulting in longer PL depolarisation times and a PL blue-shift. Both these considerations suggest that PVA may form supramolecular complexes with both PDV.Li and PDV.Li$\subset\beta$-CD similarly to what has been observed for polyethylene oxide (PEO).[27-29] While these experiments have been carried out on Li-rotaxanes and analogues, significant changes in the alignment behaviour upon substitution of Li with larger ions are not expected: the only effect likely to occur is a slight reduction of intermolecular interactions brought by larger cations, as discussed in ref.[20]. To investigate this futher, steady-state and time-resolved PL measurements on diluted water solutions of both polymers, in the presence and in the absence of PVA were performed.

For aqueous solutions without PVA, $\Phi_{PL} = 0.17$ for PDV.Li and $\Phi_{PL} = 0.35$ for PDV.Li$\subset\beta$-CD at the concentration of 10^{-3} mg/ml.[19] Importantly, the addition of $9\text{x}10^{-3}$ mg/ml of PVA significantly increases the quantum yield of both polymers: $\Phi_{PL} = 0.73$ for PDV.Li and $\Phi_{PL} = 0.65$ for PDV.Li$\subset\beta$-CD. This high quantum yield is maintained in the films: $\Phi_{PL}= 0.70$ for PDV.Li and $\Phi_{PL}= 0.60$ for PDV.Li$\subset\beta$-CD. For unthreaded PDV.Li, the increase of PL quantum yield is accompanied by a drastic change in the PL decay dynamics (Fig. 3.9). The PL decay kinetics of PDV.Li in the absence of PVA can be fitted with an expression:

$$I(t) = I_0^1 e^{-t/\tau_1} + I_0^2 e^{-t/\tau_2}, \tag{3.20}$$

With τ_1 = 860 ps (intrachain exciton) and τ_2 = 2.6 ns (long-lived interchain species).[30] The addition of PVA strongly suppresses the long-lived component, thus leading to a PL-dynamic:

$$I(t) = I_0 e^{-t/\tau}, \tag{3.21}$$

In this case, a single exponential decay with τ = 870 ps (intrachain exciton), typical of isolated chromosphores in diluted solutions is observed.[19, 30]

As expected, only small changes in the PL-dynamics are observed for PDV.Li$\subset\beta$-CD, since intermolecular interactions are strongly inhibited by the cyclodextrins, especially for polyrotaxanes with high threading ratio (τ = 880 ps).[19]

Interestingly, Φ_{PL} for the polyrotaxane increases by a factor of 1.8 upon addition of PVA to the solution.

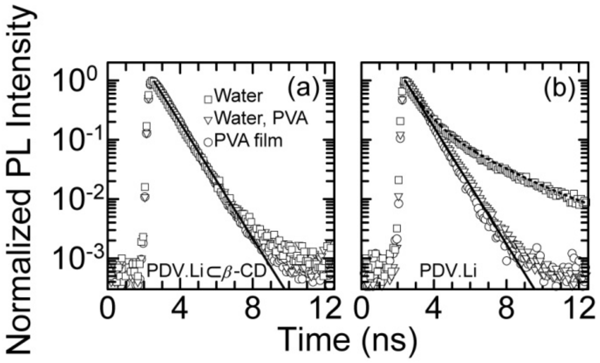

Figure 3.9 PL time decays for water solutions (10^{-3} mg/ml, squares) of (a) PDV.Li$\subset\beta$-CD and (b) PDV.Li in the presence and in the absence of PVA ($9\mathrm{x}10^{-3}$ mg/ml, reversed triangles) and for PVA films (circles). The best fits are reported as solid curves apart from the PDV.Li water solution (dashed curve).

This effect is ascribed to a combination of further reduction of intermolecular aggregation and to the potential sequestering of Li cations (by the PVA matrix) away from the conjugated cores, thus reducing the electrostatic quenching, as observed in the case of PEO.[29]

	τ_1 (ps)	τ_2 (ps)	Φ_{PL} (%)
PDV.Li⊂β-CD			
Water solution (10^3 mg/ml)	**880 ± 40**	**/**	**35 ± 3**
Water solution + PVA ($9*10^3$ mg/ml)	**880 ± 40**	**/**	**65 ± 6**
Film	**880 ± 40**	**/**	**60 ± 6**
PDV.Li			
Water solution (10^3 mg/ml)	**860 ± 40**	**2600 ± 130**	**17 ± 2**
Water solution + PVA ($9*10^3$ mg/ml)	**870 ± 40**	**/**	**73 ± 7**
Film	**870 ± 40**	**/**	**70 ± 7**

Table 3.2 Life time values (τ_1 and τ_2) used in the fit-curves and the Φ_{PL} value for solutions and films.

It is also very interesting to look at the evolution of the average energy, as a function of time, as reported in Fig. 3.10. This clearly shows that the exciton diffusion process is slowed down by addition of PVA to both conjugated moieties, and implies that the emission of photons is mainly from intrachain exciton, in line with previous literature showing that intrachain exciton diffusion is far slower than interchain one.[31]

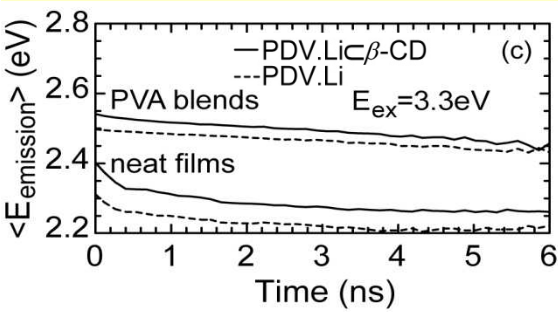

Figure 3.10 Average energy of the emitted photons for PVA and spin-coated films for both conjugated moieties. Data has been calculated from Time-Resolved Emission Spectra (TRES).

3.3.5. Excitation with non-polarised light (hybrid device)

To study the possibility of using these films in actual devices as polarising filters, a hybrid device based on non-polarised inorganic LEDs array as excitation source for our oriented films was fabricated (Fig. 3.11).

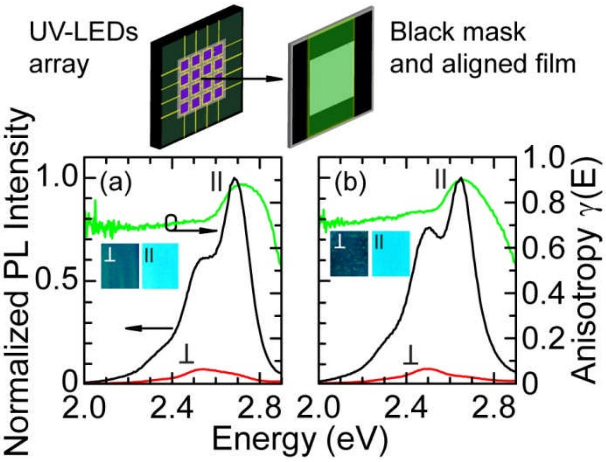

Figure 3.11 PL spectra of stretch-oriented PVA films containing (a) PDV.Li$\subset\beta$-CD and (b) PDV.Li excited by non-polarised light from an GaN LEDs array (E_{peak} = 3.3eV, maximum light output = 1150mW). The respective calculated spectral anisotropy is reported as a green curve. Inset: Pictures of the stretch-oriented films excited by the LEDs array in the two different orientations (parallel and perpendicular to the stretching direction).

$R_{\parallel/\perp}$ = 21 for PDV.Li$\subset\beta$-CD and $R_{\parallel/\perp}$ = 27 for PDV.Li. The spectral anisotropy undergoes a sharp decrease from its highest values of 0.88 (0.90) at 2.6 eV to a lower 0.68 (0.72) for PDV.Li$\subset\beta$-CD (PDV.Li).

3.4. Conclusions

I have shown a new type of highly oriented film prepared using a stretchable polymeric matrix (PVA) embedding conjugated polymers. The remarkable polarisation ratio obtained ($R_{\parallel\parallel/\perp\perp}$= 111 for PDV.Li) indicate that a high degree of orientation is achieved.

The effect of intermolecular interaction on the emission anisotropy has been investigated using supramolecularly encapsulated polymers. Suppressed interchain interactions in polyrotaxanes combined with the PVA matrix result in slower depolarisation of the emitted light which contributes to the overall PL anisotropy. PVA interacts with the conjugated moieties by sequestering Li^+ cations, thus reducing the electrostatic quenching and increasing the PL quantum yield.

A hybrid organic/inorganic device has been fabricated to show that oriented PVA films have significant applicative potential as polarising filters with average polarisation yields of about 80%.

References

[1] M. Grell, D. D. C. Bradley, *Advanced Materials* **1999**, *11*, 895.

[2] D. D. C. Bradley, R. H. Friend, H. Lindenberger, S. Roth, *Polymer* **1986**, *27*, 1709.

[3] D. D. C. Bradley, *Journal of Physics D-Applied Physics* **1987**, *20*, 1389.

[4] U. Lemmer, D. Vacar, D. Moses, A. J. Heeger, T. Ohnishi, T. Noguchi, *Applied Physics Letters* **1996**, *68*, 3007.

[5] C. Soci, D. Comoretto, F. Marabelli, D. Moses, *Physical Review B* **2007**, *75*, 11.

[6] V. Morandi, M. Galli, F. Marabelli, D. Comoretto, *Physical Review B* **2009**, *79*, 8.

[7] J. Cognard, *Molecular Crystals and Liquid Crystals* **1982**, 1.

[8] M. F. Toney, T. P. Russell, J. A. Logan, H. Kikuchi, J. M. Sands, S. K. Kumar, *Nature* **1995**, *374*, 709.

[9] N. Vanaerle, M. Barmentlo, R. W. J. Hollering, *Journal of Applied Physics* **1993**, *74*, 3111.

[10] T. Uchida, M. Hirano, H. Sakai, *Liquid Crystals* **1989**, *5*, 1127.

[11] A. Bolognesi, G. Bajo, J. Paloheimo, T. Ostergard, H. Stubb, *Advanced Materials* **1997**, *9*, 121.

[12] K. Sakamoto, K. Usami, Y. Uehara, S. Ushioda, *Applied Physics Letters* **2005**, *87*, 3.

[13] S. A. Schmid, K. H. Yim, M. H. Chang, Z. Zheng, W. T. S. Huck, R. H. Friend, J. S. Kim, L. M. Herz, *Physical Review B* **2008**, *77*, 8.

[14] Z. J. Zheng, K. H. Yim, M. S. M. Saifullah, M. E. Welland, R. H. Friend, J. S. Kim, W. T. S. Huck, *Nano Letters* **2007**, *7*, 987.

[15] S. Moynihan, P. Lovera, D. O'Carroll, D. Iacopino, G. Redmond, *Advanced Materials* **2008**, *20*, 2497.

[16] M. Mas-Torrent, S. Masirek, P. Hadley, N. Crivillers, N. S. Oxtoby, P. Reuter, J. Veciana, C. Rovira, A. Tracz, *Organic Electronics* **2008**, *9*, 143.

[17] W. Pisula, A. Menon, M. Stepputat, I. Lieberwirth, U. Kolb, A. Tracz, H. Sirringhaus, T. Pakula, K. Mullen, *Advanced Materials* **2005**, *17*, 684.

[18] F. Di Stasio, P. Korniychuk, S. Brovelli, P. Uznanski, S. O. McDonnell, G. Winroth, H. L. Anderson, A. Tracz, F. Cacialli, *Advanced Materials* **2010**, *23*, 1855.

[19] S. Brovelli, G. Latini, M. J. Frampton, S. O. McDonnell, F. E. Oddy, O. Fenwick, H. L. Anderson, F. Cacialli, *Nano Letters* **2008**, *8*, 4546.

[20] G. Latini, L. J. Parrott, S. Brovelli, M. J. Frampton, H. L. Anderson, F. Cacialli, *Advanced Functional Materials* **2008**, *18*, 2419.

[21] P. Bojarski, A. Kaminska, L. Kulak, M. Sadownik, *Chemical Physics Letters* **2003**, *375*, 547.

[22] G. Strobl, *The physics of polymers*, Springer, Berlin **2007**.

[23] W. Becker, *Advanced time-correlated single photon counting techniques*, Springer Science+Business Media, Berlin **2005**.

[24] J. R. Lakowicz, *Principles of Fluorescence Spectroscopy*, Springer Science+Business Media, New York **2006**.

[25] J. C. de Mello, F. H. Wittmann, R. H. Friend, *Advanced Materials* **1997**, *9*, 230.

[26] F. Cacialli, J. S. Wilson, J. J. Michels, C. Daniel, C. Silva, R. H. Friend, N. Severin, P. Samori, J. P. Rabe, M. J. O'Connell, P. N. Taylor, H. L. Anderson, *Nature Materials* **2002**, *1*, 160.

[27] M. H. Chang, M. J. Frampton, H. L. Anderson, L. M. Herz, *Physical Review Letters* **2007**, *98*, 4.

[28] M. H. Chang, M. J. Frampton, H. L. Anderson, L. M. Herz, *Applied Physics Letters* **2006**, *89*, 3.

[29] J. S. Wilson, M. J. Frampton, J. J. Michels, L. Sardone, G. Marletta, R. H. Friend, P. Samori, H. L. Anderson, F. Cacialli, *Advanced Materials* **2005**, *17*, 2659.

[30] A. Petrozza, S. Brovelli, J. J. Michels, H. L. Anderson, R. H. Friend, C. Silva, F. Cacialli, *Advanced Materials* **2008**, *20*, 3218.

[31] E. Hennebicq, G. Pourtois, G. D. Scholes, L. M. Herz, D. M. Russell, C. Silva, S. Setayesh, A. C. Grimsdale, K. Mullen, J. L. Bredas, D. Beljonne, *Journal of the American Chemical Society* **2005**, *127*, 4744.

4. Radiative-rate modifications in photonic crystals self-assembled with conjugated polyrotaxanes

4.1. Introduction

Photonic crystals (PhC) are materials possessing a regular modulation of the dielectric constant (ε_r) in one, two or three dimensions (Fig. 4.1).[1] The study of PhC started in 1987 with two independent publications from Yablonovitch[2] and John[3] on the inhibition of spontaneous emission and light localisation respectively.

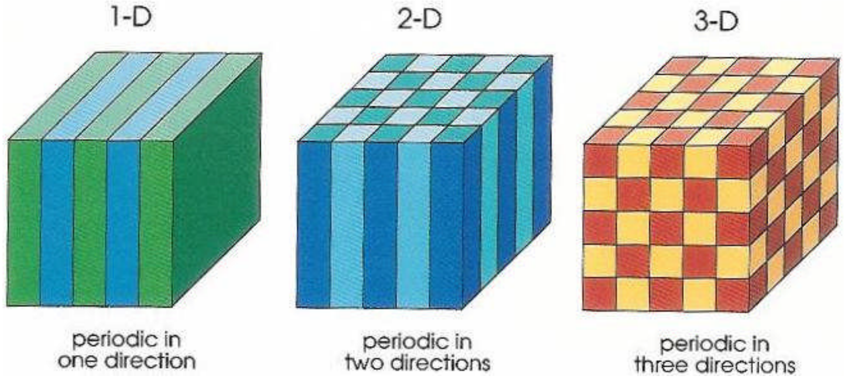

Figure 4.1 Schematic of one-dimensional (left), two-dimensional (centre) and three-dimensional (right) photonic crystals (*Photonic crystals: molding the flow of the light, J.D. Joannopulos, Princeton University Press)*

Typically, PhC are composite materials made of two different mediums (one is usually air or vacuum), of particular interest are PhC with a ε_r periodicity on the scale of visible light or near-infrared due to their technological applications. The behaviour of photons inside a PhC is analogue to charge carriers inside a periodic potential in fact; the ε_r modulation creates a photonic band structure as the electric potential inside a crystalline material, causing forbidden and allowed bands (energies, Fig. 4.2). The optical properties of PhCs can be described using a set of wave equations deriving directly from the Maxwell’s equations, an accurate description and analysis can be found in ref. [4].

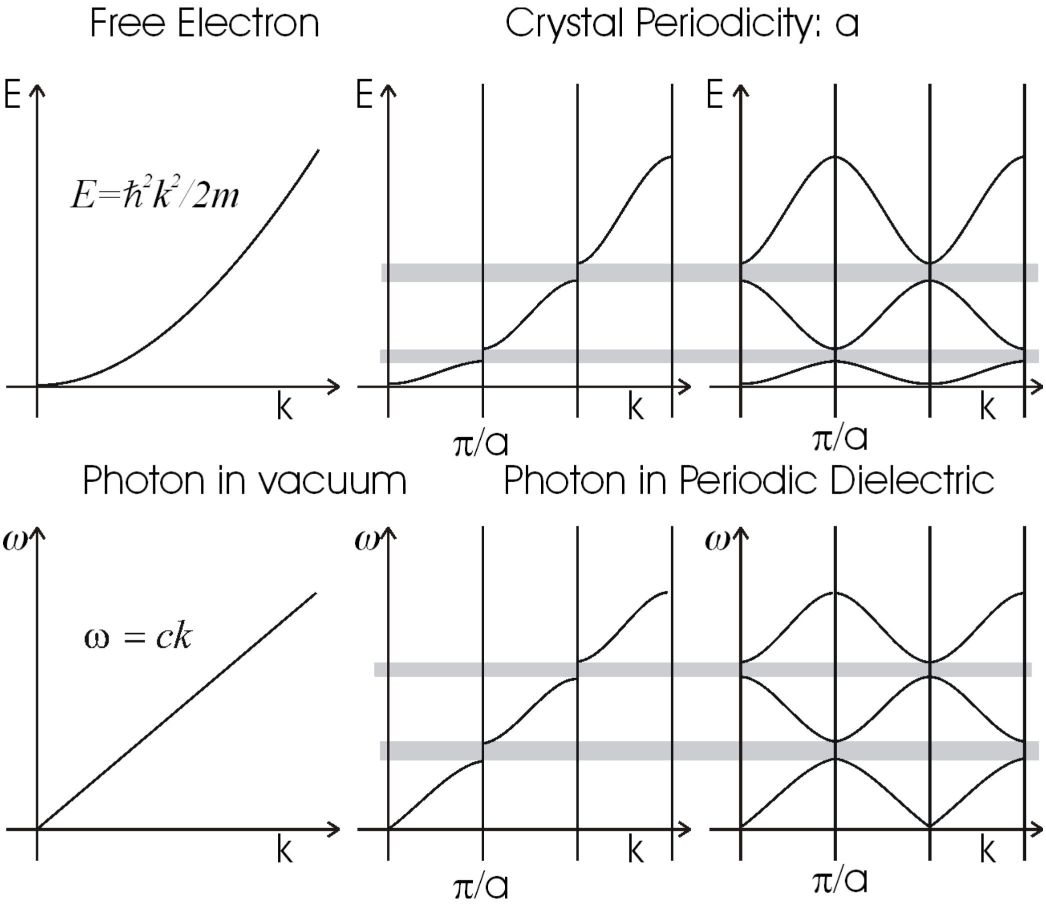

Figure 4.2 Dispersion relations for free electrons and inside a periodic potential (top) and for photons in vacuum and inside a periodic dielectric (bottom) (*Photonic crystals: molding the flow of the light, J.D. Joannopulos, Princeton University Press)*

The formation of forbidden (photonic band gap) and allowed bands in PhCs is caused by interference of diffraction phenomena due to the modulation of ε_r. A simple model to describe it is by considering the PhC as a one-dimensional planar structure.[5] In this way we can apply the Bragg's law for incidence light (Fig. 4.3).

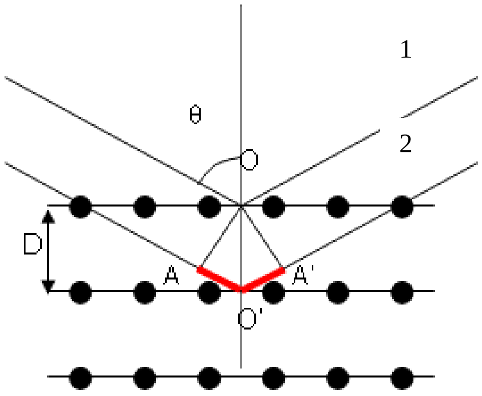

Figure 4.3 Scheme of the diffraction process of two incident beams in a one-dimensional crystal

If we consider the interference between the diffracted beam 1 and 2, their difference in phase (optical path) can be calculated from the sum of the two segments AO+A'O'=$D\cos\theta$. When the difference in optical path is equal to a multiple of the wavelength, the condition of constructive interference is fulfil:

$$m\lambda = 2D\cos\theta, \tag{4.1}$$

With λ the wavelength and θ the angle of the incidence light, D is the spacing between planes.

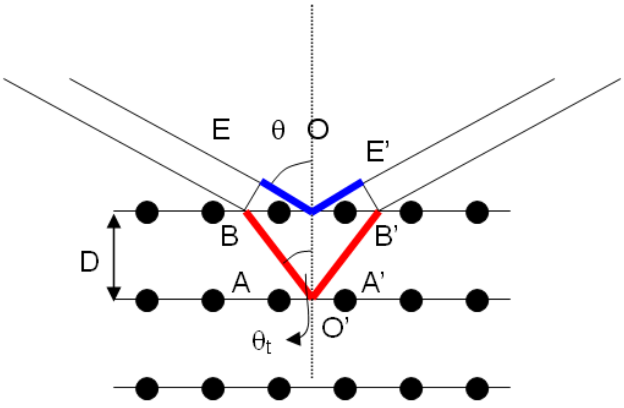

Figure 4.4 Scheme of the diffraction model of one-dimensional photonic crystal

This equation is valid until $\lambda < D$ and if the incidence light is specularly reflected. Since a PhCs possess a periodicity similar or smaller than the wavelength of the incidence light ($\lambda \sim D$), we have to consider the refractive index (n) of the PhC, applying the Snell's law (Fig. 4.4):

$$n_i \sin\theta_i = n_t \sin\theta_t, \tag{4.2}$$

Where θ_i and θ_t are the incidence and refraction angles respectively, and n_i and n_t are the refractive index of the two mediums. As discussed before, PhCs possess a periodical ε_r (hence n, since $n = \sqrt{\varepsilon_r \mu_r}$). To evaluate the refractive index of the PhC we can define an effective refractive index (n_{eff}) using this equation:[6, 7]

$$\frac{\varepsilon_{eff}-\varepsilon_0}{\varepsilon_{eff}+\varepsilon_0} = f\frac{\varepsilon_1-\varepsilon_0}{\varepsilon_1+\varepsilon_0} + (1-f)\frac{\varepsilon_2-\varepsilon_0}{\varepsilon_2+\varepsilon_0}, \tag{4.3}$$

Where ε_{eff} is the effective dielectric constant, ε_0 is the dielectric constant of vacuum ($8.8 \cdot 10^{-12}$ F*m^{-1}) and f is the volume fraction of medium 1 ($f = 0.74$ for a face-centred-cubic structure).

From Eq. 5.2 and 5.3, if $n_i = 1$ (air), we obtain:

$$\sin\theta = n_{eff}\sin\theta_t, \tag{4.4}$$

From Fig. 4.3 we can calculate the optical path once more:

$$m\lambda = 2(n_{eff}BO' - EO), \tag{4.5}$$

We can calculate both BO’ and EO from geometrical considerations from Fig. 4.4, obtaining:

$$BO' = \frac{D}{\cos\theta_t} = \frac{Dn_{eff}}{\sqrt{n_{eff}^2 - \sin^2\theta}}, \tag{4.6}$$

$$EO = BO\sin\theta = (BO'\sin\theta)\sin\theta = \frac{D\sin^2\theta}{\sqrt{n_{eff}^2 - \sin^2\theta}}, \tag{47}$$

Substitution of eq. 4.6 and 4.7 in eq. 4.5, we obtain the Bragg-Snell law:

$$m\lambda = 2\left(\frac{Dn_{eff}^2}{\sqrt{n_{eff}^2 - \sin^2\theta}} - \frac{D\sin^2\theta}{\sqrt{n_{eff}^2 - \sin^2\theta}}\right) = 2D\sqrt{n_{eff}^2 - \sin^2\theta}, \tag{4.8}$$

The energy of the photonic band gap (PBG) can be obtained from the diffraction wavelength calculated from the Bragg-Snell law. Furthermore, the position of the PBG depends on the angle of incidence light. As we will see in the following chapters this simple model describes quite well the synthetic opals here studied.

4.1.1. Optical properties of synthetic opals

Among PhCs, self-assembled structures have been studied in details due to their low fabrication cost and ease of preparation, with artificial opals[2, 3, 8, 9] being especially popular. Synthetic opals are in fact a versatile system that can be infiltrated by vapour phases,[10] or solutions,[8] and therefore enable the investigation of a variety of photonic effects and especially the fine-tuning of optical properties,[11] including the modification of the emission spectra and radiative rates,[12, 13] optical switching,[14] and Fano resonances.[9] Different active materials such as metal nanoparticles,[14] semiconductor nanocrystals[15] or conjugated molecules,[7] can be effectively incorporated into the opals via infiltration.

Synthetic opals are face-centred-cubic (FCC, Fig. 4.5 inset) structure of nanospheres, materials used for opal assembly range from polymers (mainly polystyrene or poly(methyl methacrylate)) to oxides, chalcogenides and metals. Many different deposition methods have been developed during these years, all of them starting from a suspension of nanospheres in water or other solvents. For an overview on materials and deposition techniques used to obtain synthetic opals see the review from C. Lopez et al. in ref. [10].

The dielectric contrast in artificial opals is given by air ($\varepsilon_r = 1$) and the material used for the nanospheres (in our case polystyrene $\varepsilon_r = 2.4\text{-}2.7$).[7] Polystyrene opals are usually classified as “low-dielectric contrast” PhC possessing a complex photonic band structure but a photonic band gap only along the crystallographic direction (111) (perpendicular to the growth direction, Fig. 4.5), i.e. a *pseudo*-photonic band gap (*p*-PBG).

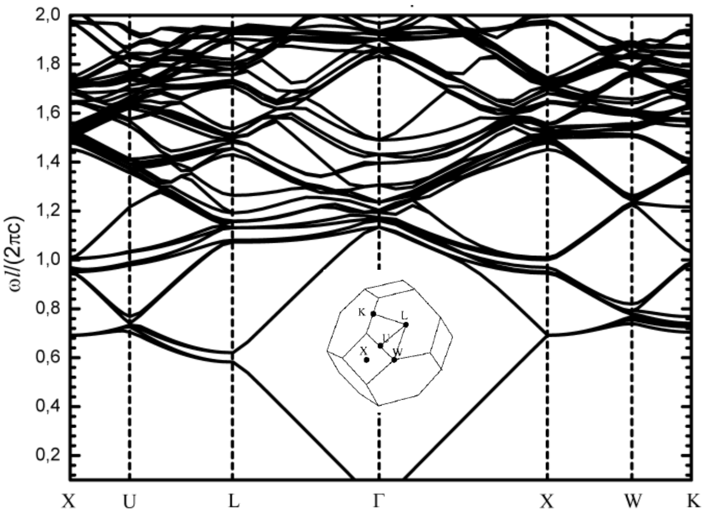

Figure 4.5 Photonic band structure of a synthetic polystyrene opal. The PBG is present along the LΓ direction Inset: FCC lattice structure. (Calculated using the MIT photonic bands software, http://ab-initio.mit.edu/wiki/index.php/MIT_Photonic_Bands)

By tuning the material and the size of the nanospheres, it is possible to change the width of the *p*-PBG and its spectral position respectively (Fig. 4.4).

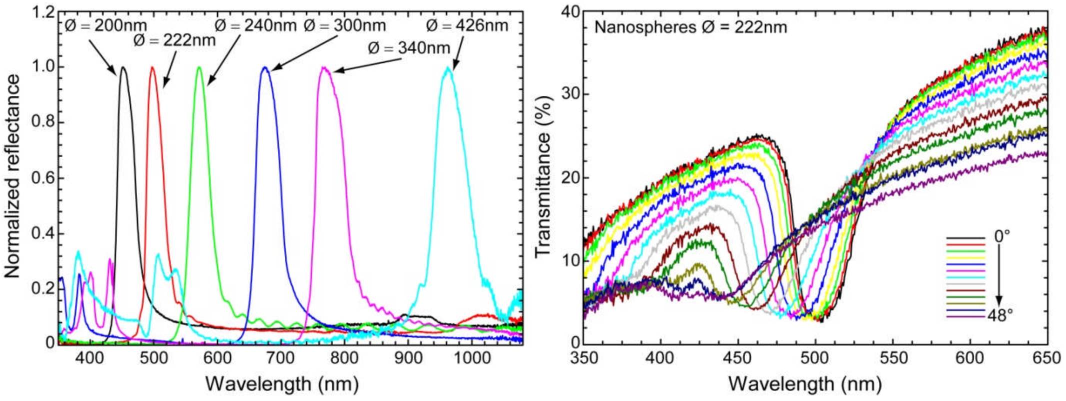

Figure 4.6 Normal incidence reflectance spectra (left) for synthetic opals with different nanospheres size and transmittance spectra at different incidence angle of light (right)

All synthetic opals investigated here were prepared using polystyrene nanospheres. Nevertheless, different diameters were studied to find the suitable nanospheres size. By tuning the size of the nanospheres, it is possible to modify the parameter D in eq. 4.8 (interplanar spacing). In fact, D depends on the diameter of the nanospheres through this simple relation: $D = a\sqrt{2/3}$ where a is the nanospheres diameter. Furthermore, Fig. 4.6 shows a transmittance spectra at different incidence angle of light for a polystyrene opal, as discussed previously the spectral position of the p-PBG depends on the angle of incidence light (θ, eq. 5.8) following the Bragg-Snell law Lattice direction LU in Fig. 4.5).

4.1.2. Photonic density of states

Controlling the density of states (DOS) of embedded emitters in a PhC is one of the main goals in order to use PhCs in actual applications. In fact, the radiative rate of an emitter depends on the density of states (Fermi's golden rule) and by tuning it, is possible to control the emission properties of an emitter inside a PhC. In particular, reducing down the DOS would lead to low-threshold lasing action since the undesirable spontaneous emission can be suppressed and population inversion can be obtained easily.

Spontaneous emission spectra in the surroundings of a *p*-PBG not only show dips connected to forbidden energies, but usually show enhancements too,[7, 13, 16] due to angular redistribution of the emitted photons. Recently Barth et al.[13] have shown that the angular and spectral redistribution of emitted photons from an embedded organic emitter can be explained by considering a redistribution of the DOS along specific directions and positions inside a polystyrene synthetic opal. In particular, by defining the fractional local density of states (FLDOS), i.e. a local density of the states calculated along specific directions, they were able to demonstrate that the photoluminescence (PL) enhancement at the *p*-PBG edge and the PL suppression inside the *p*-PBG observed in the steady-state spectra were due to the FLDOS of the synthetic opal (Fig. 4.6).

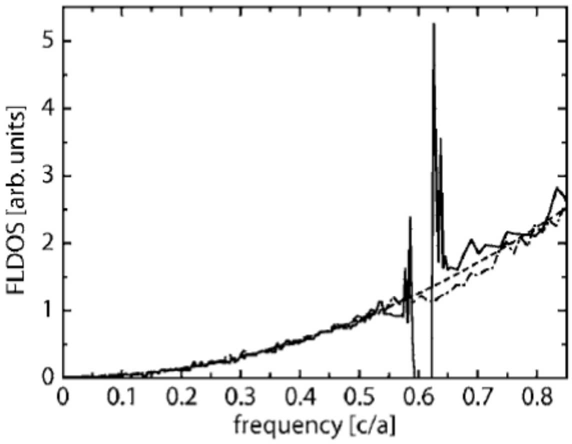

Figure 4.7 Mean value of the FLDOS (solid line) averaged over the whole sphere surface. The dashed line indicates the corresponding behaviour of an effective homogeneous medium. The LDOS (dash-dotted line) is also shown for comparison. (Taken from M. Barth, A. Gruber, F. Chicos, Physical Review B **2005**, 72, 10)

At this is point is quite clear that the PL enhancement/suppression effects induced by the PhC DOS can be observed on the steady-state PL spectra. A more accurate way to study the effect of the DOS on emitters would be study their PL-dynamics. In fact, as discussed before, the radiative rate (K_R) depends on the DOS (Fermi's golden rule):

$$K_R(\omega) = \frac{2\pi}{\hbar}\rho(\mathbf{r},\omega), \tag{4.9}$$

Furthermore, the cross-section for stimulated emission ($\sigma_{SE}(\lambda)$) is directly dependant to the radiative rate of the optical transition (eq. 4.10):

$$\sigma_{SE}(\lambda) = \frac{\lambda^4 f(\lambda) K_R}{8\pi n^2 c}, \tag{4.10}$$

Where $f(\lambda)$ is the normalized PL spectral distribution, n is the refractive index, c is the speed of light. Therefore, by increasing the radiative rate we directly increase $\sigma_{SE}(\lambda)$ i.e. the probability of population inversion.[17]

Petrov et al.[18] in 1998 claimed a modification of the decay rate of an organic emitter inside a SiO_2/polymer opal. Their results became quickly a matter of controversy[19, 20] and still now, many publications report either an increase in the PL-lifetime [13, 15, 21, 22] due to a decrease in the DOS at the PBG, no modifications[23] and a shortening effectof the PL-lifetime[24] due to the DOS.

Considering all the different results in this field, we decided to study the effect of *p*-PBG of a synthetic polystyrene opal on the emission properties of conjugated polyrotaxanes. Processability of emissive materials is obviously crucial to their incorporation into PhCs and, interestingly, water-soluble conjugated polymers with high PL efficiency provide an intriguing opportunity for use in combination with synthetic opals, although only a few attempts have been reported so far.[25-29]

With the *p*-PBG overlapping the PL of the incorporated polyrotaxanes, a suppression of the PL correspondent to the *p*-PBG and an enhancement in correspondence of its high-energy edge was observed. Furthermore, time-resolved measurements revealed a wavelength-dependent modification of the emission lifetime which is shortened at the high-energy edge, but longer inside the stop-band. Both effects are assigned to the modification of the density of photonic states upon tuning the opal stop-band over the PL spectrum of the polyrotaxane.

PhCs preparation was carried out at the "Dept. of Chemistry and Industrial Chemistry, University of Genoa" in collaboration with Mr. Luca Berti and Prof. Davide Comoretto. The conjugated polymers were synthesised at the "Chemistry Research Laboratory, Department of Chemistry, University of Oxford" by Dr. Shane O. McDonnel and Prof. Harry L. Anderson. This study was carried out within the Marie Curie RTN-THREADMILL (MRTN-CT-2006-036040), ITN-SUPERIOR (PTN-CT-2009-238177), the EC FP7 ONE-P large-scale project N. 212311. Work in Genoa is partially supported by the PHOENICS project (CARIPLO FOUNDATION). A manuscript regarding this topic is currently in preparation: "F. Di Stasio, L. Berti, S. O. McDonnel, H. L. Anderson, D. Comoretto, F. Cacialli, *in preparation*"

4.2. Experimental methods

4.2.1. Synthetic opals preparation

Artificial opals are grown by spontaneous assembly of nanospheres into stable and well-defined structures on glass substrates (Fig. 4.8).[30] For the deposition, commercially available polystyrene monodisperse nanospheres water suspension (Duke Scientific, 10% in volume, diameter a = 200, 222 and 260 nm; standard deviation < 5%; refractive index, $n_{PS} = 1.59$), diluted with de-ionized water as necessary to obtain the desired crystal thickness upon complete evaporation of the water were used (d ~ 5 μm).[6, 7] Even though different sphere diameters have been used, the main results discussed here concern spheres with a = 200 nm since these ensure an optimal spectral overlap of the polyrotaxane PL spectrum and the opal stop-band.

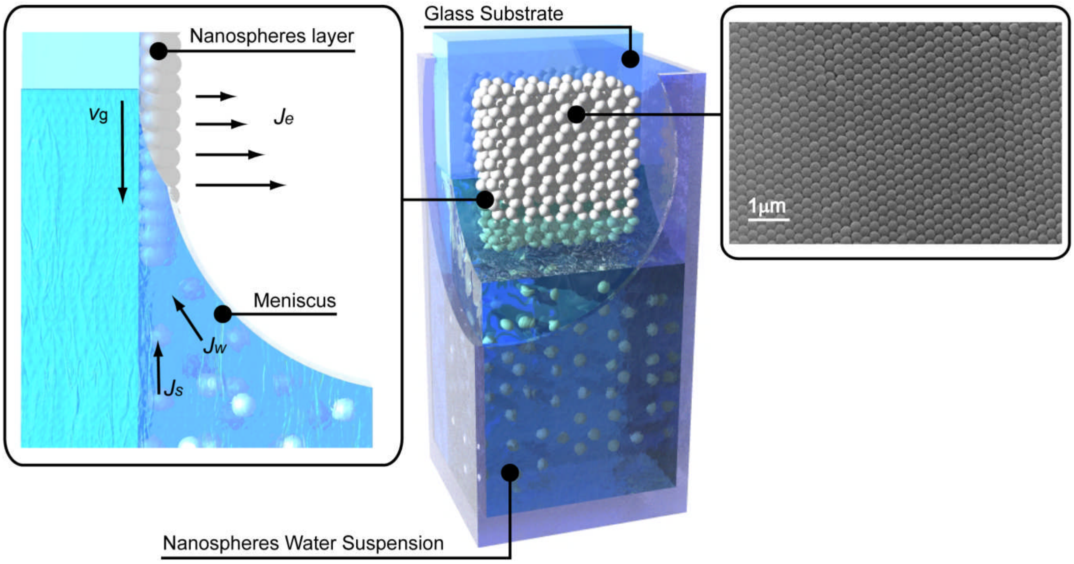

Figure 4.8 Schematic of the vertical deposition technique used to prepare the synthetic polystyrene opals used in this study.

As luminescent semiconductor *β*-CD threaded PDV was used, a polyelectrolytic derivative of poly-*para*-phenylene where sulfonated sidegroups balanced by Li^+ ions afford solubility in polar solvents (PDV.Li⊂*β*-CD, threading ratio = 2,[31] molecular structure in Fig. 4.10). The incorporation of the polyrotaxane takes place during the vertical deposition of the PhC and to make sure that the presence of the polyrotaxane does not hinder or negatively affects the growth of the PhC, a range of concentration for the polyrotaxane water solutions was investigated. A PDV.Li$\subset\beta$-CD concentration of 8x10^{-3} mg/ml yielded homogeneously infiltrated opals without giving rise to the deposition of a polymer layer on its surface (which could affected the intrinsic PhC spectral properties). Furthermore, partial infiltration of voids preserves a reasonable dielectric contrast within the structure, as inferred from lack of spectral shifts and narrowing (broadening) of the stop-band.

4.2.2. Reference sample preparation

As a reference sample to study PL modifications induced by the PhC, the very same opal was used but thermally annealed at 75 °C for 5 minutes. Thermal annealing at 75 °C (Fig. 4.9) is enough to destroy any photonic property of the structure[32] (as proven by the PL spectrum in Fig. 4.11) without changing the PL properties of the conjugated polyrotaxane, due to the higher thermal stability of this class of supramolecular systems.

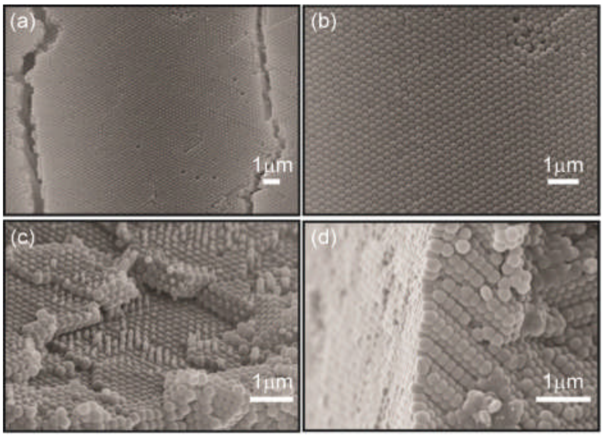

Figure 4.9 SEM micrographs of a polystyrene opal made with 260 nm diameter nanospheres before (a, b) and after (c, d) the thermal annealing at 75 °C for 5 minutes in air.

A modification of the PL properties upon annealing at 75 °C is instead observed for the un-threaded analogue PDV.Li. To be able to compare the different properties, both measurements were carried out in the same area of the sample before and after the thermal process and the PL spectra were normalized at λ = 550 nm, far away from the photonic stop-band (Fig. 4.11).[13]

4.2.3. Optical measurements

Steady-state PL spectra at different incidence angle of the exciting beam were carried out using a pulsed laser diode (λ_{ex} = 371 nm, pulse width ~ 40 ps), a spectrometer (Andor Shamrock 163i) coupled with a CCD camera (Andor Newton CCD, cooled at -50°C) and a rotating stage (M-060.DG, Physik Instrumente, resolution ~ 0.0001°). Time-resolved PL measurements were carried out using a time-correlated single photon counting unit (Edinburgh instruments, F900, time response ~150 ps) and the previous pulsed laser diode as the excitation source. All transmittance (T) and normal incidence reflectance (R) spectra were collected with a setup described in ref. [6, 7].

4.3. Optical properties

4.3.1. Reflectance and transmittance spectra

Fig. 4.10 shows R and T spectra of a typical synthetic opal made with polystyrene beads with diameter *a* = 200 nm. As expected, the peak of reflectance at 455 nm (E_B = 2.74 eV) corresponds to a minimum in the transmittance spectrum. Importantly, no significant changes in the optical properties of the stop-band of the PhC were observed, upon incorporation of the rotaxanes, namely the spectral position of the stop-band and its full width at half-maximum (ΔE_B = 0.16 eV), are unchanged compared to a bare opal.[6, 7] This proves that the incorporation process does not completely fill the interstices between the spheres and then does not significantly change the dielectric contrast of the PhC as well as the lattice periodicity.[14, 33, 34]

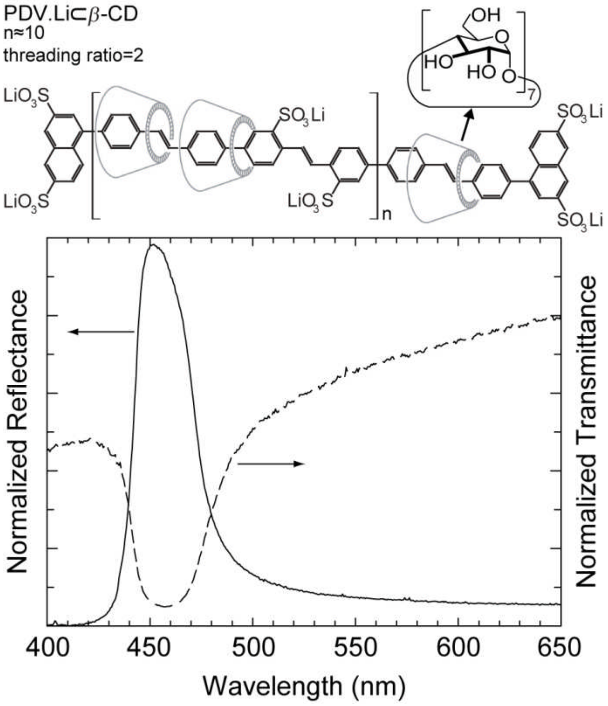

Figure 4.10 Top: Chemical structure of PDV.Li$\subset\beta$-CD, threading ratio = 2, with an average number of repeat units n = 10. Bottom: Reflectance (R, solid line) and transmittance (T, dashed line) spectra of a polystyrene opal film infiltrated with PDV.Li$\subset\beta$-CD (sphere diameter a = 200 nm, refractive index, n_{PS} = 1.59). The full-width-half-maximum of the PBG is not affected by the incorporation process.

4.3.2. Photoluminescence spectra

In Fig. 4.11, PL spectra at different incidence angle of excitation light for the PhCs incorporating PDV.Li$\subset\beta$-CD and the reference sample are shown. First of all, a 50 nm blue-shift of the PL peak and a small increase of the PL quantum yield (Φ_{PL}) to 38 ± 3% (for reference samples) compared to a neat spin-coated film of PDV.Li$\subset\beta$-CD is observed.[35, 36] Such a blue-shift and Φ_{PL}, might be explained by the electrostatic interactions of the Li cations with the negatively charged surface of the polystyrene nanospheres thus changing the polymer structure and then the electronic structure of semiconducting chains close to the surface.

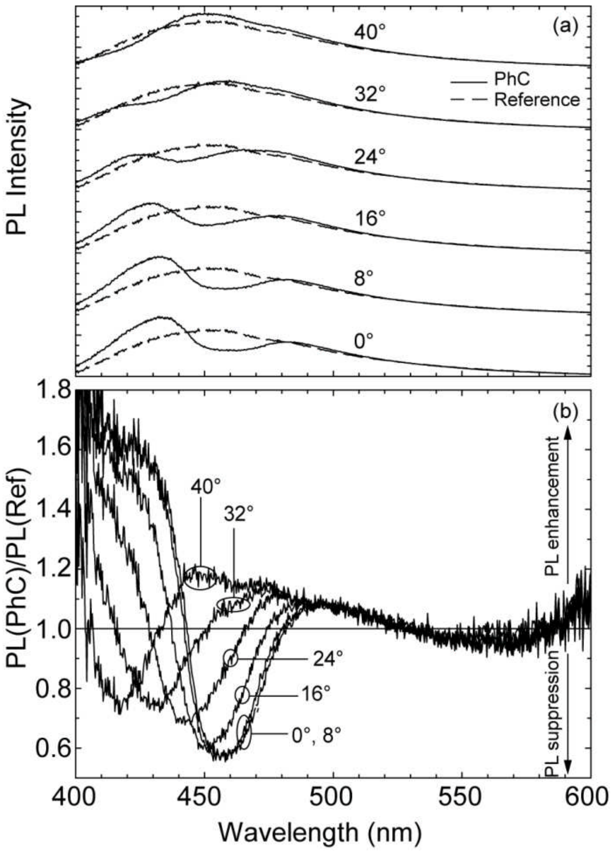

Figure 4.11 (a) PL spectra of an opal film infiltrated with PDV.Li$\subset\beta$-CD before (solid line) and after (dashed line) the thermal treatment at 75 °C at different incidence angle of the exciting beam,[32] (b) ratio between the two PL spectra before and after the thermal process. All spectra were collected in air and at room temperature.

It must be remembered that the conjugated polymer is introduced in the PhC during the opal growth process, which is mainly driven by capillary forces[30] that would also act on the polyrotaxanes and are likely to impose geometrical constraints. These forces might induce an additional interaction of Li cations with the negatively charged surface of the polystyrene nanospheres[30] thus giving a modification of the polymer supramolecular structure affecting the PL dynamics of the polyrotaxane compared to a neat-polymer film or solution.[31] An additional support to this interpretation comes to the similar situation observed in solution of poly(phenylene-ethynylene) polyelectrolytes neat and grafted to silica microspheres, for which a spectral blue shift is observed in agreement with this data.[28]

The PL spectrum of PDV.Li$\subset\beta$-CD (Fig. 4.2 (a) solid line) is strongly modified by the PBG: in particular, the PBG acts as a filter and partially suppresses the light propagation between 448 nm and 482 nm (at 0°). Not only does the filtering effect of the PhC modify the shape of the PL spectrum but, it also induces a decrease (increase) of 33% (measured with respect to our reference system) of the PL intensity in the PBG spectral region (short-wavelength edge of the PBG). Both enhancement and suppression depend on the incidence angle of the excitation light as the PBG suggesting that both effects are connected to a directional redistribution of the photonic density of states.[7, 13]

The enhancement/suppression effects driven by the PhC are even clearer if we calculate the ratio between the two PL spectra (Fig. 4.11 (b)). Note that within the PBG the ratio is lower than 1, instead the ratio is above 1 for the short-wavelength edge of the PBG.[7, 13, 15, 16]

4.3.3. Time resolved photoluminescence measurements

To gain further insight into the underlying photophysics of these photonic structures time-resolved PL measurements at the relevant wavelengths were carried out, i.e. at 437 nm, where an enhancement of the PL spectrum is observed, and at 460 nm within the photonic stop-band, where the emission is suppressed (Fig 12). In previous studies, the PL decay dynamics of polyrotaxane films have been fitted with a double exponential expression and assigned to the *intramolecular* singlet exciton and *inter*-molecular aggregate states.[31] Surprisingly, for these photonic structure a triple exponential expression had to be used: $I(t) = I_0 + I_1 e^{-(\frac{t}{\tau_1})} + I_2 e^{-(\frac{t}{\tau_2})} + I_3 e^{-(\frac{t}{\tau_3})}$ whose parameters are reported in Table 4.1. The longer decays, namely τ_2 and τ_3, are assigned to the ones previously reported for this type of polyrotaxane (τ_{exciton} ~ 850 ps, $\tau_{\text{aggregate states}}$ ~ 2600 ps).[31] This suggests that the (fast) additional decay mechanism could be related to a new emissive specie arising from the interaction of the polyrotaxane with the nanospheres surfaces inside the PhC. Such interaction is also likely to induce the observed blue-shift of the PL and the increase in Φ_{PL}. This hypothesis is further supported by the observation of a three-exponential decay in the annealed reference sample too, thus indicating that such complicated de-excitation pathway is observed only in the presence of polyrotaxane/colloid interaction. Furthermore, this interpretation is in agreement with the relative intensities of all processes which are substantially the same for the PhC and the reference at both wavelengths.

Turning to the analysis of the PL-decays and radiative rates, the long decay in the ns domain is not affected by the opal having almost the same value in the reference film (2650 ps at 437 nm and 2750 ps at 460 nm) as well as in neat spin-coated films.

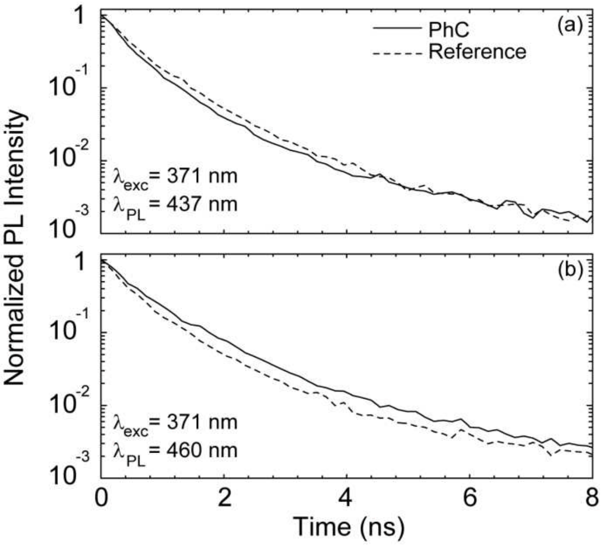

Figure 4.12 Temporal evolution of the PDV.Li⊂β-CD PL measured at the short-wavelength edge (a, 437 nm) and inside (b, 460 nm) the PBG before (solid line) and after (dashed line) the thermal treatment at 75°C for 5 minutes. All measurements were carried out in air and at room temperature.

At the short-wavelength edge of the stop-band (437 nm) the decay for the infiltrated opal is shorter than for the reference (~ 11%, estimated from the weighted mean of τ_1 and τ_2) whereas within the stop-band (460 nm) the reverse situation occurs (~ 13%). Expectedly, Both these effects are smaller than those observed for PhC with higher dielectric contrast,[15] but it is remarkable to observe such modifications at such a low-dielectric contrast as that achieved with the polystyrene opals investigated here.[13, 15, 16]

	τ_1, ps (I_1)	**τ_2**, ps (I_2)	**τ_3**, ps (I_3)
437 nm (high energy PBG edge)			
PhC	300 ± 15 (0.33)	790 ± 40 (0.56)	2720 ± 140 (0.11)
Reference	370 ± 20 (0.33)	860 ± 40 (0.57)	2650 ± 130 (0.10)
460 nm (PBG)			
PhC	430 ± 20 (0.32)	950 ± 50 (0.55)	2850 ± 140 (0.13)
Reference	365 ± 20 (0.34)	860 ± 40 (0.53)	2750 ± 140 (0.13)

Table 4.1 Lifetime values (τ_1, τ_2, τ_3) used in the fit-curves the temporal evolution of the PL (the relative contribute of each time constant is included in parentheses). We estimated an error of 5% on the measured value

Indeed, a sizable effect on the radiative lifetime (Purcell effect)[37] can only be observed in photonic crystals for which the photonic density of states is strongly modified in the whole *k*-space. In this case the PBG is present only along the [111] (ΓL) crystallographic direction and it is spectrally narrow when compared to the width of the PL spectrum, thus reducing the observable effect.[13] Furthermore, Φ_{PL} of PDV.Li$\subset\beta$-CD in the reference sample is ~ 38 ± 4%, meaning that the radiative rate (K_R) is smaller than the non-radiative rate (K_{NR}, $K_R < K_{NR}$) and so, any modification caused by a redistribution of the photonic density of the states will have a small effect on the PL lifetime.

Interestingly, the PL lifetime modification here observed is wavelength dependent with a precise overlap with the PBG spectrum. According to this observation and previously reported experiments[7, 13] this effect can be assigned to the modification of the density of photonic states along the ΓL direction, even though alternative explanations cannot be ruled out.[16]

4.3.4. Radiative rate analysis

As a first order approximation, the modification of the PL lifetime can be considered as only induced by the redistribution of the photonic density of states. If we consider Φ_{PL} as the sum of contributions of the 3 emissive species, we obtain:

$$\Phi_{PL} = I_1\Phi_{PL1} + I_2\Phi_{PL2} + I_3\Phi_{PL3}, \tag{4.11}$$

Where I_x is the relative contribution to the total PL intensity (as obtained from the PL-decays) of all emissive species. As previously discussed, τ_2 and τ_3 are similar to previously measured values; we can assume that τ_2 corresponds to a Φ_{PL} of ~ 35% being its PL-lifetime is similar to the one measured in PDV.Li$\subset\beta$-CD diluted water solutions (where the emission is mainly due to intrachain exciton).[31] Instead, we can assume τ_3 corresponds to a Φ_{PL} of ~ 3% since its PL-lifetime is similar to the one measured for PDV.Li films (where the emission is mainly due to aggregate states).[38] From these two considerations, we can calculate a Φ_{PL} for the "blue-emitting specie" (τ_1) of ~ 52 ± 5 %.

From Φ_{PL} and τ we can calculate K_R and K_{NR} using this simple equation:

$$\Phi_{PL} = \frac{K_R}{K_R + K_{NR}}, \tag{4.12}$$

Since we do not know Φ_{PL} for PDV.Li$\subset\beta$-CD after the photons redistribution takes place in the PhC, we can only calculate K_R and K_{NR} for the reference sample. Nevertheless, the variation of the photonic density of states only affects K_R leaving K_{NR} unchanged (Fermi's golden rule, $K_R(\omega) = \frac{2\pi}{\hbar}\rho(\mathbf{r},\omega)$, where ρ is the photonic density of states). Knowing K_{NR} from the reference sample we can calculate K_R from $\tau = \frac{1}{K_R + K_{NR}}$.

	Blue-emitting specie (τ_1)	**Intrachain exciton (τ_2)**	**Aggregate states (τ_3)**
437 nm (high energy PBG edge)			
$K_{R(PhC)}$ s^{-1} ($x10^8$)	19.8 ± 2	5.1 ± 0.5	0.10 ± 0.01
$K_{R(Reference)}$ s^{-1} ($x10^8$)	13.5 ± 2	4.1 ± 0.4	0.10 ± 0.01
460 nm (PBG)			
$K_{R(PhC)}$ s^{-1} ($x10^8$)	9.5 ± 0.9	3.0 ± 0.3	0.10 ± 0.01
$K_{R(Reference)}$ s^{-1} ($x10^8$)	13.6 ± 2	4.1 ± 0.4	0.10 ± 0.01
K_{NR} s^{-1} ($x10^8$)	13.7 ± 2	7.5 ± 0.7	3.5 ± 0.3

Table 4.2 Radiative (K_R) and non-radiative (K_{NR}) rates for PDV.Li$\subset\beta$-CD incorporated inside the PhC and in the reference sample. All rates were calculated using the model proposed in the text. We include an error of 10% on the calculated value.

From this model we are able to calculate an increase of K_R of 46 and 24% at the high-energy PBG edge (437 nm), and a decrease of 31 and 27% inside the PBG (460 nm) for τ_1 and τ_2 respectively. τ_3 seems completely unaffected by the redistribution of the photonic density of states; a possible explanation of this is once again the large K_{NR} that is not modified by the presence of the PhC leaving the modification of the K_R too small to be estimated or measured (Table 4.2).

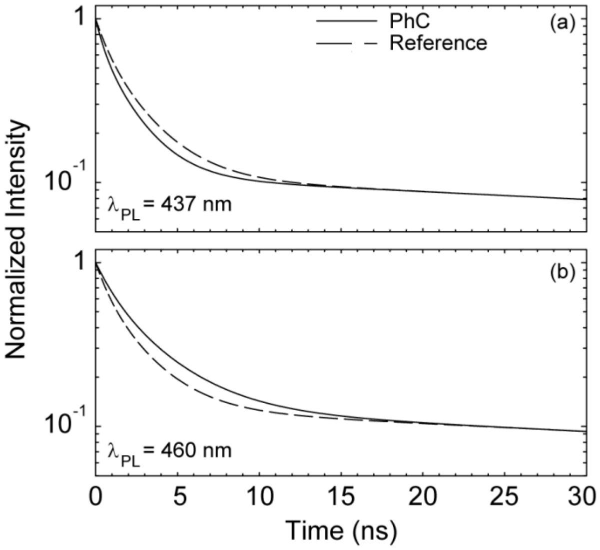

Figure 4.1013 Radiative decay for PDV.Li$\subset\beta$-CD incorporated into the PhC (solid line) and in the reference sample (dashed line) at 437 nm (a, high energy PBG edge) and at 460 nm (b, inside the PBG).

By plotting the radiative decay $I(t) = I_0 + I_1 e^{-K_{R1}t} + I_2 e^{-K_{R2}t} + I_3 e^{-K_{R3}t}$ (Fig. 4.13), the modification in dynamics between PDV.Li$\subset\beta$-CD incorporated into the PhC and in the reference sample is even clearer, showing a sizeable effect of the PhC on the radiative lifetime of PDV.Li$\subset\beta$-CD.

4.4. Conclusions

In conclusion, an all-plastic water solution processable photonic crystal functionalized with a novel class of supramolecular conjugated polymer grown in a single step process was investigated. The photoluminescent PhC exhibits an enhancement and suppression (both 33%) of the steady-state PL intensity of the embedded polyrotaxane. Furthermore, a wavelength dependent modification of the PL lifetime is observed correspondent to the enhancement/suppression spectral regions. Using a simple model to analyse the various rates an increase in the radiative of 46% and 24% at the high-energy PBG edge (437 nm), and a decrease of 31 and 27% inside the PBG (460 nm) for τ_1 and τ_2 respectively is observed. All effects can be connected to a modification of the photonic density of states occurring at the photonic band gap and at its short-wavelength edge which modify the radiative rate of the incorporated conjugated polymer even though alternative explanations cannot be ruled out.

References

[1] J. D. Joannopulos, R. D. Meade, J. N. Win, *Photonic crystals: molding the flow of the light*, Princeton University Press, Princeton **1995**.

[2] E. Yablonovitch, *Physical Review Letters* **1987**, *58*, 2059.

[3] S. John, *Physical Review Letters* **1987**, *58*, 2486.

[4] K. Sakoda, *Optical properties of photonic crystals*, Springer, New York **2001**.

[5] E. Hecht, *Optics*, Addison Wesley Longman New York **1998**.

[6] F. Di Stasio, L. Berti, M. Burger, F. Marabelli, S. Gardin, T. Dainese, R. Signorini, R. Bozio, D. Comoretto, *Physical Chemistry Chemical Physics* **2009**, *11*, 11515.

[7] L. Berti, M. Cucini, F. Di Stasio, D. Comoretto, M. Galli, F. Marabelli, N. Manfredi, C. Marinzi, A. Abbotto, *Journal of Physical Chemistry C*, **2010**, *114*, 2403.

[8] C. Lopez, *Advanced Materials* **2003**, *15*, 1679.

[9] M. V. Rybin, A. B. Khanikaev, M. Inoue, K. B. Samusev, M. J. Steel, G. Yushin, M. F. Limonov, *Physical Review Letters* **2009**, *103*, 4.

[10] J. F. Galisteo-Lopez, M. Ibisate, R. Sapienza, L. S. Froufe-Perez, A. Blanco, C. Lopez, *Advanced Materials* **2011**, *23*, 30.

[11] A. Pasquazi, S. Stivala, G. Assanto, V. Amendola, M. Meneghetti, M. Cucini, D. Comoretto, *Applied Physics Letters* **2008**, *93*, 3.

[12] I. S. Nikolaev, P. Lodahl, W. L. Vos, *Physical Review A* **2005**, *71*, 10.

[13] M. Barth, A. Gruber, F. Cichos, *Physical Review B* **2005**, *72*, 10.

[14] V. Morandi, F. Marabelli, V. Amendola, M. Meneghetti, D. Comoretto, *Advanced Functional Materials* **2007**, *17*, 2770.

[15] P. Lodahl, A. F. van Driel, I. S. Nikolaev, A. Irman, K. Overgaag, D. Vanmaekelbergh, W. L. Vos, *Nature* **2004**, *430*, 654.

[16] L. Bechger, P. Lodahl, W. L. Vos, *Journal of Physical Chemistry B* **2005**, *109*, 9980.

[17] S. Schols, *Device architecture and materials for organic light-emitting devices*, Springer Science+Business Media, New York **2011**.

[18] E. P. Petrov, V. N. Bogomolov, Kalosha, II, S. V. Gaponenko, *Physical Review Letters* **1998**, *81*, 77.

[19] M. Megens, H. P. Schriemer, A. Lagendijk, W. L. Vos, *Physical Review Letters* **1999**, *83*, 5401.

[20] E. P. Petrov, V. N. Bogomolov, Kalosha, II, S. V. Gaponenko, *Physical Review Letters* **1999**, *83*, 5402.

[21] A. C. Arsenault, T. J. Clark, G. V. Freymann, L. Cademartiri, R. Sapienza, J. Bertolotti, E. Vekris, S. Wong, V. Kitaev, I. Manners, R. Z. Wang, S. John, D. Wiersma, G. A. Ozin, *Nature Materials* **2006**, *5*, 179.

[22] I. S. Nikolaev, P. Lodahl, W. L. Vos, *Journal of Physical Chemistry C* **2008**, *112*, 7250.

[23] A. F. Koenderink, L. Bechger, H. P. Schriemer, A. Lagendijk, W. L. Vos, *Physical Review Letters* **2002**, *88*, 143903.

[24] S. Kubo, A. Fujishima, O. Sato, H. Segawa, *Journal of Physical Chemistry C* **2009**, *113*, 11704.

[25] T. L. Kelly, Y. Yamada, C. Schneider, K. Yano, M. O. Wolf, *Advanced Functional Materials* **2009**, *19*, 3737.

[26] Q. L. Fang, J. L. Geng, B. H. Liu, D. M. Gao, F. Li, Z. Y. Wang, G. J. Guan, Z. P. Zhang, *Chemistry-a European Journal* **2009**, *15*, 11507.

[27] R. C. Polson, A. Chipouline, Z. V. Vardeny, *Advanced Materials* **2001**, *13*, 760.

[28] K. Kim, S. Webster, N. Levi, D. L. Carroll, M. R. Pinto, K. S. Schanze, *Langmuir* **2005**, *21*, 5207.

[29] M. Deutsch, Y. A. Vlasov, D. J. Norris, *Advanced Materials* **2000**, *12*, 1176.

[30] A. S. Dimitrov, K. Nagayama, *Langmuir* **1996**, *12*, 1303.

[31] S. Brovelli, G. Latini, M. J. Frampton, S. O. McDonnell, F. E. Oddy, O. Fenwick, H. L. Anderson, F. Cacialli, *Nano Letters* **2008**, *8*, 4546.

[32] M. Cucini, M. Alloisio, A. Demartini, D. Comoretto, in *Biomimetic and Supramolecular System Research*, (Ed: A. H. Lima), Nova Science, New York **2008**, 91.

[33] V. Morandi, F. Marabelli, V. Amendola, M. Meneghetti, D. Comoretto, *Journal of Physical Chemistry C* **2008**, *112*, 6293.

[34] W. L. Vos, R. Sprik, A. v. Blaaderen, A. Imhof, A. Lagendijk, G. H. Wegdam, *Physical Review B* **1996**, *53*, 16231.

[35] F. Cacialli, J. S. Wilson, J. J. Michels, C. Daniel, C. Silva, R. H. Friend, N. Severin, P. Samori, J. P. Rabe, M. J. O'Connell, P. N. Taylor, H. L. Anderson, *Nature Materials* **2002**, *1*, 160.

[36] G. Latini, L. J. Parrott, S. Brovelli, M. J. Frampton, H. L. Anderson, F. Cacialli, *Advanced Functional Materials* **2009**, *19*, 3679.

[37] E. M. Purcell, *Physical Review* **1946**, *69*, 681.

[38] A. Petrozza, S. Brovelli, J. J. Michels, H. L. Anderson, R. H. Friend, C. Silva, F. Cacialli, *Advanced Materials* **2008**, *20*, 3218.

5. Organic light-emitting diodes with self-assembled monolayers functionalized anodes

5.1. Introduction

Achieving high efficiency organic light-emitting diodes (OLED) is a crucial step to guarantee the exploitation of this class of devices in modern technology. Two main roads have been followed so far, the synthesis of conjugated polymers with high photoluminescence efficiency and the engineering of device structures.[1, 2] Modification of electrodes using self-assembled monolayers (SAMs) is a promising technique for organic emitting diodes (LEDs) and thin-film transistors (TFTs). In fact, SAMs can be used to tune the work function (WF) of electrodes,[3-7] changing charge-injection barriers at the metal/organic film interface.

The most common materials used as anode is indium tin oxide (ITO), mainly because of its distinctive property of being conductive and transparent to visible light. However, the WF of as-deposited ITO (4.7 eV) still remains lower than the HOMO level of conjugated polymers (usually between 5.7 and 6.3 eV) hindering the injection of holes into the active layer. Multiple transport/injection interlayers can be used to provide an energy stepping profile for holes to be injected into the emissive polymer.[1] On the other hand, a direct change of the WF of the anode would reduce the cost of multiple polymer layers deposition and the risk of polymer intermixing. As an example, recently Helander et al.[8] have demonstrated that, by directly functionalising the ITO anode with Cl, the ITO WF increases up to 6.1 eV, thus enhancing the efficiency of the OLED as a consequence of the lower hole injection barrier at the anode.

SAMs are highly ordered supramolecular arrays of molecules chemisorbed on metal substrates[9] and the design of their molecular structure is crucial to confer specific functions to the resulting surface.[10] In general, the presence of an interfacial dipole associated to a SAM is responsible for changing the WF (Fermi level, E_F) of metallic contacts[11-13]. Among the vast family of SAMs, azobenzenes are known to undergo a well-defined isomerisation from -trans to –cis conformation (Fig. 5.1) around the N=N bond, in response of an external stimulus such as UV-light.[14-16] The two conformations show different properties[17, 18] and when in a SAM they show different wettability,[19] conductance[20] and dipole moment.[21] The UV-induced change in conformation (and properties) of the azobenzenes SAMs (AZO-SAMs) here investigated has been studied in ref.[10].

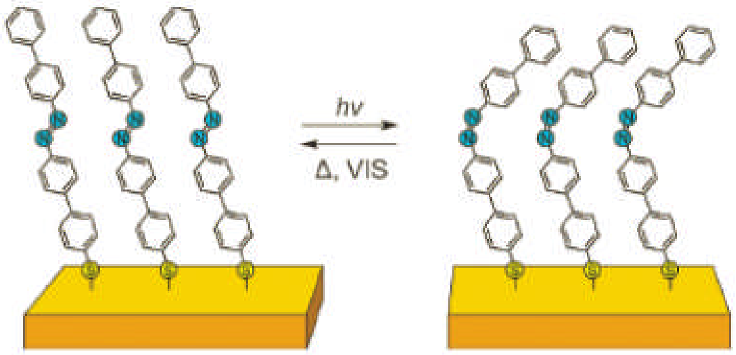

Figure 5.1 Scheme of the trans- cis- transition of the AZO-SAM. (Reproduced from ref. 10)

In this work, SAMs based on two different conjugated azobenzene derivatives and their influence on the gold work function (WF_{Au}) was studied. In particular, these SAMs ahow an increase in the external quantum efficiency (EQE) of polyfluorene base light-emitting diodes (LEDs) connected with an increase in the anode WF. Photoluminescence (PL) and electroluminescence (EL) measurements showed that AZO-SAMs did not modify the emission properties of the active layer. Instead, AZO-SAMs enhanced the EQE of LEDs from 0.018% to 0.18% and decreased the turn-on voltage from 7.9 V to 6.2 V by reducing the injection barrier at the anode thus providing a better balance between holes and electrons in the active layer. This phenomenon was studied experimentally using electroabsorption spectroscopy.

AZO-SAMs preparation was carried out by Dr. Nuria Crivillers and Prof. Paolo Samori at "ISI-CNRS, University of Strasbourg". This work was supported by the EC Marie-Curie IEF-OPTSUFET (PIEF-GA-2009-235967), ITN-SUPERIOR (PITN-GA-2009-238177) and RTN-THREADMILL (MRTN-CT-2006-036040), the EC FP7 ONE-P large-scale project no. 212311, the NanoSci-E+ project SENSORS and the International Center for Frontier Research in Chemistry (FRC, Strasbourg). The results in experimental methods, optical and electronic properties and conclusions are published in: "N. Crivillers, A. Liscio, F. Di Stasio, C. Van Dyck, S. Osella, D. Cornil, S. Mian, G. M. Lazzerini, O. Fenwick, E. Orgiu, F. Reinders, S. Braun, M. Fahlman, M. Mayor, J. Cornil, V. Palermo, F. Cacialli, P. Samori, *Physical Chemistry Chemical Physics* **2011**, *13*, 14302,". Other two publications regarding this topic are currently in preparation: "G. M. Lazzerini, S. Mian, F. Di Stasio, N. Crivillers, P. Samori, F. Cacialli, *in preparation*" and "N. Crivillers, A.

Liscio, G.M. Lazzerini, C. Van Dyck S. Osella, D. Cornil, S. Mian, F. Di Stasio, O. Fenwick E. Orgiu, F. Reinders, S. Braun, M. Fahlman, M. Mayor, J. Cornil, V. Palermo, F. Cacialli, P. Samorì, *in preparation*"

5.2. Experimental Methods

5.2.1. Self-assembled monolayers preparation

Azobenzene based self-assembled monolayers (AZO-SAMs, Fig. 5.2) were prepared by immersion of the Au substrates in a 0.1 mM solution of the azobenzene derivative in chloroform for 48h. Afterward samples were rinsed and finally dried with nitrogen gas. As a substrate, an Au film of 5 nm thickness deposited onto indium-tin-oxide (ITO) treated with oxygen plasma (15 min at 10.2 W)[22-25] was used obtaining a homogeneous Au grains size.[10, 16, 26] Thermal deposition of the Au adhesion layer was performed at 450 °C, deposition rate 0.01 nm*s^{-1} and pressure 1*10^{-6} mbar.

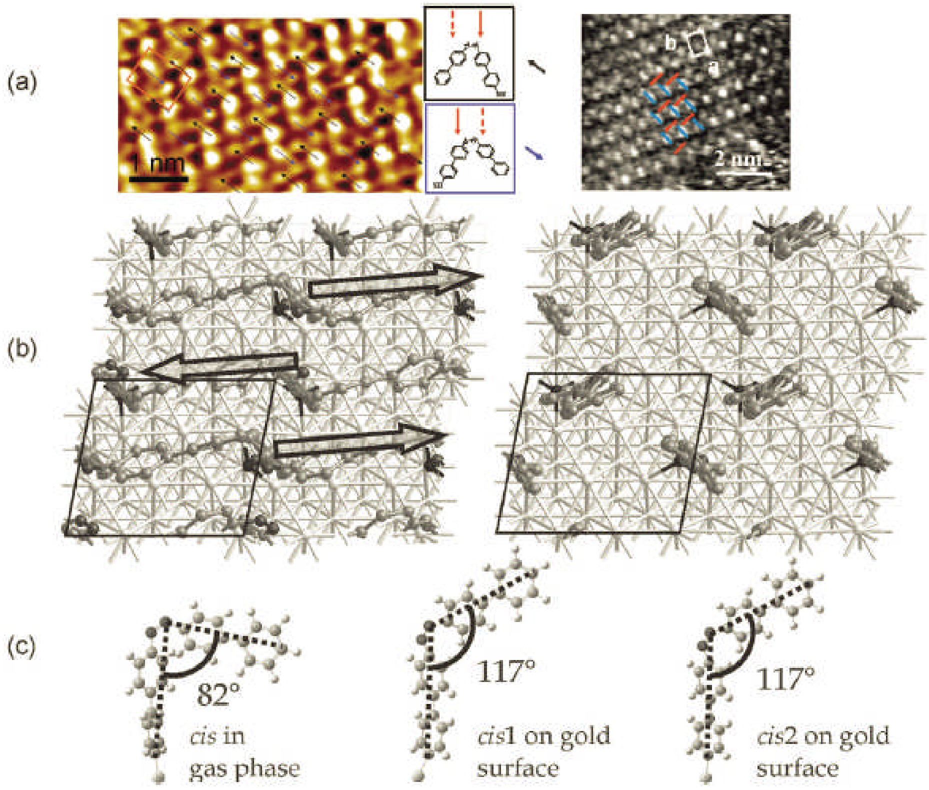

Figure 5.2 (a) Scanning tunnelling microscope images of the cis- and trans- configurations of the AZO-SAM. (b) Optimized geometries of the unit cell for the cis- (left) and trans- (right) configurations, arrows show the opening direction of the cis-form to compare with the STM image; (c) optimized geometry of the cis- configuration in a gas phase (left) and of the two independent molecules in the unit cell on the Au surface (right). (Reproduced from ref. 10 and ref. 16)

5.2.2. Devices preparation

Devices (Fig. 5.3) were prepared using the SAM/Au/ITO-coated glass substrates previously described.

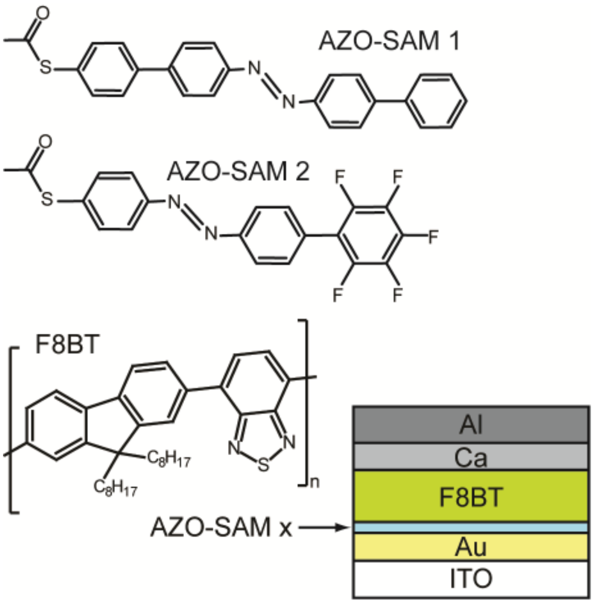

Figure 5.3 Chemical structures of the two self-assembled monolayers studied and poly(9,9'-dioctylfluorene-alt-benzothiadiazole) (F8BT) used as active layer in light-emitting diodes. Bottom: structure of the light-emitting diodes studied.

The steps following oxygen plasma treatment and Au functionalization were then carried out inside a N_2 glove-box (M-Braun) and consisted in spincoating (1.8 krpm) a 120 nm thick poly(9,9'-dioctylfluorene-alt-benzothiadiazole) (F8BT, American Dye Source, Mw = 73000, 2% w/w in toluene, Chemical structure in Fig. 5.3) emissive layer on top of the AZO-SAM x/Au/ITO anode and the thermal evaporation of a Ca (30 nm) cathode with a 150 nm Al protective layer (for LEDs used in the electroabsorption study only Al was used). In addition to the functionalized Au, two types of reference samples were also prepared: ITO/F8BT/Ca-Al (ITO samples, F8BT spin-coated directly on oxygen-plasma-treated ITO) and ITO/Au/F8BT/Ca-Al (Au samples, with no AZO-SAMs on the Au anode). AZO-SAMs were exposed to air prior the spin-coating of the active layer. The set-ups used for EL and PL characterization of devices and films is reported in ref.[27, 28].

Electrical characterisation was carried out measuring the device current and light output as a function of the applied voltage. The current was measured by a Keithley 2400 source meter, which also supplied the voltage. The luminous output was measured with a calibrated silicon photodiode. The electroluminescence spectrum was collected with an Andor Newton EMCCD camera coupled with an Andor SHAMROCK 163 spectrograph.

5.2.3. Electroabsorption measurements

Electroabsorption spectroscopy (Fig. 5.4) is a technique that studies the optical absorption of a sample under the influence of a modulated electric field. The optical absorption change is due to the Stark effect affecting excitons in the conjugated polymer (named after J. Stark, who discovered it in 1903). [29-31]

In general, the intensity of transmitted light (I) depends on the absorption coefficient α and can be written as:[32-34]

$$I = I_0(1-R)^2 e^{-\alpha d}, \tag{5.1}$$

Where I_0 is the intensity of incidence light, R is the reflection coefficient and d is the thickness of the sample. The application of an electric field (E) induces a change in R and α (the modification of R is usually neglected for high absorption):[32, 34]

$$\frac{\partial I}{\partial E} \sim -\, d I_0 e^{-\alpha d} \frac{\partial \alpha}{\partial E}, \tag{5.2}$$

If we divide eq. 5.2 for the initial intensity (E=0) we obtain:

$$\frac{\Delta I}{I} = -d\Delta\alpha, \tag{5.3}$$

As written before, the change in the optical absorption is due to the Stark effect, i.e. splitting of energy levels. In particular the Stark effect can de described with two different components: one linear (linear Stark effect) and a second one quadratic to the applied electric field (quadratic Stark effect).

The linear Stark effect is induced by permanent dipoles in the electronic states, this effect can be described by:

$$\Delta\varepsilon^{(1)} = -\Delta\boldsymbol{m} * \boldsymbol{E}, \tag{5.4}$$

Where Δm is the dipole moment variation between two states. Conjugated polymers do not possess a permanent dielectric dipole. However, disorder and defects in the structure allows the formation of permanent dipoles, i.e. a linear Stark effect.[34, 35]

The quadratic Stark effect is caused by the interaction between the electric field and the field induced dipole. In general, it can be expressed in terms of difference in the polarizability of the ground and the excited state (Δp):[34, 35]

$$\Delta\varepsilon^{(2)} = -\frac{1}{2}\Delta p E^2, \tag{5.5}$$

Finally, if we combine the two effects the complete shift ($\Delta\varepsilon$) can be written as:

$$\Delta\varepsilon = -\boldsymbol{m} * \boldsymbol{E} - \frac{1}{2}\Delta p E^2, \tag{5.6}$$

The linear effect induces usually bigger shifts (177 μeV) than the quadratic ones (33 μeV, as reported by Harrison et al.).[35] Interestingly, for the linear component the optical absorption follows the line shape of the second derivative, while for the quadratic one it follows the first derivative.[34]

Changes in the absorption coefficient ($\Delta\alpha = \alpha(E) - \alpha(0)$) can be connected to $\Delta\varepsilon$ via a Taylor expansion of $\alpha(E+\Delta E)$ until the second power of ΔE:[32-34, 36, 37]

$$\Delta\alpha = \langle\frac{\partial\alpha}{\partial E}\Delta E\rangle + \frac{1}{2}\langle\frac{\partial^2\alpha}{\partial E^2}\Delta E^2\rangle, \tag{5.7}$$

If we insert eq. 6.7 in eq. 6.3 we obtain:[32]

$$\frac{\Delta I}{I} = -dE^2\left(b\frac{\partial\alpha}{\partial E} + c\frac{\partial^2\alpha}{\partial E^2}\right), \tag{5.8}$$

From eq. 6.8 we can see as the electroabsorption signal ($\Delta I/I$) depends on E^2. This can be used to probe the internal field of organic light-emitting diodes. Experimentally, the electroabsorption signal is small and a modulation technique based on lock-in amplifiers is necessary to measure it thus using an applied voltage V containing a DC component (V_0) and an AC one ($V_{AC}\cos(\omega t)$) obtaining:[32]

$$\frac{\Delta I}{I} \propto \chi\left(V_{AC}^2\frac{1+\cos(2\omega t)}{2} + 2V_{Ac}V_0\cos(\omega t) + V_0^2\right), \tag{5.9}$$

Where χ is the optical susceptibility($\Delta I/_I \sim \chi E^2$). Using lock-in amplifiers is possible to select either the first harmonic (ωt) or the second one (2ωt):

$$\frac{\Delta I}{I}(\omega) \propto \chi(V_{Ac}V_0\cos(\omega t)), \tag{5.10}$$

$$\frac{\Delta I}{I}(2\omega) \propto \chi\left(V_{AC}^2\frac{\cos(2\omega t)}{2}\right), \tag{5.11}$$

Considering that $V_0=V_{DC}+V_{BI}$, (V_{BI} is the built-in potential of the device), if $\Delta I/I = 0 \Rightarrow V_{DC} = V_{BI}$, this allows us to directly evaluate the built-in potential (i.e. the difference in work functions of electrodes) using the electroabsorption technique.[38]

A scheme of the electroabsorption set-up used in this study is shown in Fig. 5.4. The set-up was build and optimized during the last 10 years by three PhD student: Thomas Brown,[33] Vladimir Bodrozic[34] and Gustaf Winroth.[32]

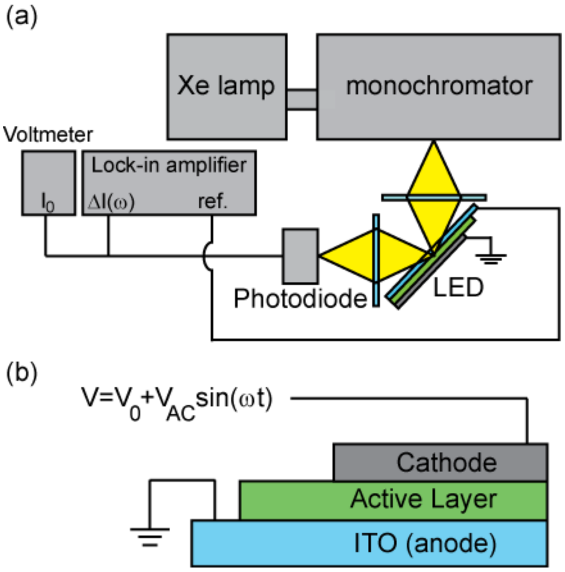

Figure 5.4 (a) Scheme of the electroabsorption set-up used in this study. (b) Scheme of an LED and how it is driven.

The electroabsorption set-up consists of three different parts: a monochromatic light source (ozone-free Xenon lamp coupled with a monochromator, working range 300-900 nm), a lock-in amplifier (Stanford Research Systems SRS830, driving the device with a DC and AC voltage, Fig. 5.4b) and a detection system, i.e. a photodiode connected to the same lock-in amplifier, and a voltmeter to so as to detect the AC and DC components corresponding to the change in transmission (ΔI) and the intensity of the light beam (I_0) respectively.[32]

As described before, an second lock-in amplifier can be used to detect the second harmonic of the output signal (I(2ω)). The entire user interface was developed by Thomas Brown and Vladimir Bodrozic using LabView software.

5.3. Optical and electronic properties

5.3.1. Electroabsorption measurements (built-in voltage)

As previously described, the linear dependence of the electroabsorption (EA) signal on the applied voltage can be used to determine the built-in voltage of light-emitting diodes (LEDs).[39-41] All measurements were carried out at room temperature at the EA signal peak, by irradiating at λ = 505 nm, while applying a sinusoidal voltage V_{AC} = 0.5 V at frequency f= 2 kHz, and with the optical probe entering the device through the semitransparent electrode (Au/ITO). The wavelength used to probe the device (λ = 505 nm) will not induce a trans- to cis- isomerisation since this phenomenon takes place only when the sample is irradiated with UV light.[10] The zero crossing voltages were obtained from an average of 10 measurements over 2 different pixels.

In Fig. 5.5 the EA signals as a function of the applied voltage is shown for LEDs embedding AZO-SAM 1 and AZO-SAM 2. In the ideal condition of negligible charge building up in the active layer (F8BT) the EA signal is null (V_{null}) when the applied voltage is equal and opposite to the built-in voltage (V_{BI}) of the LED (i.e. generated by the equalisation of the Fermi energies through the LED and so equal to the WF difference between cathode and anode).[10, 38]

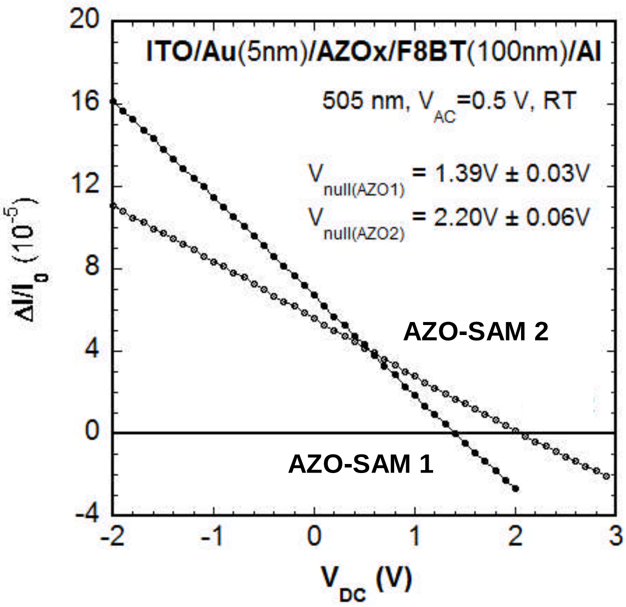

Figure 5.5 EA signal as function of the applied voltage for AZO-SAM 1 (filled circles) and AZO-SAM 2 (open circles). The V_{null} values are reported as inset

V_{null} values of 1.39 V and 2.20 V for AZO-SAM 1 and AZO-SAM 2 respectively were measured. In order to estimate the WF of the self-assemble monolayer, it is necessary to know the WF of the anode (Al) and the lowest unoccupied molecular orbital (LUMO) energy of the active layer (F8BT, only in case of cathodic pinning of the Fermi energy to the F8BT LUMO). The F8BT LUMO energy lies between 3.2 and 3.5 eV, instead the Al WF decreases below 3.5 eV only upon exposure to oxygen during evaporation.[42-44] Our Al electrodes give an average WF of 3.7-3.8 eV.[45] Considering this cathodic pinning can be ruled out and it is possible to calculate the anode WF using eq. (5.12):[44]

$$V_{null} = \frac{(WF_{anode} - WF_{cathode})}{e}, \tag{5.12}$$

Where e is the elementary charge. Using this equation,values of 5.2 and 5.9 eV for AZO-SAM 1 and AZO-SAM 2 respectively were calculated. Both AZO-SAMs induce an increase of the WF of the anode from ~ 5.1 eV for Au.[44]

5.3.2. Current density-Voltage-Luminance curves

In Fig. 5.6 the current density (J, Fig. 5.6a) and luminance (L, Fig. 5.6b) vs applied bias (V) for the ITO, Au, AZO-SAM 1 and AZO-SAM 2 LEDs are reported. For a given voltage (15.5 V), J drastically drops from 95 mA/cm^2 (ITO samples) to 7 mA/cm^2 for Au samples and then increases again to 62 mA/cm^2 and 110 mA/cm^2 for AZO-SAM 1 and AZO-SAM 2 samples respectively. Similarly, the luminance L at J = 120 mA/cm^2 decreases from 54 cd/m^2 for the ITO sample to 13 cd/m^2 for AZO-SAM 1 and then increases one order of magnitude up to 650 cd/m^2 for AZO-SAM 2. For the Au sample, only a maximum L = 5 cd/m^2 at 20 V with J = 34 mA/cm^2 is reached. The external quantum efficiencies (EQEs) are 0.018 % for the ITO sample, 0.006 % for the Au sample, 0.004 % for AZO-SAM 1 and 0.18 % for AZO-SAM 2. Finally, the light turn-on voltage, V_{on}, increases from 7.9 V for the ITO sample to 13.1 V for the Au sample and then reduces progressively to 8.1 V and 6.2 V for AZO-SAM 1 and AZO-SAM 2 respectively.

Although the insertion of the 5 nm Au layer causes an increase of V_{on} from 7.9 V to 13.1 V, as well as a drastic reduction of the conductivity and EQE from 0.018 % to 0.006 %, the insertion of the AZO-SAM 2 compensates for this detrimental effect.

For AZO-SAM 1, the EQE slightly reduces to 0.004 %, however the conductivity increases and the light turn-on voltage reduces from 13.1 V (Au sample) to 8.1 (AZO-SAM 1), which allows to reduce the driving voltage of the device and subsequent device degradation. This can be attributed to the reduction of conductivity and increase of V_{on} upon insertion of the Au layer to a decrease of the WF, thus reducing the number of holes injected into the F8BT layer (HOMO = 5.9 eV).

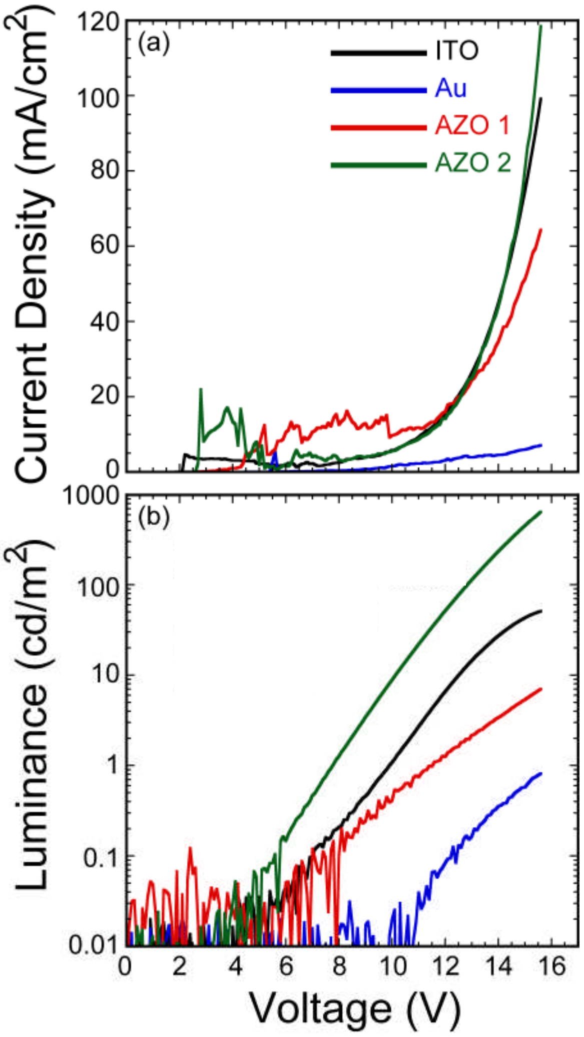

Figure 5.6 Current density-voltage (a) and (semi-logarithmic) luminance-voltage (b) plots for all OLEDs. Color code is the same in both panels.

Upon functionalization of the Au layer with AZO-SAM 1, the WF of the anode increases[10] of ~ 0.1 eV to ~ 5.2 eV, thus providing a lower injection barrier than Au anodes. However, AZO-SAM 1 EQE does not increase with the conductivity and it is possible that the number of holes injected is still too low compared to the number of electrons injected in the active layer, thus keeping the recombination-zone near the F8BT/AZO-SAM 1/Au interface. As a consequence, the emission can suffer from electrostatic quenching induced by the Au/ITO (image charge effect).

Instead, the EQE of the AZO-SAM 2 device is 30 times higher than the EQE of the Au one and shows a tenfold increase with respect to the ITO one. Furthermore, a reduction of V_{on} to 6.2 V is observed and it can be attributed to the increase in WF. As a consequence the e^--h^+ balance in the F8BT layer improves, thus leading to an increase of the EQE and reduction of V_{on}.

5.3.3. Photoluminescence and electroluminescence spectra

In Fig. 5.7 (a, b) the spectral characteristics of emission, PL and EL, of all LEDs are shown. They all show 2 main peaks at 2.15 eV and 2.24 eV, which correspond to the emission of F8BT,[46] and any further peak in either PL or EL spectra was observed. In addition, time resolved PL measurements (Fig. 5.8) reveal a mono-exponential decay with time constant τ of 1.0 ± 0.1 ns for ITO, 0.89 ± 0.09 ns for Au, 0.90 ± 0.09 ns for AZO-SAM 1 and 0.95 ± 0.1 ns for AZO-SAM 2 which can be attributed to singlet decay in F8BT. [46] The use of AZO-SAMs does not induce changes in the PL-dynamics at the AZO-SAM/F8BT interface, and radiative recombination only occurs in the F8BT active layer.

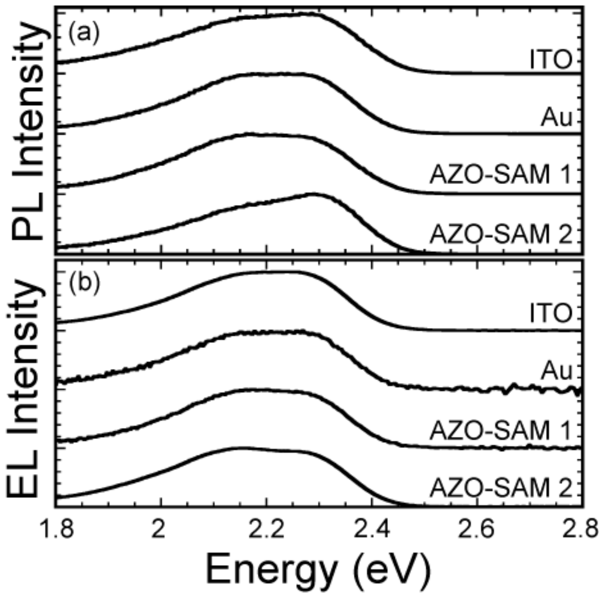

Figure 5.7 Steady-state PL (a) and EL (b) spectra of all devices investigated (from top to bottom, ITO, Au, AZO-SAM 1 and AZO-SAM 2, curves have been offset for clarity). All measurements were conducted at room temperature, and the PL was excited by a pulsed diode laser (E_{ex} = 3.3 eV, pulse width ~ 40 ps).

The functionalization of the Au anode with the AZO-SAMs does not affect the spectral emission. Furthermore, the PL-lifetime (τ) of ITO samples is lower ($\tau < 1$ ns) that the one reported by Kim et al.[46] (2.4 ns) with a similar device structure. This might be explained by a higher non-radiative rate of the F8BT used and a more efficient PL quenching at the interface between F8BT and ITO. This would also explain the lower EQE for ITO samples compared to the one reported by Kim et al. As the ITO is coated with 5 nm Au, τ reduces from 1.0 ns to 0.89 ns and it can be assigned to a further increase of the non-radiative component caused by electrostatic quenching at the Au/F8BT interface. Interestingly, after the functionalization of Au with AZO-SAMs, τ increases to 0.90 ns and 0.95 ns due to AZO-SAMs acting as spacers between the Au and the F8BT, thus reducing the PL quenching. However, it is worth noting that τ varies < 7 % between Au and AZO-SAM 2 and so is possible that the small thickness of the AZO layer (~ 5 nm) only limits the PL quenching, but does not completely prevent it.

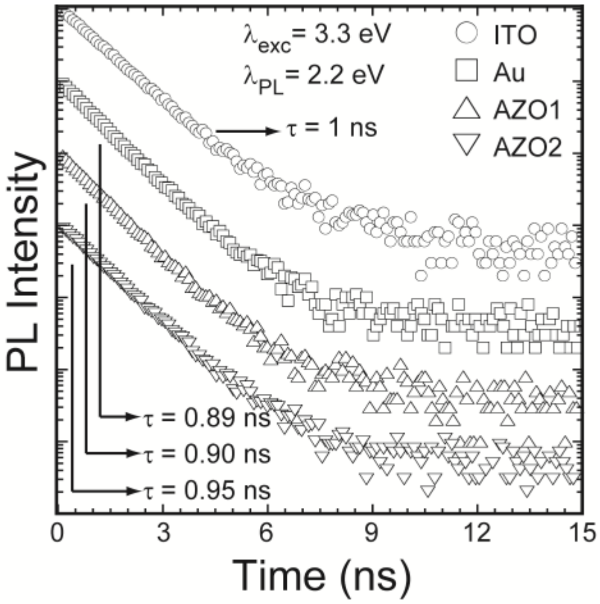

Figure 5.8 Temporal evolution of the PL collected at 2.24 eV for all OLEDs (from top to bottom, ITO, Au, AZO-SAM 1 and AZO-SAM 2, curves have been offset for clarity). A single exponential decay of the type: $I(t) = I_0+I\exp(-t/\tau)$ is used to fit the decay of all the samples (values of τ are reported in figure). All measurements were conducted at room temperature.

5.4. Conclusions

In conclusion, despite the EQE of LEDs with Au anodes reduce in comparison to LEDs with oxygen-plasma-treated ITO anodes, the functionalization of Au with azobenzene-based SAMs tune the WF of Au and eventually increase the EQE up to 10 times. Steady-state PL and EL and time-resolved PL measurements of these devices prove that AZO-SAMs do not modify the emission spectra (EL or PL) of F8BT and the emission only occurs from decay of singlets in the emissive layer.

References

[1] P. K. H. Ho, J.-S. Kim, J. H. Burroughes, H. Becker, S. F. Y. Li, T. M. Brown, F. Cacialli, R. H. Friend, *Nature* **2000**, *404*, 481.

[2] R.-Q. Png, P.-J. Chia, J.-C. Tang, B. Liu, S. Sivaramakrishnan, M. Zhou, S.-H. Khong, H. S. O. Chan, J. H. Burroughes, L.-L. Chua, R. H. Friend, P. K. H. Ho, *Nature Materials* **2010**, *9*, 152

[3] G. S. Tulevski, C. Nuckolls, A. Afzali, T. O. Graham, C. R. Kagan, *Applied Physics Letters* **2006**, *89*, 3.

[4] N. Koch, *Chemphyschem* **2007**, *8*, 1438.

[5] D. Natali, L. Fumagalli, M. Sampietro, *Journal of Applied Physics* **2007**, *101*, 12.

[6] J. Zaumseil, H. Sirringhaus, *Chemical Reviews* **2007**, *107*, 1296.

[7] L. J. Wang, G. M. Rangger, L. Romaner, G. Heimel, T. Bucko, Z. Y. Ma, Q. K. Li, Z. Shuai, E. Zojer, *Advanced Functional Materials* **2009**, *19*, 3766.

[8] M. G. Helander, Z. B. Wang, J. Qiu, M. T. Greiner, D. P. Puzzo, Z. W. Liu, Z. H. Lu, *Science* **2011**, *332*, 944.

[9] J. C. Love, L. A. Estroff, J. K. Kriebel, R. G. Nuzzo, G. M. Whitesides, *Chemical Reviews* **2005**, *105*, 1103.

[10] N. Crivillers, A. Liscio, F. Di Stasio, C. Van Dyck, S. Osella, D. Cornil, S. Mian, G. M. Lazzerini, O. Fenwick, E. Orgiu, F. Reinders, S. Braun, M. Fahlman, M. Mayor, J. Cornil, V. Palermo, F. Cacialli, P. Samori, *Physical Chemistry Chemical Physics* **2011**, *13*, 14302.

[11] R. W. Zehner, B. F. Parsons, R. P. Hsung, L. R. Sita, *Langmuir* **1999**, *15*, 1121.

[12] K. Asadi, F. Gholamrezaie, E. C. P. Smits, P. W. M. Blom, B. de Boer, *Journal of Materials Chemistry* **2007**, *17*, 1947.

[13] P. Stoliar, R. Kshirsagar, M. Massi, P. Annibale, C. Albonetti, D. M. de Leeuw, F. Biscarini, *Journal of the American Chemical Society* **2007**, *129*, 6477.

[14] N. Tamai, H. Miyasaka, *Chemical Reviews* **2000**, *100*, 1875.

[15] Griffith.J, *Chemical Society Reviews* **1972**, *1*, 481.

[16] G. Pace, V. Ferri, C. Grave, M. Elbing, C. von Haenisch, M. Zharnikov, M. Mayor, M. A. Rampi, P. Samori, *Proceedings of the National Academy of Sciences of the United States of America* **2007**, *104*, 9937.

[17] N. Katsonis, J. Vicario, T. Kudernac, J. Visser, M. M. Pollard, B. L. Feringa, *Journal of the American Chemical Society* **2006**, *128*, 15537.

[18] G. C. Dol, K. Tsuda, J. W. Weener, M. J. Bartels, T. Asavei, T. Gensch, J. Hofkens, L. Latterini, A. Schenning, B. W. Meijer, F. C. De Schryver, *Angewandte Chemie-International Edition* **2001**, *40*, 1710.

[19] W. H. Jiang, G. J. Wang, Y. N. He, X. G. Wang, Y. L. An, Y. L. Song, L. Jiang, *Chemical Communications* **2005**, 3550.

[20] S. Karpe, M. Ocafrain, K. Smaali, S. Lenfant, D. Vuillaume, P. Blanchard, J. Roncali, *Chemical Communications* **2011**, *46*, 3657.

[21] L. F. N. A. Qune, H. Akiyama, T. Nagahiro, K. Tamada, A. T. S. Wee, *Applied Physics Letters* **2008**, *93*, 083109.

[22] J. S. Kim, F. Cacialli, M. Granström, R. H. Friend, N. Johansson, W. R. Salaneck, R. Daik, W. J. Feast, *Synthetic Metals* **1999**, *101*, 111.

[23] J. S. Kim, F. Cacialli, R. Friend, *Thin Solid Films* **2003**, *445*, 358.

[24] G. Winroth, S. Brovelli, R. Daik, W. J. Feast, F. Cacialli, *Organic Electronics* **2011**, *11*, 1445.

[25] G. Winroth, G. Latini, D. Credgington, L.-Y. Wong, L.-L. Chua, P. K. H. Ho, F. Cacialli, *Applied Physics Letters* **2008**, *92*, 103308.

[26] D. Samanta, A. Sarkar, *Chemical Society Reviews* **2011**, *40*, 2567.

[27] F. Di Stasio, P. Korniychuk, S. Brovelli, P. Uznanski, S. O. McDonnell, G. Winroth, H. L. Anderson, A. Tracz, F. Cacialli, *Advanced Materials* **2011**, *23*, 1855.

[28] G. Winroth, G. Latini, D. Credgington, L.-Y. Wong, L.-L. Chua, P. K.-H. Ho, F. Cacialli, *Applied Physics Letters* **2008**, *92*, 103308.

[29] W. Barford, *Electronic and optical properties of conjugated polymers*, Clarendon press, Oxford **2005**.

[30] G. Weiser, *Physica Status Solidi a-Applied Research* **1973**, *18*, 347.

[31] J. Stark, *Nature* **1913**, *92*, 401.

[32] G. Winroth, *Physical characterisation of interfaces in organic devices*, PhD thesis, London **2010**.

[33] T. M. Brown, *Electroabsorption investigation of light-emitting diodes with efficient electrodes*, PhD thesis, Cambridge **2001**.

[34] V. Bodrozic, *Electroabsorption investigations of advanced polymer light-emitting diodes*, PhD thesis, London **2005**.

[35] M. G. Harrison, S. Moller, G. Weiser, G. Urbasch, R. F. Mahrt, H. Bassler, U. Scherf, *Physical Review B* **1999**, *60*, 8650.

[36] G. Weiser, A. Horvath, *Chemical Physics* **1998**, *227*, 153.

[37] A. Horvath, G. Weiser, G. L. Baker, S. Etemad, *Physical Review B* **1995**, *51*, 2751.

[38] I. H. Campbell, T. W. Hagler, D. L. Smith, J. P. Ferraris, *Physical Review Letters* **1996**, *76*, 1900.

[39] V. Bodrozic, T. M. Brown, S. Mian, D. Caruana, M. Roberts, N. Phillips, J. J. Halls, I. Grizzi, J. H. Burroughes, F. Cacialli, *Advanced Materials* **2008**, *20*, 2410.

[40] T. M. Brown, F. Cacialli, *Journal of Polymer Science Part B-Polymer Physics* **2003**, *41*, 2649.

[41] T. M. Brown, R. H. Friend, I. S. Millard, D. J. Lacey, T. Butler, J. H. Burroughes, F. Cacialli, *Journal of Applied Physics* **2003**, *93*, 6159.

[42] G. Winroth, O. Fenwick, M. A. Scott, D. Yip, S. Howorka, F. Cacialli, *Applied Physics Letters* **2010**, *97*, 043304.

[43] R. I. R. Blyth, S. A. Sardar, F. P. Netzer, M. G. Ramsey, *Applied Physics Letters* **2000**, *77*, 1212.

[44] T. M. Brown, G. M. Lazzerini, L. J. Parrott, V. Bodrozic, L. Buergi, F. Cacialli, *Organic Electronics* **2010**, *12*, 623.

[45] S. Brovelli, H. Guan, G. Winroth, O. Fenwick, F. Di Stasio, R. Daik, W. J. Feast, F. Meinardi, F. Cacialli, *Applied Physics Letters* **2010**, *96*, 213301.

[46] J.-S. Kim, R. H. Friend, I. Grizzi, J. H. Burroughes, *Applied Physics Letters* **2005**, *87*, 023506.

6. Low-temperature treatment of semiconducting interlayers in organic light-emitting diodes

6.1. Introduction

A major issue in organic electronics is the difference in mobility and injection efficiency of holes and electrons. In fact, most organic light-emitting diodes (OLEDs)[1] have one type of carriers (usually holes) in excess, hindering the formation of excitons and thus emission of photons. Additional layers can be introduced in OLEDs between the conjugated polymer active-layer and electrodes to obtain a balanced charge transport. These interlayers can either reduce the majority carriers by introducing an energy barrier at the heterojunction, or facilitate the injection of minority carriers by coupling the work function of the electrode and the polaronic levels of the active-layer. An early example on the use of multilayer structure is the work from N.C. Greenham et al.[2]: an OLED prepared using PPV and a cyano-substituted polymer (CN-PPV) showing high external quantum efficiency (Fig. 6.1).

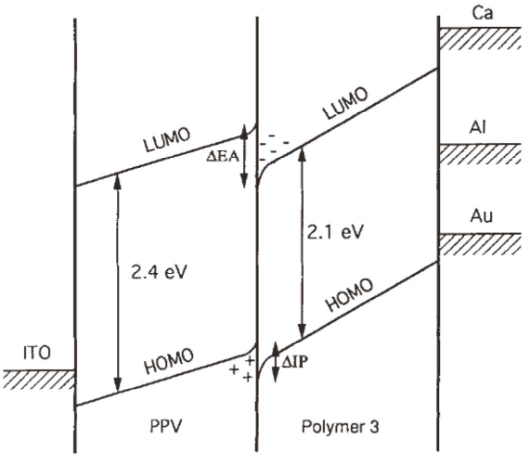

Figure 6.1 Scheme of energy levels alignment for ITO/PPV/CN-PPV/cathode OLEDs. (Reproduced from ref. 2)

The CN-PPV facilitate the injection of electrons providing a “graded barrier” at the cathode while it confines hole at the interface PPV/CN-PPV.

During the last 20 years many different types of interlayer have been developed. Nevertheless, some OLEDs components still require relatively high-temperature (above 150 °C) annealing procedures that reduce the choice of materials, and potentially the device performance. Achieving low-temperature processing of OLEDs is an important milestone on the path to all-plastic, printable, and mass-produced organic displays.

For example, poly(ethylene dioxythiophene):poly(styrene sulphonic acid), PEDOT:PSS[3-5] is a well known hole injection layer[6, 7] (or anode itself)[8] that grants OLEDs with lower turn-on voltages, higher efficiency and stability,[9-11] but it involves an annealing step usually done at temperatures above 150 °C, that is preferably avoided for certain plastic or substrates.[12]

Poly(9,9'-dioctylfluorene-alt-N-(4-butylphenyl)-diphenylamine), TFB,[13-15] as well as poly(p-phenylene vinylene), PPV,[16] and/or other interlayers have also been used on top of PEDOT:PSS to increase the efficiency.[17] They also require annealing at temperatures in excess of 150-160 °C to prevent re-solubilization when the emissive layer is spin-coated on top.[13] However, a degree of mixing between the polymers may become acceptable as a trade-off to achieve simultaneous low-temperature (low-T) processability and high efficiency. In fact, it is possible to forego the high-T annealing of TFB in indium-tin-oxide(ITO)/TFB/poly(9,9'-dioctylfluorene-alt-benzothiadiazole)(F8BT)/Ca-Al OLEDs, and still achieve a significant increase of the electroluminescence (EL) efficiency. Using continuous wave (CW) and time-resolved photoluminescence (PL), the intermixing (presence of exciplexes)[18] is monitored, showing how it influences the overall EL or PL can be tailored by controlling the TFB layer thickness.

A low-temperature treatment of exciton/electron blocking interlayers in light-emitting diodes based on poly(9,9'-dioctylfluorene-alt-benzothiadiazole) (F8BT) is here presented. Poly(9,9'-dioctylfluorene-alt-N-(4-butylphenyl)-diphenylamine (TFB) interlayers processed at temperatures up to 50 °C, i.e. far below the glass transition temperature of TFB (~156 °C) were used. Continuous wave and time-resolved photoluminescence studies confirmed the formation of both excitons and exciplex species, as a result of the F8BT/TFB intermixing. Interestingly, an increase the electroluminescence external quantum efficiency from 0.05% to 0.5% and 1% for progressively thicker TFB films can still be observed.

Cyclic voltammetry measurements were carried out in collaboration with Dr. Daren Caruana, Dept.

of Chemistry, University College London. This work was supported by the EC Marie Curie RTN-THREADMILL (MRTN-CT-2006-036040), ITN-SUPERIOR (PTN-CT-2009-238177), the EC FP7 ONE-P large-scale project N. 212311 and the NanoSci-E+ project SENSORS. A manuscript concerning the results here shown is currently under revision (G. M. Lazzerini, F. Di Stasio, C. Fléchon, D. Caruana, F. Cacialli)

6.2. Experimental methods

6.2.1. Interlayer and devices preparation

Devices were fabricated and tested using TFB (Fig. 6.2, American Dye Source, ADS, molecular weight, M_w = 68000 g/mol) as electron/exciton/exciplex blocking layer (EBL) and F8BT (ADS, M_w = 46000 g/mol) as the “active” layer. 5 different TFB “initial” (before the F8BT deposition) thicknesses were investigated. The LEDs were prepared by spin-coating at 3000 rpm TFB solutions of different concentrations on top of ITO-coated glass substrates previously treated with oxygen plasma (15 min at 10.2 W).[19, 20]

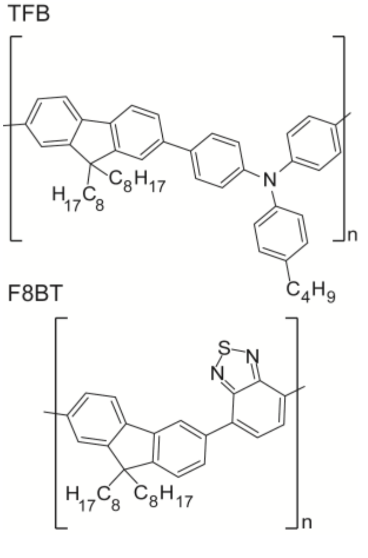

Figure 6.2 Chemical structure of Poly(9,9’-dioctylfluorene-alt-N-(4-butylphenyl)-diphenylamine) (TFB, top) and poly(9,9’-dioctylfluorene-alt-benzothiadiazole) (F8BT, bottom)

The initial thickness (t_i) of the TFB films, was measured with a Dektak profilometer to be t_i = 29 ± 3 nm, 90 ± 6 nm, 395 ± 5 nm, 1800 ± 160 nm for TFB concentrations of 1%, 2%, 5%, 10% (w/w in toluene), respectively. After the oxygen plasma all sample handling was conducted within a N_2 glove-box (M-Braun). The samples, except the ones with t_i = 0 nm, were then held at ~50 °C for 16 h to completely evaporate any residual solvent prior to the spin coating of the F8BT (Fig. 6.2) layer from a 2% toluene solution.[20, 21] As this temperature is much lower than TFB glass transition temperature, T_g^{TFB}=156 °C,[15, 20] and toluene is a solvent for TFB, a degree of intermixing and a reduction of the pure TFB layer thickness upon spin-coating of F8BT is expected. The precise determination of the thickness of the pure TFB layer in these conditions is not trivial, but a rough estimate by measuring the film thickness after spin-rinsing a TFB layer with toluene was obtained: for t_i = 1800 nm we measure 270 nm, and similarly 28 nm for t_i = 395 nm, and < 8 nm for t_i = 90 nm or 29 nm. Ca (30 nm) and Al (150 nm) thermal evaporation completed the device preparation. Electrical characterisation of all devices was carried out using the set-up shown in chapter. 6.[22, 23]

6.3. Optical and Electronic properties

6.3.1. Current density-Voltage-Luminance curves

In Fig. 6.3 the current density (J) and luminance (L) vs. voltage (V) curves of all devices are shown. Current densities are similar for all samples, especially for V > 5 V (excluding the sample with t_i = 1800 nm). Interestingly, the luminance increases progressively with t_i: at J = 300 mA/cm^2, L increases from 360 cd/m^2 for t_i = 0 nm up to 4000 cd/m^2 for t_i = 395 nm. On the contrary, for t_i = 1800 nm, J is reduced to 1.2 mA/cm^2 and L = 2240 cd/m^2 is reached at 30 V with J = 88 mA/cm^2. External quantum efficiencies (EQEs, the number of photons emitted per electron injected into the device) show values of 0.05 %, 0.23 %, 0.36 %, 0.5 % and 1 % for t_i = 0, 29, 90, 395 and 1800 nm, respectively. In addition, the light turn-on voltage, V_{on} (defined as the voltage at which the luminance is 0.06 cd/m2 (with the noise level at 0.01 cd/m^2 and extracted out of an average of the 8 pixels in each sample) decreases progressively from 4.4 ± 0.1 V to 2.38 ± 0.15 V for t_i = 0 and 395 nm, respectively, and then increases again to 2.99 ± 0.35 V for t_i = 1800 nm. The electric field during EL operation is > 5x105 V/cm, which should result in charge injection across the heterojunction, and therefore emission from both exciplexes at the TFB/F8BT interface and excitons from the polymers bulk.

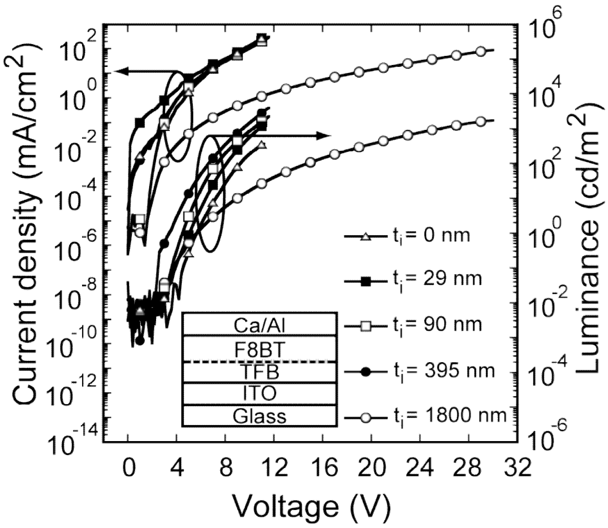

Figure 6.3 Current density-voltage (logJ-V) and luminance-voltage (logL-V) curves for ITO/TFB(ti)/F8BT(120 nm)/Ca-Al OLEDs for ti=0, 29, 90, 395 and 1800 nm (pixel area = 0.35 mm^2). Luminance progressively increases upon insertion of the TFB layer up ti=395 nm. A drastic reduction of J and L is measured for ti=1800 nm.

The progressive increase of L and the reduction of the light-emission threshold V_{on} with t_i is mainly caused by the electron/exciton-blocking effect of TFB and only partially to the fragmentation of the energy barrier (graded energy barrier) for holes at the anode. The electron/exciton blocking effect moves the recombination zone from near the ITO to the TFB/F8BT interface, thus reducing the electrostatic quenching at the ITO/F8BT interface (image charge effect). Furthermore, the hole-barrier fragmentation improves the electron-hole balance, and consequently the luminance,[24] as the HOMO of TFB (5.4 eV) acts as an intermediate step to favour hole injection from plasma-treated ITO (work function of 5.2 eV)[25] and F8BT (HOMO = 6.0 eV, as measured by cyclic voltammetry, Fig. 6.4).

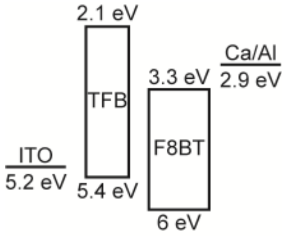

Figure 6.4 Energy bands diagram of OLEDs components before contact is created. ITO and Ca work function values[26] and TFB and F8BT[27, 28] polaronic levels (conduction band and valence band). The energy barrier at the TFB/F8BT for electrons injected trough the Ca/Al cathode increases the charge carrier balance in the device.

All these effects result in an increase of EQEs of one order of magnitude from 0.05 % for t_i = 0 nm to 0.5 % for t_i = 395 nm. Interestingly, the EQE for t_i = 1800 nm is even higher EQE (1%), although high operating voltage is necessary (30 V for L=2240 cd/m2) due to a relatively thick TFB layer remaining (> 30 nm) after the deposition of F8BT, as also confirmed by the PL measurements.

6.3.2. Photoluminescence and electroluminescence spectra

Fig. 6.5 reports photoluminescence (PL, a) and electroluminescence (EL, measured at V = 11 V for all the devices except for ti = 1800 nm, for which we applied a 20 V bias, b) spectra for all OLEDs here studied.

In the PL spectra it is possible to observe three main peaks at 2.16, 2.28[13] and 2.85 eV, with the peak at 2.85 eV (TFB) not observed for t_i = 0 nm, as expected. Higher intensities of the peak at 2.85 eV (only just visible on a linear scale for t_i = 1800 nm), as well as higher PL emission at energies below 2.28 eV (second peak) can be observed for increasing t_i.

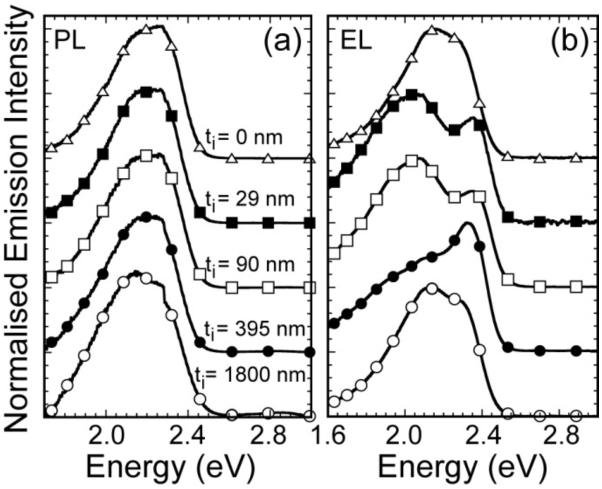

Figure 6.5 (a) PL and (b) EL spectra for OLEDs with different initial TFB layer thickness. PL spectra were collected at room temperature in air, using the TCSPC system described in chapter 4. As excitation source a pulsed laser diode was used (E = 3.3 eV, ~40 ps)

In agreement with A. C. Morteani et al.,[29, 30] the increase of the PL emission at energies below 2.28 eV can be connected to the presence of exciplexes in the TFB:F8BT blend (interface). Furthermore, the TFB peak (2.85 eV) confirms the presence of relatively thick (> 10 nm) domains of pure TFB and the dependence of the peak intensity with t_i confirms that the thicker the initial deposited TFB layer, the larger the amount of pure TFB left after the deposition of F8BT.

In the EL spectra (Fig. 6.5) there is no emission from TFB, thus confirming EL does not originate from TFB. For the sample without TFB and the one with t_i = 1800 nm, the main EL peaks are at 2.17 eV and 2.28 eV whereas for all other samples the two EL peaks occur at 2.10 eV and 2.33 eV. Furthermore, EL spectra show increased emission at E < 2.1 eV for all OLEDs with TFB, and a narrowing for t_i = 395 nm.

The EL red-shift for t_i = 0 nm and t_i = 1800 nm (Fig. 6.3b) can be ascribed to interference effects induced by the shift of the recombination region.[15, 31] Some minor spectral variability of the EL peaks among different pixels of the same device was observed as well, thus suggesting some non-uniformity of the TFB/F8BT multilayer structure. However, the CIE colour coordinates have a mean and standard deviation value of x = 0.45 ± 0.02 and y = 0.53 ± 0.02,16 respectively, thus confirming that there is an acceptable variation of the perceived colour. As a comparison, the green phosphorous of RGB displays have to lie within $\Delta x = 0.02$ and $\Delta y = 0.03$.

6.3.3. Time-resolved photoluminescence measurements

PL time-resolved measurements (Fig. 6.6, at the PL peak value of 2.28 eV) reveal a single-exponential dynamics with τ =1.4 ns for t_i = 0 nm, and a non-mono-exponential decay for $t_i \neq 0$, with a long tail extending over several ns, which strongly suggests an interchain state as an exciplex. The non-mono-exponential decay at relatively short times (<3 ns) might be indicative of a decay from a distribution of states, but a triple exponential ($I(t) = I_{01}\exp(-t/\tau_1) + I_{02}\exp(-t/\tau_2) + I_{03}\exp(-t/\tau_3)$) can be used to fit these decays over the whole range with good accuracy (χ^2 <1.1 with three exponentials and 1.3-1.7 when fitting with two exponentials; χ^2 =1.2 for t_i =0).

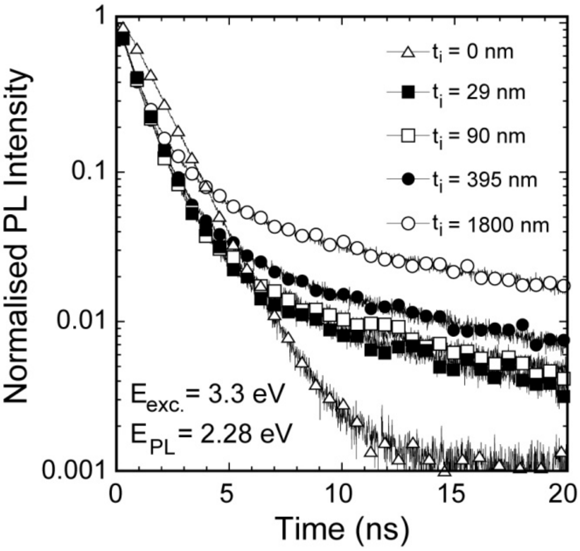

Figure 6.6 Normalised PL time-resolved measurements collected at 2.28 eV, comparing the time decay of the samples with different initial TFB thicknesses. A single exponential decay is used to fit the decay of the reference sample, whereas a triple exponential is used for all others. The presence of exciplexes is confirmed by the longer decay time for the samples with TFB.

For all the various samples τ_2=1.4 ns was used (as for neat F8BT) and τ_1=0.6-0.8 ns and τ_3 = 8.9-10.8 ns. In addition, the relative weight of the exponential associated to τ_3 progressively increases with t_i from 15% for t_i = 0 nm to 43% for t_i = 1800 nm. This provides strong evidence of TFB/F8BT intermixing, as the τ_3 time constant for OLEDs with TFB is > 8.9 ns, i.e. not compatible with the accepted photophysics of intrachain singlets.

Quantitative analysis of the dynamics for t_i>0 is complicated by the fact that the decays are non-mono-exponential. While previous literature identifies a short and a long-decay constant (readily assigned to a singlet and an exciplex), a three-exponential function yields the most accurate fits in our case. This could result from three different decay pathways, but a similar decay profile for times up to 1-3 ns could also be justified by a distribution of states (e.g. due to conformational disorder). In either case the extended temporal range of the overall decay provides strong evidence of TFB:F8BT intermixing.

This PL lifetime is shorter than some of the previously reported for TFB/F8BT exciplexes (27 ns),[18] but in agreement, with data from J. -S. Kim et al.[13] Therefore, such a long-lived species is best assigned to an exciplex but, the possibility that the non-mono-exponential decay in the first few ns is due to the already mentioned distribution of states cannot be ruled out. The difference with A. C. Morteani et al. can be ascribed to ITO-induced electrostatic quenching (image charge effect). Differences in other polymer/blends properties (PL efficiency, purity, the degree of mixing) may also play a role. As expected, also the weight of the exciplexes in the decay dynamics increases with t_i, thus confirming an increasing number of exciplexes formed.

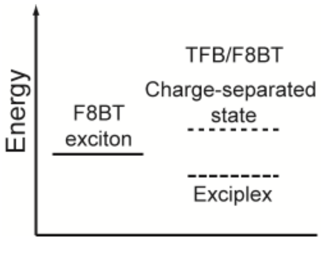

Figure 6.7 Energy level scheme for excitons in F8BT, charge-separated states and exciplexes at the TFB/F8BT interface.
(Reproduced and adapted from ref. 27)

The fast decay (τ1 < 1 ns) can be explained as due to energy transfer to the exciplex state (Fig. 6.7) and to the charge separation of the excitons at the interface.[18]

6.4. Conclusions

In conclusion, low-T processing of TFB can be used to increase the EQE of the LEDs. The best trade-off among EQE, Von and driving voltage, is offered by the devices with a TFB thickness of 395 nm, prior to the F8BT deposition, which were found to provide the best performance in terms of EQE and V_{on}. Exciplex formation through EL, PL and time-resolved measurements was also confirmed. An associated change in the perceived colour is observed, which is within the same tolerance allowed to the green phosphorous of RGB, and thus confirming that the effect of the intermixing of F8BT and TFB due to the low-T treatment can be accepted for LED applications.

References

[1] J. H. Burroughes, D. D. C. Bradley, A. R. Brown, R. N. Marks, K. Mackay, R. H. Friend, P. L. Burns, A. B. Holmes, *Nature* **1990**, *347*, 539.

[2] N. C. Greenham, S. C. Moratti, D. D. C. Bradley, R. H. Friend, A. B. Holmes, *Nature* **1993**, *365*, 628.

[3] S. Kirchmeyer, K. Reuter, *Journal of Materials Chemistry* **2005**, *15*, 2338.

[4] B. L. Groenendaal, F. Jonas, D. Freitag, H. Pielartzik, J. R. Reynolds, *Advanced Materials* **2000**, *12*, 481.

[5] G. Heywang, F. Jonas, *Advanced Materials* **1992**, *4*, 116.

[6] G. Greczynski, T. Kugler, M. Keil, W. Osikowicz, M. Fahlman, W. R. Salaneck, *Journal of Electron Spectroscopy and Related Phenomena* **2001**, *121*, 1.

[7] M. Sun, Q. Niu, R. Yang, B. Du, R. Liu, W. Yang, J. Peng, Y. Cao, *European Polymer Journal* **2007**, *43*, 1916.

[8] C. Yin, B. Pieper, B. Stiller, T. Kietzke, D. Neher, *Applied Physics Letters* **2007**, *90*.

[9] T. M. Brown, F. Cacialli, *Journal of Polymer Science Part B: Polymer Physics* **2003**, *41*, 2649.

[10] T. M. Brown, J. S. Kim, R. H. Friend, F. Cacialli, R. Daik, W. J. Feast, *Applied Physics Letters* **1999**, *75*, 1679.

[11] G. Winroth, G. Latini, D. Credgington, L.-Y. Wong, L.-L. Chua, P. K. H. Ho, F. Cacialli, *Applied Physics Letters* **2008**, *92*, 103308

[12] V. Zardetto, T. M. Brown, A. Reale, A. Di Carlo, *Journal of Polymer Science Part B: Polymer Physics* **2011**, *49*, 638.

[13] J.-S. Kim, R. H. Friend, I. Grizzi, J. H. Burroughes, *Applied Physics Letters* **2005**, *87*, 023506.

[14] R. Jin, P. A. Levermore, J. Huang, X. Wang, D. D. C. Bradley, J. C. deMello, *Physical Chemistry Chemical Physics* **2009**, *11*, 3455.

[15] M. Shakutsui, H. Matsuura, K. Fujita, *Organic Electronics* **2009**, *10*, 834.

[16] J. Morgado, R. H. Friend, F. Cacialli, B. S. Chuah, S. C. Moratti, A. B. Holmes, *Journal of Applied Physics* **1999**, *86*, 6392.

[17] R.-Q. Png, P.-J. Chia, J.-C. Tang, B. Liu, S. Sivaramakrishnan, M. Zhou, S.-H. Khong, H. S. O. Chan, J. H. Burroughes, L.-L. Chua, R. H. Friend, P. K. H. Ho, *Nature Materials* **2010**, *9*, 152.

[18] A. C. Morteani, R. H. Friend, C. Silva, *Organic Light Emitting Devices: Synthesis, Properties and Applications*, WiLEY-VCH, Weinheim, **2006**

[19] J. S. Kim, F. Cacialli, M. Granström, R. H. Friend, N. Johansson, W. R. Salaneck, R. Daik, W. J. Feast, *Synthetic Metals* **1999**, *101*, 111.

[20] G. M. Lazzerini, F. Di Stasio, C. Fléchon, D. Caruana, F. Cacialli, *submitted*.

[21] L. V. Govor, I. A. Bashmakov, F. N. Kaputski, M.Pientka, J. Parisi, *Macromolecular Chemistry and Physics* **2000**, *201*, 2721.

[22] G. Winroth, G. Latini, D. Credgington, L.-Y. Wong, L.-L. Chua, P. K. H. Ho, F. Cacialli, *Applied Physics Letters* **2008**, *92*, 103308.

[23] F. Di Stasio, P. Korniychuk, S. Brovelli, P. Uznanski, S. O. McDonnell, G. Winroth, H. L. Anderson, A. Tracz, F. Cacialli, *Advanced Materials* **2010**, *23*, 1855.

[24] S. A. Choulis, V. E. Choong, A. Patwardhan, M. K. Mathai, F. So, *Advanced Functional Materials* **2006**, *16*, 1075.

[25] T. M. Brown, G. M. Lazzerini, L. J. Parrott, V. Bodrozic, L. Burgi, F. Cacialli, *Organic Electronics* **2011**, *12*, 623.

[26] T. M. Brown, J. S. Kim, R. H. Friend, F. Cacialli, R. Daik, W. J. Feast, *Applied Physics Letters* **1999**, *75*, 1679.

[27] L. L. Chua, J. Zaumseil, J. F. Chang, E. C. W. Ou, P. K. H. Ho, H. Sirringhaus, R. H. Friend, *Nature* **2005**, *434,* 194.

[28] E. Moons, *Journal of Physics-Condensed Matter* **2002**, *14*, 12235.

[29] A. C. Morteani, R. H. Friend, C. Silva, *Chemical Physics Letters* **2004**, *391*, 81.

[30] A. C. Morteani, A. S. Dhoot, J. S. Kim, C. Silva, N. C. Greenham, C. Murphy, E. Moons, S. Cina, J. H. Burroughes, R. H. Friend, *Advanced Materials* **2003**, *15*, 1708.

[31] T. Granlund, L. A. A. Pettersson, M. R. Anderson, O. Inganas, *Journal of Applied Physics* **1997**, *81*, 8097.

7. Supramolecular architecture for near-infrared emission

7.1. Introduction

Infrared light-emitting diodes (NIR-LEDs) are of particular interest in many different applications like optical communications and remote controls. Many different materials for solution processable NIR-LEDs have been investigated using semiconducting nanoparticles[1, 2] and conjugated molecules.[3-6]

The energy-gap rule[7, 8] predicts a decrease of the photoluminescence quantum yield for molecular emitters as the energy-gap starts reducing. This is caused by an increase in the vibrational overlap of the excited and ground states. This intrinsic limitation cause lower external quantum efficiency (EQE, ratio between the number of injected charges and the number of emitted photons) in organic NIR-LEDs compared to OLEDs operating in the visible range, inviting to innovative molecular approaches to reach higher EQEs in the NIR.[3]

Among conjugated systems, porphyrins are an interesting class of naturally occurring emitting molecules consisting of a metal ion complexed by heterocyclic macrocycles. They possess an extended conjugation length and, as a consequence they usually show intense absorption bands. Furthermore, they are highly tunable through substitution of different metal ions into the centre of the ring, as well as by covalent chemistry on the peripheral positions of the ring.[3] An example of this class of molecular compounds versatility is Platinum containing porphyrins showing electrophosphorescence in the NIR.[3, 9, 10]

To be able to obtain NIR absorption and emission, an extended π–conjugation is necessary .To fulfil this requirement porphyrins oligomers with π–conjugation extending on the overall molecule have been synthesized.[11-16] Nevertheless, porphyrins oligomers have a strong tendency to create non-emissive aggregates but, by using ligands it is possible to create a supramolecular structure able to prevent the aggregation, hence the suppression of the photoluminescence. On the other hand, curved molecular π-systems such as the one investigated in this study represent an alternative approach to reducing aggregation as well.

In this work, organic light-emitting diodes incorporating two hexamers of *meso*-butadiyne-linked zinc porphyrin oligomers: a linear P6 and a cyclic one bound to a hexapyridyl template, c-P6T were prepared and studied. Both hexamers possess red-shifted emission (λ_{PL} = 873 and 920 nm, respectively) compared to single porphyrin ring as a consequence of their extended π-conjugation. Photoluminescence and electroluminescence of blends with poly(9,90-dioctylfluorene-alt-benzothiadiazole) show a high photoluminescence quantum yield of 7.7% for the linear hexamer when using 4-benzyl pyridine to create supramolecular structures in order to prevent aggregation and achieving near-infrared electroluminescence. For all porphyrin structures studied in this work, emission at room temperature is known to originate from the singlet excited states.

All porphyrins used in this study were synthesized at the "Chemistry Research Laboratory, Department of Chemistry, University of Oxford" by Johannes K. Sprafke, Dmitry V. Kondratuk and Prof. Harry L. Anderson. This study was funded by the EC (Contracts MRTN-CT-2006-036040 (THREADMILL), PITN-GA-2009-238177 (SUPERIOR), and Grant Agreement No. 212311 FP7/2007-2013 (ONE-P)) and the EPSRC.

7.2. Optical and Electronic properties:

7.2.1. Samples preparation

Samples for optical studies were spin-coated to a thickness of ~70 nm from a 2 wt.% xylene solution as a blend of poly(9,90-dioctylfluorene-alt-benzothiadiazole) (F8BT, 90 wt. %) with the porphyrin hexamer (Fig. 7.1a, 10 wt. %). To prevent aggregation (i.e. photoluminescence quenching) of the linear hexamer, 4-benzyl pyridine (BP) was added to the blend in a quantity of 18 BP molecules per hexamer (87 wt. % F8BT, 10 wt. % P6, 3 wt. % BP).

OLEDs were prepared spin-coating ~80 nm hole injection layer of Poly(3,4-ethylenedioxythiophene) poly(styrenesulfonate) (PEDOT:PSS, Sigma Aldrich 560596) from 2.8 wt. % dispersion in water onto an oxygen plasma treated ITO film on a glass substrate.[17] Devices were then baked at 200°C for 10 minutes in N_2 atmosphere. The active layer was spin-coated to a thickness of ~70 nm from a

2 wt. % solution in xylene, using identical blend compositions as those for the optical experiments. A 45 nm Ca electrode was evaporated on top of the active layer, then a 150 nm protective layer of Al.

7.2.2. Optical properties

The absorption spectra of blended films are plotted alongside their photoluminescence (PL) spectra in Fig. 7.1b. The characteristic double-peaked F8BT absorption can be observed in the UV, and peaks associated with the hexamers in the NIR region (800 - 900 nm). The PL spectrum of the cyclic hexamer (c-P6T, $\lambda_{PL\text{-}peak}$ ~ 920 nm) shows a slight red-shift compared to the linear hexamer (P6, $\lambda_{PL\text{-}peak}$ ~ 920 nm), a broader absorption and emission profiles, and a larger Stokes' shift.[18, 19] Blends with either P6 or c-P6T spun-coated from xylene show relatively low PL quantum yields ($\eta_{PL} < 1$ %) compared to the neat F8BT films (48 ± 5%).[20, 21]

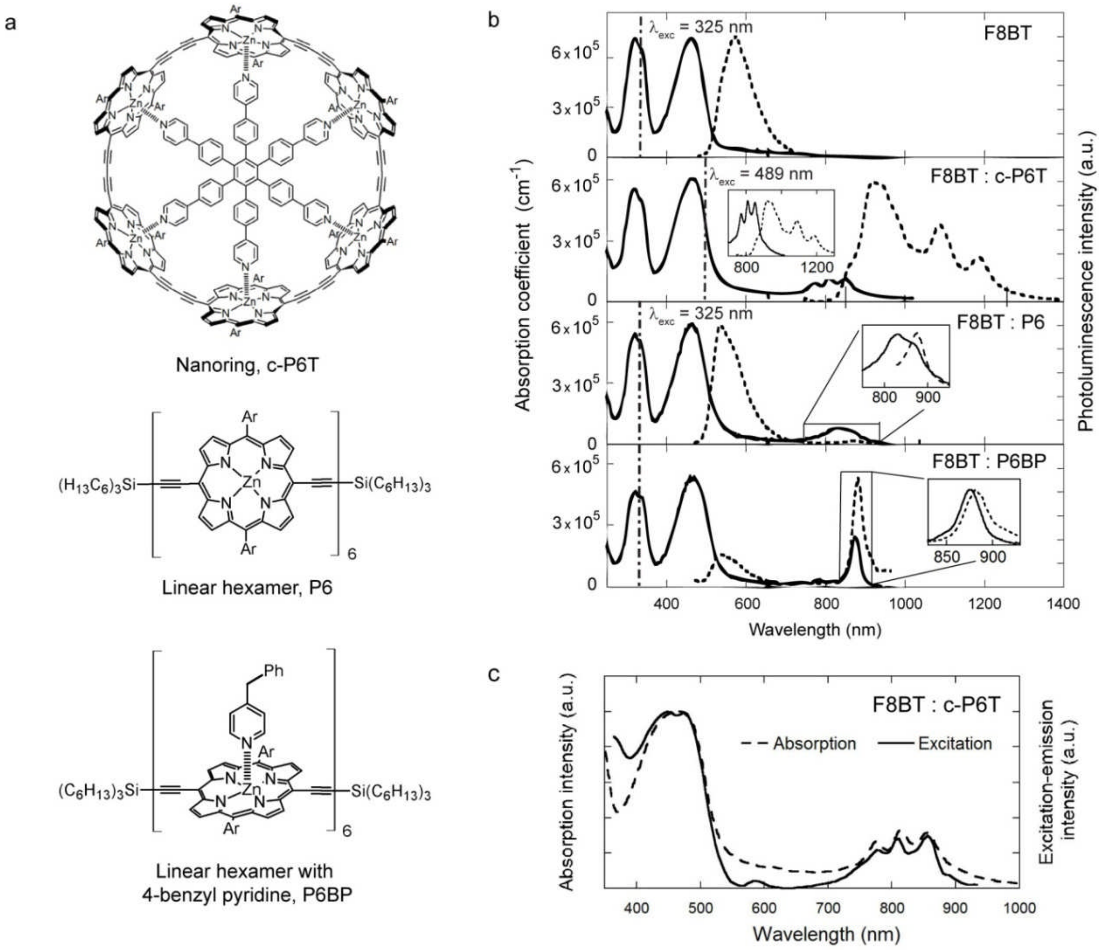

Figure 7.1 (a) Chemical structures of the porphyrin hexamers used and the complex of the linear hexamer, P6, with 4-benzyl pyridine, BP. (Ar = 3,5-bis(octyloxy)phenyl in P6 and 3,5-bis(tert-butyl)phenyl in c P6T.) (b) Optical absorption (solid lines) and photoluminescence (dashed lines) spectra of pure F8BT and blended films. Insets show the overlap of the absorption and emission of the hexamer component of the spectrum. (c) Excitation-emission spectrum for an F8BT : c-P6T blend for a collection wavelength of 1090 nm, plotted alongside the absorption intensity. (Reproduced from ref. 3)

By adding 4-benzyl pyridine (BP) to the F8BT : P6 blend, BP is expected to co-ordinate metal ions with the lone pair of electrons on its nitrogen atom,[12] and so, decorate the P6 molecules and prevent aggregation. This method is analogous to other supramolecular insulation methods used to prevent aggregation and increase η_{PL}, such as in the case of polyrotaxanes (Chapters 4 and 5). [22, 23] A narrowing of both absorption and PL spectra can be observed by adding BP to the P6:F8BT blend, suggesting a suppression of aggregates, supported by a significant increase in η_{PL} to 11.8 ± 1.2 % (or 7.7 % if one considers just the NIR component of the PL). The NIR η_{PL} was measured with direct excitation of F8BT (λ_{EXC} ~ 412 nm), indicating an efficient energy transfer to the P6-BP complex. Furthermore, the value (7.7 %) is in remarkable agreement with the η_{PL} measured in toluene solution (8 ±1 %) with 1% pyridine,[10] suggesting once again that PL concentration quenching is suppressed in the P6-BP complex. Addition of BP to F8BT: c-P6T blends did not caused an enhancement of the η_{PL}, indicating that the molecule itself hinders the formation of aggregates due to the steric hindrance arising from its curved π-surface. The solution η_{PL} of c-P6T, was however much lower than P6 at 0.1±0.01 %. [18] The efficient PL quenching of F8BT (>98 % for P6 and c-P6T; 91% for P6BP) suggests a strong energy or charge transfer to both types of porphyrin hexamer.

To gain further insight, HOMO and LUMO levels from redox potentials were estimated (measured electrochemically in THF containing Bu_4NBF_4).[3, 13, 19, 24] For c-P6T: -5.00 eV and -3.46 eV, and for P6: -5.12 eV and -3.34 eV for HOMO and LUMO respectively (Fig. 7.2a). The measured LUMO level of P6 is very similar to literature values for the F8BT LUMO[3, 25, 26] (i.e. between 3.3 and 3.5 eV below vacuum) suggesting that either energy transfer or exciton splitting may occur (the mismatch of the HOMOs being 0.8 ± 0.2 eV). Note that 65 % of the PL in the F8BT:P6-BP blend is from the hexamer despite using direct excitation of F8BT (λ_{exc} = 325 nm). This suggests that energy transfer does dominate the PL quenching of F8BT. However, although the ratio of the emission from the hexamer to F8BT is greater for F8BT: P6-BP than for F8BT:P6, the η_{PL} of P6 (<1%) is significantly lower than that of P6-BP (7.7± 0.8 %), and a slightly reduced PL quenching of F8BT in the blend with P6-BP (91 % quenching in P6BP compared to >98 % in P6) is observed, indicating a small energy barrier for energy transfer processes induced by the BP complexation.

For the F8BT:c-P6T blends, the excitation-emission spectrum was used, monitoring emission from c-P6T whilst scanning the excitation wavelength (7.1c). The ratio of emission to absorption in the F8BT absorption band differs by no more than 20% from the ratio in the absorption band of c-P6T, suggesting that the vast majority of excitons on F8BT transfer to c-P6T.[3]

7.2.3. Light-emitting diodes

For OLEDs incorporating both hexamers, the electroluminescence (EL) show a strong NIR component and >99 % emission quenching of the F8BT emission. For c-P6T, ~94 % of the EL was in the NIR region (Fig. 7.2) with $\lambda_{PL\text{-}peak}$ ~ 960 nm and a ~ 40 nm red-shift with respect to the PL. Interestingly, the current turns on at lower voltages in all hexamer blends devices than for analogue F8BT OLEDs. This can be due to the higher-lying HOMOs of hexamers allowing hole injection at low voltages (Table 7.1).

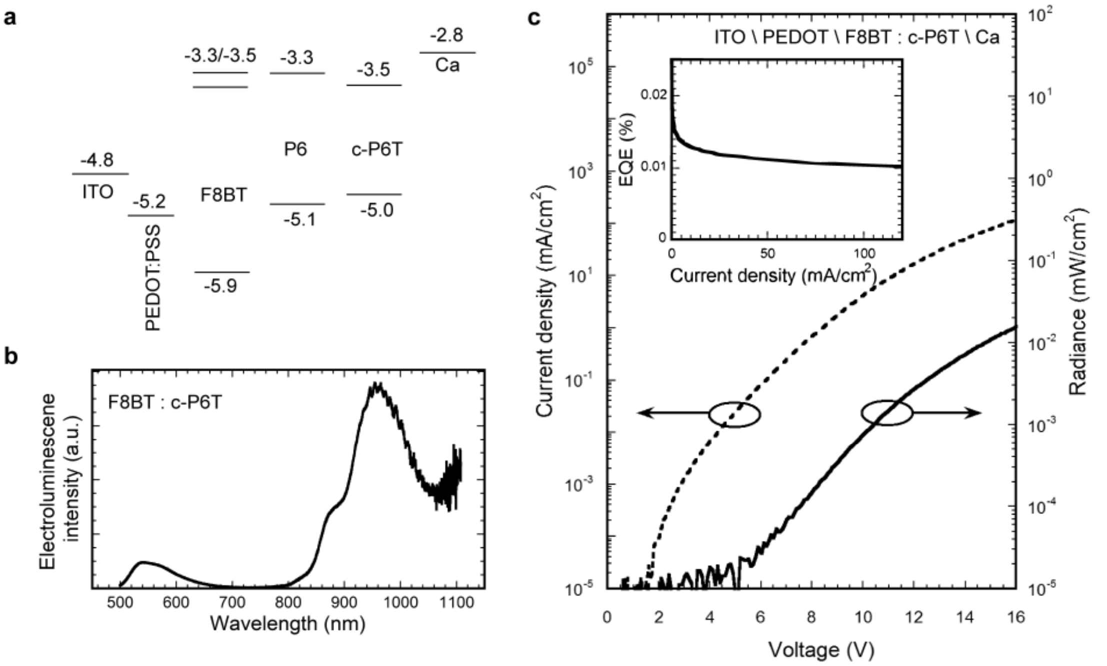

Figure 7.2 (a) Energy levels of electrodes,[27] F8BT[25, 26] and the porphyrin hexamers, P6 and c-P6T. OLEDs were fabricated with the structure ITO\PEDO:PSS(85 nm)\active layer(70 nm)\Ca(45 nm)\Al (150 nm). The device area was 3.5 mm^2. (b) Electroluminescence spectrum of an F8BT:c-P6T OLED measured at 15.5 V. (c) Current density and radiance plotted against driving voltage for a typical F8BT:c-P6T device. The inset shows the external quantum efficiency (EQE) as a function of current density, where the EQE has been calculated for the full spectrum including 6 % of the emission that originates from the F8BT. (Reproduced from ref. 3)

This lower current turn-on in porphyrin hexamer devices also implies that at just 10 % of the cyclic hexamer, we are already above the percolation threshold. External quantum efficiencies (EQE) in the F8BT:c-P6T devices were just 0.024 ± 0.001 %. One can relate this EL EQE to an internal quantum efficiency, IQE, by $IQE = \varepsilon^{-1} \cdot EQE$, where ε is the out-coupling efficiency and $0.5n^{-2} \leq \varepsilon \leq 0.75n^{-2}$ for isotropic dipoles[28, 29] or up to $1.2n^{-2}$ for in plane dipoles[30], where n is the refractive index of the active layer (we measured n = 1.9 for neat F8BT films at 550 nm by spectroscopic ellipsometry on spin-cast films of F8BT using a LOT Oriel on a VASE ellipsometer). Without knowing the position of the emission zone or dipole orientation, $IQE_{c-P6T} = 0.07$ to 0.17 % was estimated. This range incorporates the solution η_{PL}, so we do not expect large improvements by optimizing the device architecture.

	$V_{on}(I)$ [a]	$V_{on}(L)$ [b]	Maximum EQE_{EL} (%)	R_{max} (mW/cm^2)[d]	η_{PL} (%) λ_{exc} = 412 nm	PL in NIR (%)[e,f] λ_{exc} = 325 nm	EL in NIR[e,g] (%)
F8BT only	2.3 ± 0.1	2.8 ± 0.2	0.35 ± 0.03	1.1 ± 0.1	48 ± 5	-	-
F8BT:c-P6T	1.5 ± 0.3	6.4 ± 0.3	0.024 ± 0.001[c]	0.024 ± 0.001	<1	-	94 %
F8BT:c-P6TBP	0.5 ± 0.1	5.4 ± 0.3	0.011 ± 0.001[c]	0.020 ± 0.004	<1	-	-
P6	0.6 ± 0.1	9.2 ± 0.4	0.009 ± 0.001	0.019 ± 0.001	<1	2 %	76 %
P6BP	0.9 ± 0.3	3.3 ± 0.3	0.10 ± 0.01	0.10 ± 0.01	11.8 ± 1.2	65 %	99 %

Table 7.1 Table of key optical parameters for the blends, and performance parameters of devices. [a] Defined as the voltage at which the current density reaches 5 x 10-5 mA/cm2 [b] Defined as the voltage at which light output reaches 5 x 10-5 mW/cm2 (~5 times the noise level) [c] EQE has been adjusted to account for an estimated 25% that is missed through lack of sensitivity of our detector in the region beyond 1100 nm. [d] Maximum radiance at current densities ≤ 160 mA/cm2. [e] Defined as the % of emission at wavelengths longer than 750 nm. [f] Peak emission in PL was at 920 nm for c-P6T, 873 nm for P6 and 882 nm for P6BP. [g] Peak EL emission was at 960 nm for c-P6T, 883 nm for P6 and 883 nm for P6BP.
(Reproduced from ref. 3)

The F8BT:P6 devices (Fig. 7.3) showed a similar behaviour: a ~ 10 nm EL red-shift with respect to the PL, and an even lower EQE of 0.009 ± 0.001 %. However, being above the percolation threshold for P6 in devices (and the PL measurements), aggregation effects are expected, even at these modest concentrations of the hexamer in the blend (10 % by weight).

Addition of BP to the blend increased the efficiency by an order of magnitude to give the best performing devices, measuring an external quantum efficiency, $EQE_{P6BP} = 0.10 \pm 0.01\%$, corresponding to an internal efficiency $IQE_{P6BP} = 0.3\ to\ 0.7\%$. This is somewhat lower than the η_{PL}, even accounting for spin statistics, suggesting that there may be some possibility for further optimization of the device architecture by, for example, adjusting the components and ratio of the blend or by incorporating electron- or hole-blocking layers.

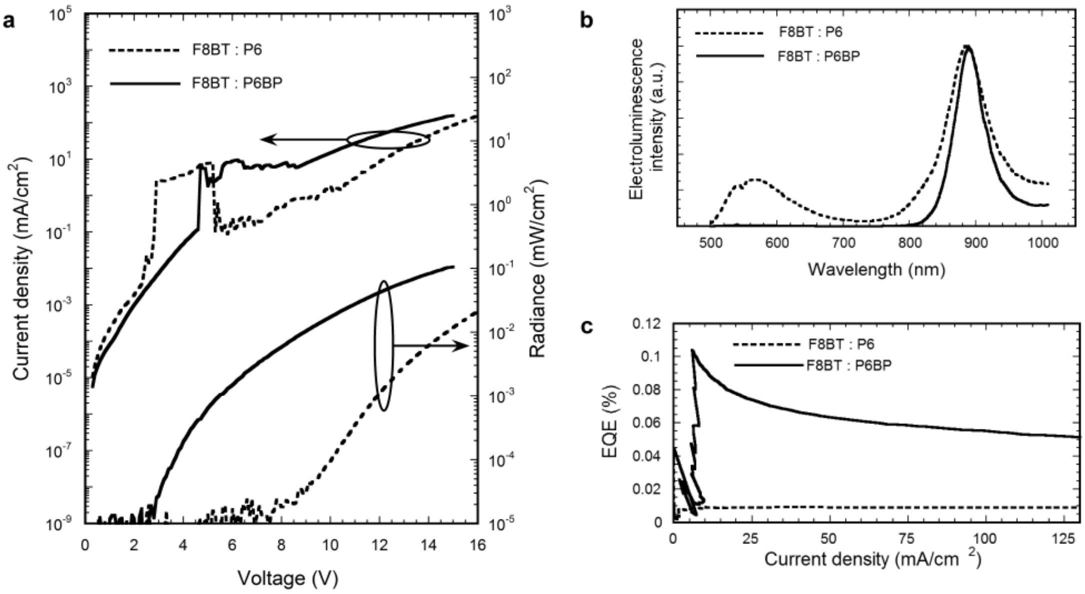

Figure 7.3 Current density and light emission plotted against driving voltage for typical F8BT blended devices with P6 and P6-BP. b Electroluminescence spectra for the F8BT:P6 and F8BT:P6BP devices recorded at 16 V and 14 V respectively. The difference in spectral shape of the NIR component is ascribed to the insulating behavior of the BP around the P6 hexamer. c External quantum efficiency (EQE) plotted as a function of current density for the same devices as a. The EQE is calculated for the full range of wavelengths (including residual F8BT emission), though for P6BP, > 99% of the emission is from the hexamer. Devices were fabricated with the structure ITO\PEDOT:PSS (85 nm)\active layer (70 nm)\Ca (45 nm)\Al (150 nm), where the active layer was a blend of P6 or P6BP in F8BT (10% P6) spin-coated from a 2% solution in xylene. The device area was 3.5 mm^2.

7.3. Conclusions

In summary, a conjugated porphyrin hexamers can be efficient an NIR-emitters, with longer wavelength electroluminescence than existing examples of porphyrin dimers and trimers.[24] The photoluminescence quantum yield of the P6 linear hexamer complexed with BP to reduce aggregation, was shown to be 7.7% ($\lambda_{PL\text{-}peak}$ = 882 nm) when blended with F8BT in solid state. The nanoring complex c-P6T shows significantly red-shifted emission (960 nm in EL) compared to the linear hexamer (883 nm in EL). Although less efficient than the linear hexamer as an emitter, the c-P6T nanoring represents an innovative approach to taking emission from organic molecules further into the NIR, and demonstrates the use of a curved π-surface to reduce aggregation. NIR emitting OLEDs incorporating both linear, P6, P6-BP, and cyclic, c-P6T, porphyrin hexamers in an F8BT charge transport matrix were fabricated and tested. By themselves, both hexamers showed low quantum yields in electroluminescence (EQE 0.024% and 0.009% for c-P6T and P6 respectively), but addition of BP to decorate the linear hexamer and provide steric hindrance for aggregation gave an order of magnitude increase in quantum efficiency to achieve 0.10% in electroluminescence (0.3 to 0.7% internal quantum efficiency) at 883 nm. It is remarkable that the presence of 3% by weight BP can suppress the aggregation of P6 in a thin film at high concentration (10% by weight). This work shows that porphyrin oligomers are promising candidates as NIR emitters in organic LEDs, with emission that can be color-tuned synthetically through control of the conjugation length.[3]

References

[1] N. Tessler, V. Medvedev, M. Kazes, S. H. Kan, U. Banin, *Science* **2002**, *295*, 1506.

[2] K. N. Bourdakos, D. M. N. M. Dissanayake, T. Lutz, S. R. P. Silva, R. J. Curry, *Applied Physics Letters* **2008**, *92*, 153311

[3] O. Fenwick, J. K. Sprafke, J. Binas, D. V. Kondratuk, F. Di Stasio, H. L. Anderson, F. Cacialli, *Nano Letters* **2010**, *11*, 2451.

[4] P. Li, O. Fenwick, S. Yilmaz, D. Breusov, D. J. Caruana, S. Allard, U. Scherf, F. Cacialli, *Chemical Communications* **2010**, *47*, 8820.

[5] Y. Yang, R. T. Farley, T. T. Steckler, S.-H. Eom, J. R. Reynolds, K. S. Schanze, J. Xue, *Journal of Applied Physics* **2009**, *106*, 044509

[6] Y. Yang, R. T. Farley, T. T. Steckler, S.-H. Eom, J. R. Reynolds, K. S. Schanze, J. Xue, *Applied Physics Letters* **2008**, *93*, 163305

[7] J. V. Caspar, E. M. Kober, B. P. Sullivan, T. J. Meyer, *Journal of the American Chemical Society* **1982**, *104*, 630.

[8] R. Englman, J. Jortner, *Molecular Physics* **1970**, *18*, 145.

[9] Y. Sun, C. Borek, K. Hanson, P. I. Djurovich, M. E. Thompson, J. Brooks, J. J. Brown, S. R. Forrest, *Applied Physics Letters* **2007**, *90*, 213503.

[10] C. Borek, K. Hanson, P. I. Djurovich, M. E. Thompson, K. Aznavour, R. Bau, Y. Sun, S. R. Forrest, J. Brooks, L. Michalski, J. Brown, *Angewandte Chemie-International Edition* **2007**, *46*, 1109.

[11] D. Beljonne, G. E. Okeefe, P. J. Hamer, R. H. Friend, H. L. Anderson, J. L. Bredas, *Journal of Chemical Physics* **1997**, *106*, 9439.

[12] H. L. Anderson, *Inorganic Chemistry* **1994**, *33*, 972.

[13] M. U. Winters, E. Dahlstedt, H. E. Blades, C. J. Wilson, M. J. Frampton, H. L. Anderson, B. Albinsson, *Journal of the American Chemical Society* **2007**, *129*, 4291.

[14] J. C. Ostrowski, K. Susumu, M. R. Robinson, M. J. Therien, G. C. Bazan, *Advanced Materials* **2003**, *15*, 1296.

[15] T. V. Duncan, K. Susumu, L. E. Sinks, M. J. Therien, *Journal of the American Chemical Society* **2006**, *128*, 9000.

[16] M. C. O'Sullivan, J. K. Sprafke, D. V. Kondratuk, C. Rinfray, T. D. W. Claridge, A. Saywell, M. O. Blunt, J. N. O'Shea, P. H. Beton, M. Malfois, H. L. Anderson, *Nature* **2010**, *469*, 72.

[17] T. M. Brown, G. M. Lazzerini, L. J. Parrott, V. Bodrozic, L. Buergi, F. Cacialli, *Organic Electronics* **2010**, *12*, 623.

[18] M. Hoffmann, J. Karnbratt, M. H. Chang, L. M. Herz, B. Albinsson, H. L. Anderson, *Angewandte Chemie-International Edition* **2008**, *47*, 4993.

[19] J. K. Sprafke, D. V. Kondratuk, M. Wykes, A. L. Thompson, M. Hoffmann, R. Drevinskas, J. Kärnbratt, J. E. Bullock, M. Malfois, M. R. Wasielewski, B. Albinsson, D. Zigmantas, D. Beljonne, H. L. Anderson, *in preparation*.

[20] L. Sardone, C. Sabatini, G. Latini, F. Barigelletti, G. Marletta, F. Cacialli, P. Samori, *Journal of Materials Chemistry* **2007**, *17*, 1387.

[21] J. C. de Mello, F. H. Wittmann, R. H. Friend, *Advanced Materials* **1997**, *9*, 230.

[22] F. Cacialli, J. S. Wilson, J. J. Michels, C. Daniel, C. Silva, R. H. Friend, N. Severin, P. Samori, J. P. Rabe, M. J. O'Connell, P. N. Taylor, H. L. Anderson, *Nature Materials* **2002**, *1*, 160.

[23] S. Brovelli, G. Latini, M. J. Frampton, S. O. McDonnell, F. E. Oddy, O. Fenwick, H. L. Anderson, F. Cacialli, *Nano Letters* **2008**, *8*, 4546.

[24] B. W. D'Andrade, S. Datta, S. R. Forrest, P. Djurovich, E. Polikarpov, M. E. Thompson, *Organic Electronics* **2005**, *6*, 11.

[25] L. L. Chua, J. Zaumseil, J. F. Chang, E. C. W. Ou, P. K. H. Ho, H. Sirringhaus, R. H. Friend, *Nature* **2005**, *434*, 194.

[26] E. Moons, *Journal of Physics-Condensed Matter* **2002**, *14*, 12235.

[27] T. M. Brown, J. S. Kim, R. H. Friend, F. Cacialli, R. Daik, W. J. Feast, *Applied Physics Letters* **1999**, *75*, 1679.

[28] N. C. Greenham, R. H. Friend, D. D. C. Bradley, *Advanced Materials* **1994**, *6*, 491.

[29] J. S. Kim, P. K. H. Ho, N. C. Greenham, R. H. Friend, *Journal of Applied Physics* **2000**, *88*, 1073.

[30] D. McBranch, I. H. Campbell, D. L. Smith, J. P. Ferraris, *Applied Physics Letters* **1995**, *66*, 1175.

8. Conclusions and outlook

Supramolecular architectures represent a powerful tool to both investigate fundamental properties of conjugated polymers, and for optoelectronic applications.

In this thesis I have shown how conjugated polyrotaxane have a potential for applications in two different fields: polarized emission and optically pumped lasers.

In Chapter 3, oriented film prepared using a stretchable polymeric matrix embedding conjugated polymers show a remarkable polarisation ratio indicating that a high degree of orientation can be achieved even for rigid supramolecular structures like conjugated polyrotaxanes. Furthermore, the suppression of interchain interactions in polyrotaxanes combined with the PVA matrix result in a slower depolarisation of the emitted light, contributing to the overall polarised photoluminescence.

In Chapter 4, an all-plastic photonic crystal functionalized with conjugated polyrotaxanes shows an enhancement (and suppression) of the photoluminescence intensity. The modification of the optical density of states by the photonic crystal causes a wavelength dependent modification of the photoluminescence lifetime correspondent to the enhancement/suppression spectral regions. The photoluminescence enhancement can potentially lead to a decrease of the lasing threshold of the conjugated polyrotaxanes.

In both this studies, the use of conjugated polyrotaxanes opened the possibility of using water-soluble materials (poly vinyl alcohol in the first case and polystyrene nanospheres in the second one) which would have been otherwise impossible using other types of conjugated polymers, usually soluble in non-polar organic solvents. Polyrotaxanes have a further advantage on other water-soluble conjugated polymers since they possess a higher photoluminescence quantum yield, thanks to the cyclodextrin encapsulation which is able to hinder the formation of aggregates and other photoluminescence quenching processes.

In the second part of this thesis I have shown how it is possible to implement self-assembled monolayers into light-emitting diodes.

In Chapter 5, by including an azo-benzene based self-assembled monolayer in the anode, the external quantum efficiency of a polymeric light-emitting diode increases 10 times. Unfortunately, the thin layer of Au necessary to the formation of the self-assembled monolayer causes a reduction of the external quantum efficiency in comparison to light-emitting diodes with oxygen-plasma-treated ITO anodes. The increase in external quantum efficiency is caused by an increase in the work function of the anode, thus decreasing the injection barrier for holes into the active layer of the device.

In Chapter 6, a novel low temperature processing of electron blocking layers is shown. By using a lower temperature than previously reported, an overall increase in device performance is observed thanks to a better balance between the number of holes and electrons in the active layer.

Finally, In Chapter 7 a supramolecular architecture between a porphyrin hexamers and benzyl pyridine is shown for near-infrared applications. The inclusion of benzyl pyridine reduces aggregation thus leading to an increase in the photoluminescence quantum yield of the linear hexamer. Although less efficient than the linear hexamer as an emitter, the porhyrin nanoring represents an innovative approach to taking emission from organic molecules further into the NIR, and demonstrates the use of a curved π-surface to reduce aggregation.

Near-infrared emitting polymeric light emitting diodes incorporating both the linear and the cyclic porphyrin hexamers showed low external quantum efficiencies but, addition of BP provide steric hindrance for aggregation giving an order of magnitude increase.

Both projects on polyrotaxanes presented here can be further developed in two ways:

The oriented films used in the study in Chapter 3 have been prepared using a non-conductive matrix. By switching to a conductive one it should be possible to prepare light emitting diodes using these oriented films by simply evaporating two electrodes on the stretched films. This would be of particular interest since it will allow a comparison between the polarization of the electroluminescence and the photoluminescence.

The photonic crystals here studied represent an interesting and cheap way to modify the optical density of states, thus modifying the photoluminescence properties of embedded polyrotaxanes. Nevertheless, photonic structures possessing a complete photonic band gap (in all three dimensions) are available, therefore opening the possibility to a further increase/enhancement of the phenomena here observed. Furthermore, lasing threshold measurements have still to be carried out.

Self-assembled monolayers are useful tool to modify injection barriers at interfaces. In the study here reported, the thin layer of Au represents the biggest limitation for devices, since it causes a reduction of the external quantum efficiency. By using a self-assembled monolayer directly attached to the ITO electrode, a further improvement of device performance can be expected.

Furthermore, the low thermal stability o f azo-benzene based self-assembled monolayers, prevents any further thermal annealing of the polymeric light emitting diode which is typically necessary to remove the solvent left after spin-coating.